Evaluation of Alternative Applications of LiDAR-based Enhanced Forest Inventory Methods

by

Jason William Kelley

B.Sc., University of Victoria, 2018

A Thesis Submitted in Partial Fulfillment of the
Requirements for the Degree of

MASTER OF SCIENCE

in the Department of Geography

We acknowledge and respect the lək̓ʷəŋən peoples on whose traditional territory the university stands, and the Songhees, Esquimalt and W̱SÁNEĆ peoples whose historical relationships with the land continue to this day.

Evaluation of Alternative Applications of LiDAR-based Enhanced Forest Inventory Methods

by

Jason William Kelley

B.Sc., University of Victoria, 2018

Supervisory Committee
Dr. Christopher Bone, Co-Supervisor
Department of Geography

Dr. Tony Trofymow, Co-Supervisor
Department of Biology

Abstract

Forests cover a large portion of the global land area and provide critical resources such as timber, food, and medicine in addition to playing a significant role in the global carbon cycle. As such, sustainable forest management practices are required to balance forest economies and climate change mitigation with other non-timber objectives. A key aspect of many sustainable forest management programs is forest monitoring, for which technological and methodological development has led to enhanced forest inventory (EFI) methods, many of which rely on remote sensing data from high-resolution light detection and ranging (LiDAR) and optical imagery. However, to date, current applications of EFI methods have mostly focused on timber attributes with limited research on non-timber attributes or analyses regarding multi-temporal monitoring, method scaling, or method transferability.

The objective of this thesis is to expand applications of EFIs in monitoring and analysis through two distinct studies, first evaluating the utility of LiDAR-based EFI methods in multi-temporal silvicultural treatment assessment and secondly in the pre-harvest estimation of merchantable wood and non-merchantable wood left as logging residues. The first study evaluates a process that expands the sampling of fertilization treatment effects on forest stands to the wider treatment area by utilizing paired LiDAR blocks made up of raster cell estimates from a multi-temporal area-based model. Results showed promise for detecting treatment impacts on stand volume, biomass, and height and highlights the potential for the methods to be used as a means to rapidly expand analysis from sample plots to the entire treatment area. The second study focuses on the use of a hybrid area-based and individual tree EFI approach to model merchantable and non-merchantable forest wood volumes while exploring the scalability of these models to harvest blocks and the transferability to additional blocks without prior training.

Results from this study indicated that models for both volume attributes are successfully scalable and transferable to harvest blocks. Overall, the research results presented in this thesis demonstrate the potential of enhanced forest inventory methods for the monitoring and assessment of timber attributes, such as wood volume or biomass, as well as alternative attributes, such as stand height, or non-merchantable wood volume, over multiple years. This work further demonstrates the potential for these methods to expand areas of assessment and increase prediction accuracies.

Table of Contents

Supervisory Committee ii
Abstract iii
Table of Contents v
List of Tables vii
List of Figures x
Acknowledgements xii
Chapter 1: Introduction 1
1.1 Background 1
1.2 Enhanced Forest Inventories 2
1.3 EFI Applications 4
1.4 Thesis Overview 6
1.5 References 7
Chapter 2: Use of Multi-Temporal LiDAR to Quantify Fertilization Effects on Stand Volume and Biomass in Late-Rotation Coastal Douglas-Fir Forests. 12
Abstract 12
1. Introduction 13
2. Materials and Methods 18
2.1. Study Area 18
2.2. Plot Establishment and Measurement 20
2.3. Tree-Ring Data Collection and Measurement 20
2.4. Biomass Increments Using Tree-Ring Volume Reconstructions and CBM-CFS3 21
2.5. LiDAR Data Acquisition 21
2.6. Sample Plot Data for Area-Based Models 22
2.7. LiDAR Data Processing 23
2.8. Area-Based Modelling 25
3. Results 27
3.1. Sample Plots 27
3.2. CBM-CFS3 Plot Biomass Increments Using Tree-Ring and Default Growth Curves 30
3.3. Area-Based Models 30
4. Discussion 36
4.1. Method Comparisons 36

4.2. Sources of Uncertainty 39
5. Conclusions 42
References 42
Appendix A 49
Chapter 3: Combining Area-based and Individual Tree Metrics Can Improve Merchantable and Non-merchantable Wood Volume Estimates in Coastal Douglas-fir Forests. 61
Abstract 61
1. Introduction 62
2. Methods 68
2.1 Study Area Descriptions 68
2.2 Spatial Data 71
2.3 Spatial Data Processing 73
2.4 Training Data From Plots at the OR, SWS and SWN Sites 75
2.5 Hybrid Model Development 78
2.6 Sources of Block-level Data for Testing Hybrid Models 79
2.7 Hybrid Model Testing and Comparisons 80
3. Results 81
3.1 Variable Selection 81
3.2 Model Fitting and Expansion 82
3.3 Comparison of HB Model Estimates with Block-level Data 85
4. Discussion 87
5. Conclusion 91
References 91
Chapter 4: Conclusion 98
4.1 Summary 98
4.2 Applications 100
4.3 Future Research 102
4.4 References 103

List of Tables

Table 2.1. Composition and number of final selected LiDAR-block pairs for each analysis unit. 24

Table 2.2. Plot level stem volumes ($m^3 ha^{-1}$), cumulative volume increments, and control (C) or fertilized (F) treatment averages for the subset trees in the plots, as well as all trees. 28

Table 2.3. Plot level stem biomass (Mg ha^{-1}), cumulative biomass increments, and control (C) or fertilized (F) treatment averages for the subset trees in the plots, as well as all trees. 29

Table 2.4. LiDAR metrics selected and relative importance ranking for the volume (V, Vol) or biomass (B, Bio) models using Boruta variable selection method. 32

Table 2.5. Treatment effect method comparison showing unweighted values (((Fertilized/Control)-1) x 100)[1] in pre- and post-treatment periods for stem volume ($m^3 ha^{-1}$), stem biomass (Mg ha^{-1}), and height (m) cumulative increment (gain) for plot subset trees and LiDAR blocks, and above-ground biomass carbon gain (Mg C ha^{-1}) from a model reconstruction approach using plot tree-ring growth curves. Comparisons are also shown for periodic annual increment (PAI) of above-ground biomass carbon (Mg C ha^{-1} yr^{-1}) from tree-ring curves for the same periods as volume growth ($m^3 ha^{-1} yr^{-1}$) in [22]. 39

Table A1. LiDAR predictor metrics used and selected by the Boruta variable selection method……49

Table A2. Mixed effect model F and P-value results between treatments for volume and biomass cumulative increments with subset plot trees or all plot trees……...50

Table A3. Mixed effect model F and P-value results between treatments for volume and biomass periodic annual increments with all plot trees or subset plot trees……50

Table A4. Plot level stem volumes ($m^3 ha^{-1}$), periodic annual volume increments ($m^3 ha^{-1} yr^{-1}$), and control (C) or fertilized (F) treatment averages for the subset trees in the plots, as well as all trees……51

Table A5. Plot level stem biomass (Mg ha^{-1}), periodic annual biomass increments (Mg $ha^{-1} yr^{-1}$), and control (C) or fertilized (F) treatment averages for the subset trees in the plots, as well as all trees……51

Table A6: Mixed effect model F and P-value results between treatments for volume and biomass increments in the LiDAR blocks across all AUs……...53

[1] Values have been corrected since publication

Table A7: Mixed effect model F and P-value results between treatments for volume and biomass increments in the LiDAR for individual AUs……54

Table A8: Mixed effect model F and P-value results between treatments for volume and biomass periodic annual increments in the LiDAR blocks across all AUs……55

Table A9: Mixed effect model F and P-value results between treatments for volume and biomass periodic annual increments in the LiDAR blocks for individual AUs……...56

Table A10: Mixed effect model F and P-value results between treatments for 95th percentile of LiDAR height increments and periodic annual increments in the LiDAR blocks across all AUs……57

Table A11: Mixed effect model F and P-value results between treatments for 95th percentile of LiDAR height increments and periodic annual increments in the LiDAR blocks for individual AUs……59

Table A12. Treatment effect method comparison showing weighted values ([Fertilized/2004 Fertilized x 100] – [Control/2004 Control x 100]) in pre and post treatment periods for stem volume (m^3 ha^{-1}), stem biomass (Mg ha^{-1}), and height (m) cumulative increment (gain) for plot subset trees and LiDAR blocks, and above ground biomass carbon gain (Mg C ha^{-1}) from a model reconstruction approach using plot tree ring growth curves. Comparisons are also shown for periodic annual increment (PAI) of above ground biomass carbon (Mg C ha^{-1} yr^{-1}) from tree-ring curves for the same periods as volume growth ($m^3ha^{-1}yr^{-1}$) in [22]. * Note: Plot tree ring growth curve PAI and Plot crop tree volume growth PAI values weighted as [Post-treat F/Pre-treat F x 100] - [Post-treat C/Pre-treat C x 100]……60

Table 3.1. Sample block site descriptions including earliest estimated establishment date (Est. Date), major species composition, main stand estimated site index (m), average block elevation (m ASL), average block slope (degrees) for blocks located at the Oyster River (OR), Sooke Watershed South (SWS), Sooke Watershed North (SWN), Northwest bay (NWB), and Franklin River (FR) sites. Major species include Douglas-fir (Fd), western hemlock (Hw), western red cedar (Cw), and amabilis fir (Ba). 71

Table 3.2: Point cloud and imagery characteristics and acquisition years. *Note imagery from SWN-15 from 2013 similar to SWS. 73

Table 3.3. Area based (AB) and individual tree (IT) style predictor metrics used for variable selection. 75

Table 3.4. Block digitized areas and block-level HB random forest model estimates of merchantable (m^3ha^{-1}) and non-merchantable volumes (m^3ha^{-1})……...84

Table 3.5. Block total merchantable volumes (m^3ha^{-1}) for the post-harvest scale (HS), pre-harvest forest cover (FC), pre-harvest hybrid model (HB), and differences in pre-harvest estimates from post-harvest validation. Average differences use the absolute value of block differences. 86

Table 3.6. Block total non-merchantable volumes (m^3ha^{-1}) for the post-harvest waste and residue survey (WRS) estimate, post-harvest semi-automated log delineation (SLD) estimate, pre-harvest hybrid (HB) model predictions, and differences between pre-harvest estimates and post-harvest values. Average volume differences use the average absolute difference. 87

List of Figures

Figure 2.1. Study area map showing the fertilization area (orange lines); DF49a fertilized and control sample plots (pink); and LiDAR blocks for forest stand analysis units of Hemlock-Fir (dark green), Fir (Site Index 30) (light blue); Fir (Sight Index 40+) (dark blue); and Fir-Hemlock (light green). The main stand, DF49, was the location of flux towers and plots established in 2002 and measured until 2011, when the stand was cut. White lines show the 2010 forest stand polygon boundaries. 19

Figure 2.2. LiDAR paired block design in the DF49a area showing the fertilization boundary, buffered offsets, and sample plots' location within cells (dashed circles). 25

Figure 2.3. Annual above-ground biomass carbon increments from the CBM-CFS3 model for control (123C solid line, circles) and fertilized (456F, dashed line triangle) plots using yield curves derived from plot tree-ring data (Rings), default stand type yield curves without a fertilizer effect (CBMD gray lines, open symbols), or default yield curves with a fertilizer effect (CBMF black line, closed symbols). Rings data show plot mean with one standard error. 31

Figure 2.4. Observed plot level vs. RF predicted volume (A) and biomass (B) values in 2004 (green), 2008 (orange), 2011 (purple), and 2016 (pink). 33

Figure 2.5. LiDAR block-level average (line) and standard error (shadow) of stem volume (A) and biomass (B) cumulative increments (gain) for control blocks (solid) and fertilized blocks (dashed). 34

Figure 2.6. LiDAR block-level average (line) and standard error (shadow) of 95th percentile of LiDAR heights (A) and height periodic annual increments (B) for control blocks (solid) and fertilized blocks (dashed). 36

Figure A1: LiDAR block-level average (line) and standard error (shadow) stem volume (left) and biomass (right) increments for control blocks (solid) and fertilized blocks (dashed) in AU 146 (A,B), AU 148 (C,D), AU 445 (E,F), AU 526 (G,H)……52

Figure A2: LiDAR block-level average (line) and standard error (shadow) 95^{th} percentile of LiDAR height cumulative (left) and periodic annual (right) increments for control blocks (solid) and fertilized blocks (dashed) in AU 146 (A,B), AU 148 (C,D), AU 445 (E,F), AU 526 (G,H).....58

Figure 3.1. Study site map showing layouts of block boundaries (black lines) and sample plot locations (red triangles) at Oyster River (OR), Sooke Watershed South (SWS) and Sooke Watershed North (SWN), Northwest Bay (NWB), and Franklin River (FR). All sites are located in Douglas-fir dominated sites on Vancouver Island, with central site locations shown (stars) in the lower right panel……..69

Figure 3.2. (A) Diagram depicting the areal appearance of the canopy and sub-canopy tree crowns (top) and the structure of a complex forest with live (dark and light green crown, respectively) and dead (yellow crown) trees that make up the canopy and sub-canopy. Also shown is the stem wood components of merchantable stem wood (>=12.5/17.5 cm DBH & 10 m length) (dark brown), non-merchantable stem wood (>= 10 cm diameter & < 10 m length) (light brown), and stumps and tops (grey). B) Data representations of an individual tree delineation for OR plot 11.3 (top) and the corresponding LiDAR point cloud (bottom). 77

Figure 3.3: Boruta variable selection results showing the distribution of variable importance scores for the merchantable volume component (A) and non-merchantable volume component (B). Green indicates selected metrics, blue indicates noise or shadow metrics, and red is those metrics deemed not important to the model..... 82

Figure 3.4: Observed plot level vs. RF predicted merchantable (Left) and non-merchantable volumes at the Oyster River (OR) (green), Sooke Watershed South (SWS) (Purple), and Sooke Watershed North (SWN) (orange) sites…….83

Acknowledgements

I would like to acknowledge the Natural Resources Canada - Canadian Wood Fibre Centre for providing funding support through a proposal by Dr. Trofymow for the fertilization study and the Canadian Forest Service Forest Innovation Program for providing funding support through a proposal by Dr. Trofymow and Dr. Bone for the study on non-merchantable wood volume. I am also thankful to the University of Victoria for providing me with a graduate fellowship and the Department of Geography for providing me with several teaching assistantship positions throughout my degree.

I would like to thank my co-supervisor, Dr. Tony Trofymow, for taking a chance on me as a co-op student and providing me with countless hours of support and guidance throughout the years, ultimately leading to this thesis work. I would also like to thank my other co-supervisor, Dr. Chris Bone, for welcoming me into the SURREAL lab and pushing me to discover more than I thought possible in my graduate program and, most importantly, his patience and insights throughout the writing process. Thanks are extended to my friends and lab-mates in the SURREAL lab for the many chats and laughs and their remarkable passion, which consistently inspires me to become a better academic.

I also thank my parents and sister for their amazing support throughout the years despite not really knowing what it is I do “at school”, it is their model of hard work that has led me to this point and their encouragement that made me start the post-secondary path, although they may not have known what they started. Finally, I have to thank my partner Kati for her constant support, endless patience, and hours of editing that she has provided through all of my years of school. I would not have been able to do this without you.

Chapter 1: Introduction

1.1 Background

Forests are a critical global resource covering over 30% of the world's land area (FAO, 2021). In addition to timber, forests provide additional resources and benefits such as food, medicine, therapy, and tourism opportunities (Trozzo et al., 2019; Yi et al., 2019; Lonn et al., 2019). Forests also play an essential role in the global carbon cycle, both positively and negatively, as forests often act as both a source and sink of atmospheric carbon (Pan et al., 2011). Globally, not including harvesting, deforestation as a result of land-use change accounted for over 1.8 Gt of CO_2 emissions in 2019 (Friedlingstein et al., 2020), while wildfire events produce even more emissions over short periods of time (Liu et al., 2014). Alternatively, healthy intact forests across the globe act as an immense carbon sink, with recent estimates showing that forests have the potential to remove 3.29 Gt of CO_2 from the atmosphere in one year (FAO, 2021). The ability to balance this source-sink relationship lies in part with proper and sustainable forest management, which, if implemented appropriately, could lead to emissions reductions up to 30% of the Paris Climate Agreement targets that were established in 2015 (Griscom et al., 2017, Nesha et al., 2021). This agreement between 196 countries aims to limit global warming to below 2 degrees Celsius and recognizes, through article 5, the need to increase and protect greenhouse gas sinks, particularly in forests (United Nations, 2015).

Many sustainable forest management programs have been established in countries around the world, and several certification bodies allow the industry to declare their products as coming from sustainable forestry practices (van Kooten et al., 2005). A crucial part of sustainable forest management that lies at the core of many programs is forest monitoring. On a global scale, the Food and Agriculture Organization of the United Nations conducts global forest assessments

every year (FAO, 2021). However, these assessments include relatively few tracked variables and rely on member countries contributing data with a vast range of collection methods and overall quality (FAO, 2021; Nesha et al., 2021). Alternatively, in countries with large areas of temperate forest and similarly large forest industries, such as those seen in Scandinavia or North America, forest monitoring or inventory programs have been long established to track key timber aspects such as forest area, volume, biomass, and height (Tomppo et al., 2010). Traditionally, these inventory methods involve a level of mapping using aerial photography and validation using ground sample plots (Tompalski et al., 2021, Gillis et al., 2005). In addition, these methods utilize ancillary information such as disturbance histories, previous inventories, or any other information that aids in delineating and interpreting the forest stands (Leckie and Gillis, 1995). Highly skilled photo interpreters can then use the total data collection to delineate forest stands and interpret their general characteristics based on uniformity, age, and structure. However, despite a system of validation checks and expert interpreters, traditional inventory methods are inherently subjective, and variations of interpretations are an expected outcome of these methods (Thompson et al., 2007).

1.2 Enhanced Forest Inventories

As remote sensing technologies have advanced, additional data sources such as digital airborne or satellite imagery or light detection and ranging (LiDAR) data were introduced to augment traditional forest inventory methods. The inclusion of these data allows for the automation of some of the interpretation steps, such as segmenting forest and non-forest areas (Gougeon & Leckie, 2003) or directly measuring certain attributes such as stand height (White et al., 2016). As technological and methodological development continues, new enhanced forest inventory

(EFI) methods have been created with an aim to limit the amount of subjective interpretation in forest inventories (Gougeon & Leckie, 2003; White et al., 2013).

EFI methods take advantage of high-resolution passive and active remote sensing platforms to describe the forest environment in a finer spatial resolution than traditional inventories. These enhanced methods can generally be broken into two main classes: the area-based (AB) and individual tree (IT) approaches, as well as an approach using a hybrid of the two. Improving on the stand level delineations for traditional inventory methods done by photo interpreters, EFI methods generally have a spatial resolution at the level of a rasterized grid (AB) or even individual trees (IT), both of which provide multiple levels of measurement within a single stand boundary.

The AB approach uses LiDAR data and a network of training sample plots to develop a statistical model of various forest attributes, which is done using a set of LiDAR metrics generated from data clipped to the plot boundaries (Næsset, 2002; Woods et al., 2008). These statistical models can be developed at the plot level using either parametric (Ferster et al., 2009) or non-parametric (White et al., 2014) methods. Once plot level models are trained for forest attributes (i.e. height, volume, biomass), they can be applied to the wider forest area for which there is data collected using a rasterized grid of predictor metrics with a similar spatial resolution as the footprint of training plots (White et al., 2013).

The IT approach can also use LiDAR or optical imagery and relies on segmentation techniques to delineate individual tree crowns while allowing direct measurement of attributes like tree height and crown area (Dalponte & Coomes, 2016). With the inclusion of species classification, additional tree attributes such as diameter at breast height (DBH), volume, or

biomass can be calculated (Jucker et al., 2014; Kozak, 1994; Ung et al., 2008). Attributes for all detected trees can theoretically then be summed up to a stand, block, or landscape level, for which there is remote sensing data available (White et al., 2017). The major advantage of EFI methods is that both the AB and IT approaches can highlight the within-stand variation; wherein traditional inventories all areas within a delineated stand have the same attributes (White et al., 2017). However, despite the advantages of expanding EFI models, few studies have compared these estimates to other independent assessment methods at the block level (White et al., 2014), and fewer have investigated the transferability of such EFI models to forests without prior training data (Tompalski et al., 2019)

1.3 EFI Applications

Current implementations of EFI methods have generally focused on aspects similar to traditional forest inventories, tracking forest attributes primarily of interest to the timber industry (Naesett, 2002, Woods et al., 2008, White et al., 2014). Further applications of EFI methods have begun to focus on attributes that are not timber-primary such as carbon stocks (Dalponte & Coomes, 2016), fire fuels (Fernández-Álvarez et al., 2019), silvicultural treatments (Hilker et al., 2010), and non-merchantable logging residues (Barrette et al., 2018). Additionally, most applications of EFI methods focus on data from a single time slice, similar to traditional inventory methods. However, multi-temporal applications for change detection have also been applied as data required for EFI methods have become more available (Hudak et al., 2012). One area of multi-temporal analysis that is relatively unexplored with EFI methods is the assessment of silvicultural treatments over time.

Traditionally, silvicultural treatments such as fertilization are evaluated using forest sample plots, similar to those used by the AB approach, measured pre-treatment and several

years post-treatment (Filipescu et al., 2017; Harrington & Devine, 2011). These sample plot methods provide a snapshot of forest conditions at each location, but the overall accuracy is linked to the number and location of sampling plots. However, with the increased availability of LiDAR data, the AB approach can be used in a multi-temporal approach to augment a sample plot network and describe the treatment effects for a wider set of EFI plots or raster cells around the treatment area. This would provide the ability for rapid assessment of treatment effects without increasing the number of ground-based sample plots.

Expanding estimates to the entire extent of the remote sensing data coverage is the largest advantage of EFI methods. However, few studies have investigated the ability to transfer models to areas of similar forest types without additional ground sample plots (White et al., 2014; Tompalski et al., 2019). From a forest manager perspective, the ability to transfer developed models to other stands of similar forest types is highly desirable, as this would limit the need for additional sample plots with every expansion. Furthermore, as most EFI applications focus on merchantable timber attributes, few studies have applied EFI style methods to estimate non-merchantable timber attributes (Barrette et al., 2018; Mansuy et al., 2017). This is also desirable due to increasing pressures posed by climate change making forest managers search to increase the utilization of non-merchantable material for bio-fuel or bio-products (Titus et al., 2021). The ability to forecast or estimate the availability of non-merchantable material would increase the utilization of non-merchantable timber that is generally left dispersed in harvest blocks or piled and burned (Trofymow et al., 2014). With improved forecasting of available non-merchantable material, the residues from logging could be used to produce bio-energy or bio-products in areas where it is economical to do so. Using these residues, which are generally piled and burned, increases the utilization of harvested material and is one of the several forest management

strategies recognized by the Intergovernmental Panel on Climate Change to improve the positive climate change mitigation potential of forest ecosystems (IPCC 2014, 2013).

1.4 Thesis Overview

The overall focus of this thesis is to expand applications of EFI methods in monitoring and analysis by evaluating the utility of LiDAR-based EFI methods in multi-temporal silvicultural treatment assessment and pre-harvest estimation of non-merchantable logging residues. Chapter Two explores the use of a multi-temporal EFI method to quantify the effects of silvicultural treatments. Specifically, this study aims to examine the utility of a multi-temporal area-based approach for expanding the sample area and detecting fertilization effects on stand height, volume, and biomass beyond the sample plots. Located in second-growth coastal Douglas-fir dominated forests on Vancouver Island, British Columbia, Canada, a total of six paired plots were used with LiDAR metrics to develop random forest model estimates one year prior to fertilization and one, four, and nine years post-fertilization. Results from models were extrapolated to 29-paired (control vs fertilized) LiDAR blocks, where relative treatment effects were calculated. Treatment effects in the LiDAR blocks were compared to observed sample plot results and estimates from a carbon budget model (CBM-CFS3) using standard growth curves as input or using growth curves derived from tree ring measurements in the sample plots.

Chapter Three comprises a study combining area-based and individual tree EFI methods in a hybrid approach to model merchantable non-merchantable forest wood volumes. This study also explores the scalability and transferability of these models to harvest blocks and additional blocks without prior training plots. Also focused on Vancouver Island, the sample blocks for this study comprise 18 harvest blocks across five different sites. A total of 38 sample plots across two of the sites were used to train models estimating merchantable and non-merchantable stem

volumes. These models were then expanded to the ten sample blocks from training sites and transferred to eight sample blocks from testing sites with no prior training. Block-level results at both training and testing sites were compared to two independent estimates of block-level merchantable volume and non-merchantable volume.

Chapter Four presents the concluding chapter that summarizes the key findings and results of the two completed studies and discusses potential limitations. Lastly, this chapter discusses the overall contributions of this research and suggestions for future work.

1.5 References

Barrette, J., Paré, D., Manka, F., Guindon, L., Bernier, P., & Titus, B. (2018). Forecasting the spatial distribution of logging residues across the Canadian managed forest. Canadian Journal of Forest Research, 48(12), 1470-1481. doi:10.1139/cjfr-2018-0080

Dalponte, M., & Coomes, D. A. (2016). Tree-centric mapping of forest carbon density from airborne laser scanning and hyperspectral data. Methods in Ecology and Evolution, 7(10), 1236–1245. https://doi.org/10.1111/2041-210X.12575

FAO. (2021). FAOSTAT – Forest Land. Available from http://www.fao.org/faostat/en/#data/GF. Last Accessed 06/27/2021

Fernández-Álvarez, M., Armesto, J., & Picos, J. (2019). LiDAR-based wildfire prevention in WUI: The automatic detection, measurement and evaluation of forest fuels. Forests, 10(2), 148. https://doi.org/10.3390/f10020148

Ferster, C. J., Coops, N. C., & Trofymow, J. A. (2009). Aboveground large tree mass estimation in a coastal forest in British Columbia using plot-level metrics and individual tree detection from lidar. Canadian Journal of Remote Sensing, 35(3), 270–275. https://doi.org/10.5589/m09-014

Filipescu, C. N., Trofymow, J. A., & Koppenaal, R. S. (2017). Late-rotation nitrogen fertilization of Douglas-fir: Growth re-sponse and fibre properties. Canadian Journal of Forest Research, 47(1), 134-138. doi:10.1139/cjfr-2016-0306

Friedlingstein, P., O'Sullivan, M., Jones, M. W., Anew, R. M., Hauck, J., Olsen, A., Peters, G. P., Peters, W., Pongratz, J., Sitch, S., Le Quere, C., Canadell, J. G., Ciais, P., Jackson, R. B., Alin, S., Aragao, Luiz E. O. C, Arneth, A., Arora, V., Bates, N. R., . . . Zaehle, S. (2020). Global carbon budget 2020. Earth System Science Data, 12(4), 3269-3340. https://doi.org/10.5194/essd-12-3269-2020

Gillis, M., Omule, A., & Brierley, T. (2005). Monitoring Canada's Forests: The National Forest Inventory. Forestry Chronicle, 81(2), 214-221. https://doi.org/10.5558/tfc81214-2

Gougeon, F. A. & Leckie, D. G. (2003). Forest information extraction from high spatial resolution images using an individual tree crown approach. Victoria: Natural Resources Canada, Canadian Forest Service, Pacific Forestry Centre.

Griscom, B. W., Adams, J., Ellis, P. W., Houghton, R. A., Lomax, G., Miteva, D. A., Schlesinger, W. H., Shoch, D., Siikamäki, J. V., Smith, P., Woodbury, P., Zganjar, C., Blackman, A., Campari, J., Conant, R. T., Delgado, C., Elias, P., Gopalakrishna, T., Hamsik, M. R., . . . Sveriges lantbruksuniversitet. (2017). Natural climate solutions. Proceedings of the National Academy of Sciences - PNAS, 114(44), 11645-11650. https://doi.org/10.1073/pnas.1710465114

Harrington, C. A., & Devine, W. D. (2011). Stand development following precommercial thinning and fertilization treatments in a western redcedar (thuja plicata) dominated forest. Canadian Journal of Forest Research, 41(1), 151-164. doi:10.1139/x10-193

Hilker, T., van Leeuwen, M., Coops, N. C., Wulder, M. A., Newnham, G. J., Jupp, D. L. B., & Culvenor, D. S. (2010). Comparing canopy metrics derived from terrestrial and airborne laser scanning in a douglas-fir dominated forest stand. Trees, 24(5), 819-832. doi:10.1007/s00468-010-0452-7

Hudak, A. T., Strand, E. K., Vierling, L. A., Byrne, J. C., Eitel, J. U. H., Martinuzzi, S., & Falkowski, M. J. (2012). Quantifying aboveground forest carbon pools and fluxes from repeat LiDAR surveys. Remote Sensing of Environment, 123, 25-40. https://doi.org/10.1016/j.rse.2012.02.023

IPCC 2014. (2013). Revised supplementary methods and good practice guidance arising from the Kyoto Protocol, Hiraishi, T., Krug, T., Tanabe, K., Srivastava, N., Baasansuren, J., Fukuda, M., and Troxler, T.G. (eds) Published: IPCC, Switzerland.

Jucker, T., Caspersen, J., Chave, J., Antin, C., Barbier, N., Bongers, F., Dalponte, M., van Ewijk, K.Y., Forrester, D.I., Haeni, M, Higgins, S.I., Holdaway, R.J., Iida, Y., Lorimer, C., Marshall, P.L., Momo, S., Moncrieff, G.R., Ploton, P., Lourens, P., … Coomes, D. A. (2017). Allometric equations for integrating remote sensing imagery into forest monitoring programmes. Global Change Biology, 23(1), 177–190. https://doi.org/10.1111/gcb.13388

Kozak, A. 1994. Development of Taper Equations by BEC Zones and Species. Retrieved from: https:// www.for.gov.bc.ca/hfd/library/documents/bib95354a.pdf. (accessed 20 October, 2018).

Leckie, D.G., & Gillis, M. D. (1995). Forest inventory in Canada with emphasis on map production. Forestry Chronicle, 71(1), 74-88. https://doi.org/10.5558/tfc71074-1.

Liu, Y., Goodrick, S., & Heilman, W. (2014). Wildland fire emissions, carbon, and climate: Wildfire–climate interactions. Forest Ecology and Management, 317, 80-96. https://doi.org/10.1016/j.foreco.2013.02.020

Lonn, P., Mizoue, N., Ota, T., Kajisa, T., & Yoshida, S. (2019). Using forest cover maps and local People's perceptions to evaluate the effectiveness of community-based ecotourism for forest conservation in Chambok (Cambodia). Environmental Conservation, 46(2), 111-117. https://doi.org/10.1017/S0376892918000462

Mansuy, N., Paré, D., Thiffault, E., Bernier, P. Y., Cyr, G., Manka, F., Lafleur, B., & Guindon, L. (2017). Estimating the spatial distribution and locating hotspots of forest biomass from harvest residues and fire-damaged stands in Canada's managed forests. Biomass & Bioenergy, 97, 90-99. https://doi.org/10.1016/j.biombioe.2016.12.014

Næsset, E. (2002). Predicting forest stand characteristics with airborne scanning laser using a practical two-stage procedure and field data. Remote Sensing of Environment, 80(1), 88-99. doi:10.1016/S0034-4257(01)00290-5

Nesha, M. K., Herold, M., De Sy, V., Duchelle, A. E., Martius, C., Branthomme, A., Garzuglia, M., Jonsson, O., & Pekkarinen, A. (2021). An assessment of data sources, data quality and changes in national forest monitoring capacities in the global forest resources assessment 2005–2020. Environmental Research Letters, 16(5), 54029. https://doi.org/10.1088/1748-9326/abd81b

Pan, Y., Birdsey, R. A., Ciais, P., Jackson, R. B., Pacala, S. W., McGuire, A. D., Piao, S., Rautiainen, A., Sitch, S., Hayes, D., Fang, J., Houghton, R., Kauppi, P. E., Kurz, W. A., Phillips, O. L., Shvidenko, A., Lewis, S. L., & Canadell, J. G. (2011). A large and persistent carbon sink in the world's forests. Science (American Association for the Advancement of Science), 333(6045), 988-993. https://doi.org/10.1126/science.1201609

Thompson, I. D., Maher, S. C., Rouillard, D. P., Fryxell, J. M., & Baker, J. A. (2007). Accuracy of forest inventory mapping: Some implications for boreal forest management. Forest Ecology and Management, 252(1), 208-221. https://doi.org/10.1016/j.foreco.2007.06.033

Titus, B. D., Brown, K., Helmisaari, H. S., Vanguelova, E., Stupak, I., Evans, A., Clarke, N., Guidi, C., Bruckman, V. J., Varnagiryte-Kabasinskiene, I., Armolaitis, K., Vries, d., Wim, Hirai, K., Kaarakka, L., Hogg, K., & Reece, P. (2021). Sustainable forest biomass :

A review of current residue harvesting guidelines. Energy, Sustainability and Society, 11(1), 1-32. https://doi.org/10.1186/s13705-021-00281-w

Tompalski, P., White, J. C., Coops, N. C., & Wulder, M. A. (2019). Demonstrating the transferability of forest inventory attribute models derived using airborne laser scanning data. Remote Sensing of Environment, 227, 110-124. https://doi.org/10.1016/j.rse.2019.04.006

Tompalski, P., White, J. C., Coops, N. C., Wulder, M. A., Leboeuf, A., Sinclair, I., Butson, C. R., & Lemonde, M. (2021). Quantifying the precision of forest stand height and canopy cover estimates derived from air photo interpretation. Forestry (London), https://doi.org/10.1093/forestry/cpab022

Tomppo E., Schadauer K., McRoberts R.E., Gschwantner T., Gabler K., Ståhl G. (2010) Introduction. In: Tomppo E., Gschwantner T., Lawrence M., McRoberts R. (eds) National Forest Inventories. Springer, Dordrecht. https://doi-org.ezproxy.library.uvic.ca/10.1007/978-90-481-3233-1_1

Trofymow, J. A., Coops, N. C., & Hayhurst, D. (2014). Comparison of remote sensing and ground-based methods for determining residue burn pile wood volumes and biomass. Canadian Journal of Forest Research, 44(3), 182–194. https://doi.org/10.1139/cjfr-2013-0281

Trozzo, K., Munsell, J., Niewolny, K., & Chamberlain, J. L. (2019). Forest food and medicine in contemporary appalachia. Southeastern Geographer, 59(1), 52-76. https://doi.org/10.1353/sgo.2019.0005

Ung, C., Bernier, P., & Guo, X. (2008). Canadian national biomass equations: New parameter estimates that include british columbia data. Canadian Journal of Forest Research, 38(5), 1123-1132. https://doi.org/10.1139/X07-224

United Nations. (2015). Framework Convention on Climate Change: Adoption of the Paris Agreement, 21st Conference of the Parties, Paris: United Nations.

van Kooten, G. C., Nelson, H. W., & Vertinsky, I. (2005). Certification of sustainable forest management practices: A global perspective on why countries certify. Forest Policy and Economics, 7(6), 857-867. https://doi.org/10.1016/j.forpol.2004.04.003

White, J. C., Wulder, M. A., Varhola, A., Vastaranta, M., Coops, N. C., Cook, B. D., Pitt, D., Woods, M. (2013). A best practices guide for generating forest inventory attributes from airborne laser scanning data using an area-based approach Information Report FI-X-010; Natural Resources Canada, Canadian Forest Service, Canadian Wood Fibre Centre, Pacific Forestry Centre: Victoria, BC, Canada, 39p. Available online: https://cfs.nrcan.gc.ca/publications?id=34887

White, J. C., Wulder, M. A., & Buckmaster, G. (2014). Validating estimates of merchantable volume from airborne laser scanning (ALS) data using weight scale data. Forestry Chronicle, 90(3), 378–385. https://doi.org/10.5558/tfc2014072

White, J. C., Coops, N. C., Wulder, M. A., Vastaranta, M., Hilker, T., & Tompalski, P. (2016). Remote sensing technologies for enhancing forest inventories: A review. Canadian Journal of Remote Sensing, 42(5), 619-641.

White, J.C., Tompalski, P., Vastaranta, M., Wulder, M.A., Saarinen, S., Coops, N.C., (2017). A best practices guide for generating forest inventory attributes from airborne laser scanning data using the area-based approach. Information Report FI-X-018. Natural Resources Canada, Canadian Forest Service, Canadian Wood Fibre Centre, Pacific Forestry Centre, Victoria, BC. 38 p. Available online: http://cfs.nrcan.gc.ca/publications?id=38945

Woods, M., Lim, K., & Treitz, P. (2008). Predicting forest stand variables from LiDAR data in the Great Lakes - St. Lawrence forest of Ontario. Forestry Chronicle, 84(6), 827–839. https://doi.org/10.5558/tfc84827-6

Yi, J., Ku, B., Kim, S. G., Khil, T., Lim, Y., Shin, M., Jeon, S., Kim, J., Kang, B., Shin, J., Kim, K., Jeong, A. Y., Park, J. H., Choi, J., Cha, W., Shin, C., Shin, W., & Kim, J. U. (2019). Traditional Korean medicine-based forest therapy programs providing electrophysiological benefits for elderly individuals. International Journal of Environmental Research and Public Health, 16(22), 4325. https://doi.org/10.3390/ijerph16224325

Chapter 2: Use of Multi-Temporal LiDAR to Quantify Fertilization Effects on Stand Volume and Biomass in Late-Rotation Coastal Douglas-Fir Forests.[2]

Abstract

Forest fertilization is common in coastal British Columbia as a means to increase wood production and potentially enhance carbon sequestration. Generally, the effects of fertilization are determined by measuring sample plots pre- and post-treatment, resulting in fertilization effects being determined for a limited portion of the treatment area. Applications of remote sensing-based enhanced forest inventories have allowed for estimations to expand to the wider forested area. However, these applications have not focused on monitoring the effects of silvicultural treatments. The objective of this research was to examine if a multi-temporal application of the LiDAR area-based method can be used to detect the fertilization effects on volume, biomass, and height in a second growth Douglas-fir (*Pseudotsuga menziesii*) stand. The study area on Vancouver Island was fertilized in January 2007, and sample plots were established in 2011. LiDAR acquisitions were made in 2004, prior to fertilization, and in 2008, 2011, and 2016, covering both treated and untreated areas. A total of 29 paired LiDAR blocks, comprised of four 20 m resolution raster cells, were selected on either side of the fertilization boundary for analysis of the effects across several different stand types differing in the percentage of Douglas-fir, site index, and age. Random forest (RF) plot-level models were developed to estimate total stem volume and total stem biomass for each year of LiDAR acquisition using an area-based approach. Plot level results showed an increase in stem volume

[2] The following chapter has been published as:
Kelley, J., Trofymow, J.A., Metsaranta, J. M., Filipescu, C. N., & Bone, C. (2021). Use of multi-temporal LiDAR to quantify fertilization effects on stand volume and biomass in late-rotation coastal Douglas-fir forests. Forests, 12(517), 517. https://doi.org/10.3390/f12050517

by 13% fertilized over control from 2005 to 2011, which was similar to a 14% increase in above-ground carbon stocks estimated using a tree-ring stand reconstruction approach. Plot-level RF models showed R^2 values of 0.86 (volume) and 0.92 (biomass) with relative cross-validated root mean square errors of 12.5% (volume) and 11.9% (biomass). For both the sample plots and LiDAR blocks, statistical results indicated no significant differences in volume or biomass between treatments. However, significant differences in height increments were detected between treatments in LiDAR blocks. The results from this research highlight the promising potential for the use of enhanced forest inventory methods to rapidly expand the assessment of treatment effects beyond sample plots to the stand, block, or landscape level.

1. Introduction

Forest fertilization as a silvicultural practice has increased in recent decades due to its observed positive impacts on tree growth (Reid et al., 2017; Saarsalmi et al., 2001; Vejre et al., 2001; Albaugh et al., 2007). Forest fertilization is the process of applying a nutrient compound, such as nitrogen (N), over a forested area to address nutrient limitations with the aim of increasing tree growth and biomass in lower-quality sites, reducing stand rotation times in higher-quality sites (Brockley, 2007), and increasing clear stem wood production with late-rotation treatment. Fertilization is also appealing to policymakers and land managers as research has shown that it can significantly increase long-term carbon storage compared to other silvicultural treatments such as thinning (i.e., the removal of trees to allow for less competition for remaining trees) (Sullivan et al., 2020). As a result, fertilization is one of several management strategies recommended by the Intergovernmental Panel on Climate Change (IPCC), to help mitigate global climate change impacts (Nabuurs et al., 2007).

Through government compliance and private markets, incentives have been introduced to land managers to implement fertilization projects focused on increasing carbon stocks (White et al., 2018). These generally take the form of a carbon offset credit program where managers are provided with a financial incentive or an emissions allowance (Shyrock et al., 2014). However, these only occur for projects that can demonstrate an additional atmospheric benefit over a defined baseline scenario. Initial predictions of fertilization gains over the baseline scenario are estimated through the use of stand-level growth and yield models such as the Table Interpolation Program for Stand Yields of the Tree and Stand Simulator model (TIPSY/TASS) (Di Lucca et al., 2011), and SIMA (Routa et al., 2019), or carbon budget models such as the Carbon Budget Model of the Canadian Forest Sector (CBM-CFS3) (Kurz et al., 2009). These models estimate the increases in volume or biomass expected under fertilization based on the results of experiments conducted on a range of species mixtures and site conditions (Brockley, 2006; Omule et al., 2011; Prescott et al., 2013). Using site-specific information such as the species mixture, site index, and stem density, these models use experimental results to estimate the gains in volume (Province of British Columbia, 2018) or biomass (Kull et al., 2019) and model the fertilization impacts in the stand. However, despite their reliance on experimental results, these models cannot account for the variability of site-specific conditions in the modelled fertilization impacts (Jang et al., 2019). Thus, any projected increases over the baseline scenario require verification of the modelled atmospheric benefits to be eligible for the incentives (Richards & Huebner, 2012a).

The verification of a project's claims is a crucial part of the process, and the methods that are chosen to do so play a critical role in the level of accuracy achieved (Richards & Huebner, 2012b). Verification projects often rely on current research and methods while balancing the

desired accuracy with the project's overall cost. Ultimately, the reliability of the verification will depend on sampling strategy, the type of data collected, and the modelling or statistical methods used (Di Lallo et al., 2017). This is important to fertilization practices because research indicates that fertilization benefits are not consistent across all forest types (Shyrock et al., 2014), and the magnitude of fertilization effects can vary with environmental conditions and species mixtures (Reid et al., 2017).

Fertilization effects are usually monitored using fixed area plots located in treated and control areas, that are otherwise similar in stand characteristics (Filipescu et al., 2017; Harrington & Devine, 2011; Brix, 1993). Measurements such as species, diameter at breast height (DBH), and height are recorded for all trees within the plots before treatment and are repeated several years after treatment (Brockley, 2006; Omule et al., 2011; Negrave et al., 2007). Using these data, volume or biomass can be calculated in both periods using allometric equations, and thus the treatment impacts on volume or biomass increments can be determined (Omule et al., 2011). Sampling designs can vary (Brockley 2006; Filipescu et al., 2017) depending on the scope of the analysis and are often limited due to available resources. Sample plot methods provide a snapshot of the forest conditions at each location for a single point in time. Having samples from these plots in multiple years allows for comparison of the periodic changes; however, they lack the temporal resolution to make annual comparisons.

To increase the temporal resolution of sample plot methods, the annual estimates of growth can be acquired using tree-ring stand reconstruction approaches (Metsaranta & Lieffers, 2009). These approaches use modelling methods to determine annual growth increments from the increment cores of all trees, live and dead, within the sample plots (Metsaranta et al., 2018). The obtained growth increments can then be used to compare the annual treatment differences

for all years prior to sampling. While stand reconstruction methods increase the temporal resolution of observations, the spatial coverage is still limited in the sampling design of plots. Research has shown that when estimating forest attributes such as carbon stocks using sample plots, the accuracy of estimates is highly sensitive to conditions such as the local disturbance history (Fisher et al., 2008) and can result in the overestimation of changes due to location bias of the sample plots (Klesse et al., 2018). Therefore, the level of accuracy for the wider area of analysis is directly linked to the number and location of sampling sites.

A method that can be applied for monitoring forests over an entire stand is tracking the carbon exchanges with Eddy covariance flux towers (Jassal et al., 2010). These towers are a common method to monitor the net exchange of carbon dioxide between forest canopies and the atmosphere and use cumulative high-frequency measurements of wind speed, direction, light, and CO_2 concentration from meteorological equipment to determine net ecosystem carbon production (NEP) (Coursolle et al., 2012). While these towers can monitor NEP over time for larger areas than plots, the footprint of the contributing canopy area can be complex to determine and interpret (Ferster et al., 2015). Additionally, analysis conducted using flux towers lacks the ability to compare fertilization treatments against controls and thus can only compare the pre- and post-fertilization periods of the treated stand (Jassal et al., 2010). While both the flux tower and sample plot methods offer advantages for forest monitoring, in the context of carbon project verification, the ability to monitor effects over a larger operational area with a sample plot design's versatility would be ideal.

Advancements in remote sensing technologies can leverage observations made from sample plots to build models that are applied to the broader area, providing estimates of attributes for the entire area of data coverage (Næsset, 2002). One of the leading modelling

methods, called the Area-Based (AB) approach, utilizes a suite of predictor metrics calculated from LiDAR data to develop a statistical model at the plot level for a forest attribute of interest, such as volume or biomass (Woods et al., 2008). This statistical model can then be applied to similar stand types across the broader area for which there is observed data collected (Woods et al., 2011). The advantage of this method is that it relies on collecting the same sample plot data that is usually collected in fertilization studies but allows for evaluating effects across a broader range of locations or even entire stands. Research using the AB approach has shown the ability to estimate variables at the stand level, such as volume (Næsset, 2002) and biomass (Bouvier, et al., 2015), with a high degree of accuracy while also showing the local within-stand variability of the estimates. In general applications of the AB approach, sample plots are established in the region of interest while sampling across the range of stand structures, primarily species mixtures and site qualities, to create a generalized model (Penner et al., 2013). If applying an established AB model or sample plot network to detect fertilization impacts, if the treatment is not explicitly captured in the sampling design, the analysis may not capture the fertilization impacts. While the collection of LiDAR data and the use of AB-style forest inventories are becoming more common in forest management, to our knowledge, these area-based methods have not yet been used in a multi-temporal approach to evaluate the impacts of fertilization.

The objective of this research was to examine if a multi-temporal application of the LiDAR area-based method can be used to detect the fertilization effects on height, volume, and biomass, in a second-growth Douglas-fir (*Pseudotsuga menziesii*) stand. Area-based method results for one, four, and nine years post-fertilization were compared against observed sample plot results, as well as results from tree-ring stand reconstruction and carbon budget model predictions.

2. Materials and Methods

2.1. Study Area

The research study area was located in the Oyster River drainage northwest of Courtenay on eastern Vancouver Island, British Columbia, Canada (Figure 2.1). The study area, located within the dry Coastal Western Hemlock biogeoclimatic subzone (Pojar et al., 1991), was part of the Fluxnet Canada research network's coastal BC station (Coursolle et al., 2012). The second-growth stands in the study area were mostly composed of Douglas-fir (*Pseudotsuga menziesii*) with components of western hemlock (*Tsuga heterophylla*), western redcedar (*Thuja plicata*), and red alder (*Alnus rubra*) (Trofymow et al., 2014). The planting of Douglas-fir seedlings in 1949 established the main stand (DF49), with other species coming from natural regeneration after harvesting (1937, 1938, and 1943) and broadcast burning operations (1939 and 1943) (Trofymow et al., 2008). The 2004 stand density index was 998 stems ha^{-1} and the stand had an estimated site index of 34 m (Filipescu et al., 2017). In January 2007, a late rotation fertilization treatment was applied aerially to a central portion of the study area (Figure 2.1) at a rate of 200 kg urea N ha^{-1}, a typical operational practice in this region (Filipescu et al., 2017).

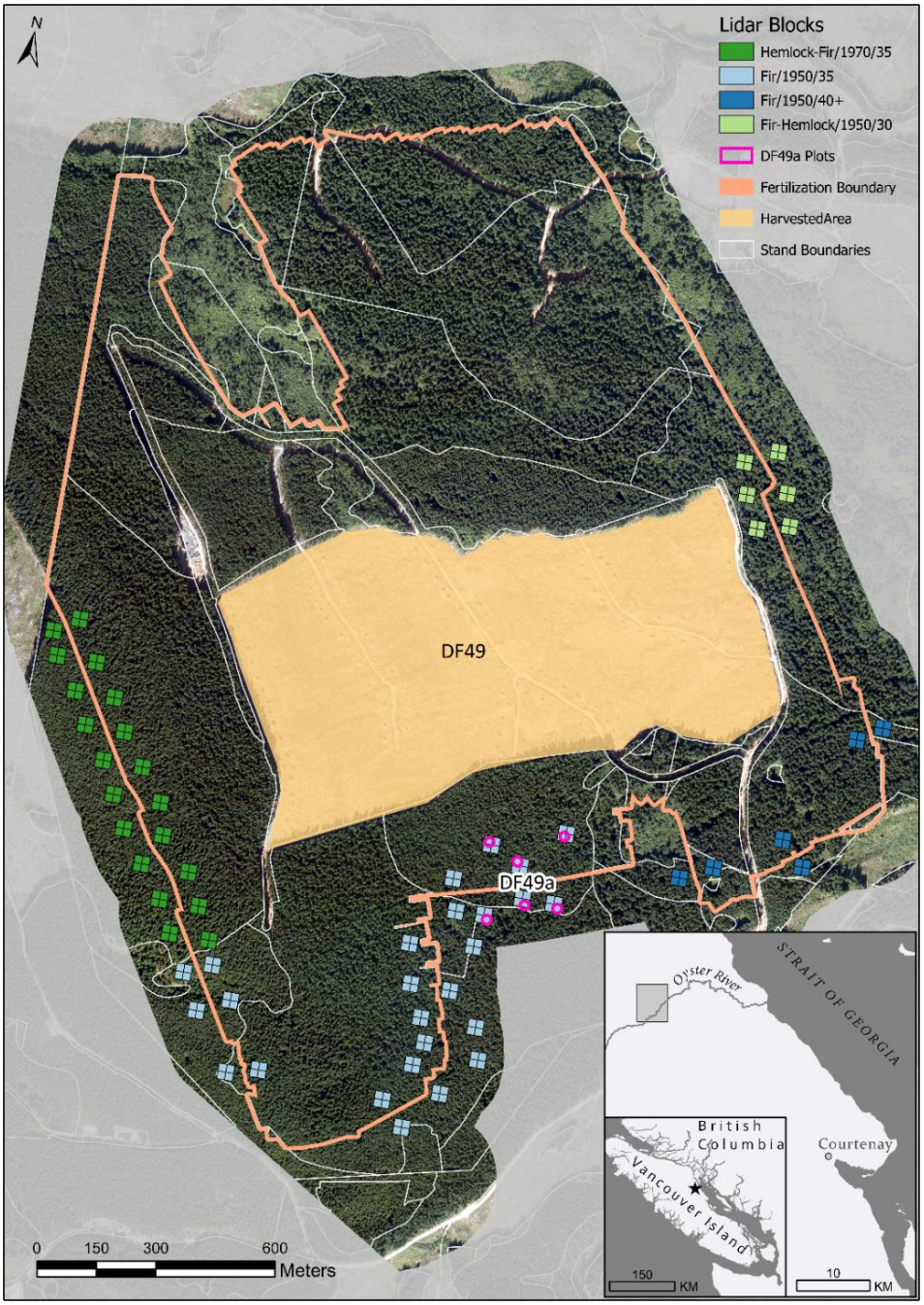

Figure 2.1. Study area map showing the fertilization area (orange lines); DF49a fertilized and control sample plots (pink); and LiDAR blocks for forest stand analysis units of Hemlock-Fir (dark green), Fir (Site Index 30) (light blue); Fir (Sight Index 40+) (dark blue); and Fir-Hemlock (light green). The main stand, DF49, was the location of flux towers and plots established in 2002 and measured until 2011, when the stand was cut. White lines show the 2010 forest stand polygon boundaries.

2.2. Plot Establishment and Measurement

In 2011, three pairs of control and fertilized 0.04 ha circular plots (11.28 m radius) were established in a forest area (DF49a) on either side of the 2007 fertilization boundary (Figure 2.1). Species and DBH were recorded for all trees above 9.0 cm DBH, heights measured for a subset of these trees, and a sample of 3 crop trees in each plot felled and stem disks cut to measure ring widths and wood properties (Filipescu et al., 2017). These tree measurements were used to calculate stem volume using equations from Kozak (1994) and biomass using equations from Canada's National Forest Inventory (https://nfi.nfis.org/en/biomass_calc, accessed on 15 August 2020). In 2017, all six plots were remeasured to record species, DBH, height, and other attributes following Canada's National Forest Inventory (National Forest Inventory, 2008) sampling guidelines. Since several crop trees were felled in 2011, there were large decreases in plot-level volume and biomass between 2011 and 2017. To account for this anomaly through the whole time series, the values of these felled trees were removed from the plot-level volume and biomass totals in each year and were only included for a separate plot-level analysis of volume and biomass increments.

2.3. Tree-Ring Data Collection and Measurement

In 2013, all trees in the plots were increment cored, and tree rings analyzed to convert yearly ring width into DBH estimates for each tree's lifespan following procedures of Metsaranta et al. (2018). The estimated DBH values were then used with the Chapman-Richards (CR) equation to estimate tree heights. The CR equation is a common method for estimating tree heights from diameter measurements (Temesgen et al., 2004), and parameters were estimated from the pre-harvest plot data from the nearby DF49 stand (Metsaranta et al., 2018). For each tree's lifespan, merchantable volume was estimated from the DBH and height using regional taper equations

from Kozak (1994). Tree volumes were then summed to the plot level and used to develop merchantable volume (m^3 ha^{-1} $year^{-1}$) over age yield curves (Metsaranta et al., 2018).

2.4. Biomass Increments Using Tree-Ring Volume Reconstructions and CBM-CFS3

The developed tree-ring yield curves were used as inputs to the CBM-CFS3 which used them to estimate above- and below-ground biomass dynamics and inputs to detrital and soil carbon pools (Kurz et al., 2009). The model was run for each of the plots using the ring curves from 1990 through 2011. The model was also run in a default mode using regional yield curves (Di Lucca & Goudie, 2011) for each plot's forest stand type and site index, without or with the model's fertilization disturbance effect (Kull et al., 2019) included. Annual above-ground biomass carbon increments were output from 2001 to 2011, which covered five years pre- and post-fertilization, similar to the periods examined by Filipescu et al. (2017). Comparisons of control and fertilized plot increments were made using two-way analysis of variance (ANOVA) for each of the pre- and post-fertilization periods.

2.5. LiDAR Data Acquisition

LiDAR acquisitions and remote sensing data for the area were obtained in 2004 (Ferster et al., 2009), 2008 (Hilker et al., 2011), 2011 (Trofymow et al., 2014), and 2016 (S. McLennan—Timberwest, personal communication, 8 December 2017) with various point densities and scan angle parameters. LiDAR points from each year were classified as ground or non-ground by the vendors using various versions of the Terrascan software (Terrasolid, Helsinki, Finland). Quality control to remove any duplicated points, air hits, or other errors was done on all point clouds through manual inspection and use of the lidR package in R (Roussel et al., 2020).

2.6. Sample Plot Data for Area-Based Models

Matching the same years of LiDAR acquisition, the tree-ring-derived DBH and height estimates described above were subset for each tree into the 2004, 2008, and 2011 seasons. To represent the 2016 growing season, the measured attributes from the 2017 sampling were used. Individual tree volumes were then estimated using these data with the regional taper equations developed by Kozak (1994), similar to Metsaranta et al. (2018). For each tree, the proportion that was considered as the stump, main stem, and treetop was determined by jurisdictional timber criteria. For these years, the British Columbia merchantability limits of a 30 cm stump height and a 10 cm top diameter were used (Timber Pricing Branch, 2011). Each tree's total stem volume consisted only of the tree's stem portions (i.e., those parts of the tree not including tops, stumps, and branches). Stem biomass was calculated using tree species, DBH, and height estimates with the online National Forest Inventory individual tree biomass calculator (https://nfi.nfis.org/en/biomass_calc, accessed on 15 August 2020) and included stem wood values only and not branches, bark, or foliage.

Individual tree volume and biomass within each plot was summed, and plot-level volume (m^3 ha^{-1}) and biomass (Mg ha^{-1}) were calculated for two groups. The first group (all trees) consisted of volume and biomass estimates from all trees within the plots in 2004, 2008, and 2011 and was only used in a plot-level analysis of treatment effects. The second group (subset trees) excluded estimates from the 2011 felled trees through all years and was used further to train the area-based models. Cumulative volume and biomass increments from 2004 (2008–2004; 2011–2004; 2016–2004) were calculated for each plot in addition to the periodic annual increments (2008–2004/4; 2011–2008/3; 2016–2011/5). A mixed-effects model with a fixed main effect of treatment and a random effect of plot (Prescott et al., 2019) was used to determine

if there were significant differences in volume or biomass cumulative or periodic increments in 2008, 2011, or 2016.

2.7. LiDAR Data Processing

As the LiDAR data was collected over several years by various vendors, there were structural differences between the acquisitions relating to point densities and scan angle ranges, with the 2016 data having almost ten times the average point density than that of the 2004 data. To address these differences in point cloud structure, all point clouds were thinned to a maximum point density of 3 points m^{-2}, and scan angles were limited to +/- 20°. These limits were chosen based on the most constraining 2004 data. Thinning was accomplished using a moving window of 25 m^2, in which points were randomly removed from the local window until the target density was reached, generating more consistent thinning results over areas of scan line overlap compared to using a global thinning target (Roussel et al., 2020). For the excluded trees removed from the field data, stem mapping information was used to geo-reference the stem locations from the plot center. Using an individual tree segmentation method (Dalponte & Coomes, 2016), LiDAR points belonging to removed trees were identified in the 2004, 2008, and 2011 data and had their heights above ground set to 0, simulating their exclusion.

Multiple LiDAR-based predictor metrics were generated over the entire study area using the thinned point clouds for each year and a 20 m resolution raster. This resolution of raster was chosen as it has a comparable ground area as the sample plots (0.04 ha). Common predictor metrics used for estimating volume and biomass at-tributes include a combination of height, density, canopy cover, and statistical metrics (White et al., 2017). In total, 47 point cloud metrics were generated using the lidR package in R (Roussel et al., 2020) (Table A1 in Appendix A).

Additionally, point clouds were clipped to the sample plots' extent, and the same predictor metrics were generated at the plot level for model training (White et al., 2017).

Next, a series of paired "LiDAR blocks" was created to examine fertilization effects over the wider forested area around the fertilization boundary (Figure 2.2). These blocks were created with a 20 m × 20 m fishnet grid aligned with the LiDAR metrics. This grid was intersected with forest inventory polygons and organized into analysis units (AUs) based on dominant species, stand age, and site index (Table 1.1). Blocks of four cells were created on either side of the fertilization boundary with a 20 m buffer on the boundary's control side and a 10 m buffer on the fertilized side (Figure 2.2). A larger buffer was used on the control side of the boundary to account for the edge effects of the treatment boundary. Pairs of blocks were selected if they shared a similar AU, and the set of blocks in the DF49a area were adjusted to ensure they contained the sample plots (Figure 2.2). Ensuring the pairs were representative of the same area, the coefficient of variation (CoV) was calculated using the 95th percentile of LiDAR height, the mean LiDAR height, and the LiDAR point density for the four cells in a block as well as the eight cells that make up a pair. Groups of cells or block pairs with a CoV greater than or equal to 20% were removed. Additionally, pairs that belonged to AUs with less than three total pairs were also removed. In total, 29 paired blocks were selected across the four AUs (Table 2.1).

Table 2.1. Composition and number of final selected LiDAR-block pairs for each analysis unit.

AU	Leading Species	Established	Site Index	Number of Paired Blocks
146	Douglas-fir	1940–1949	30–35	13
148	Douglas-fir	1940–1949	40+	3
445	Fir/Hemlock	1940–1949	25–30	3
526	Hemlock/Fir	1960–1969	30–35	10

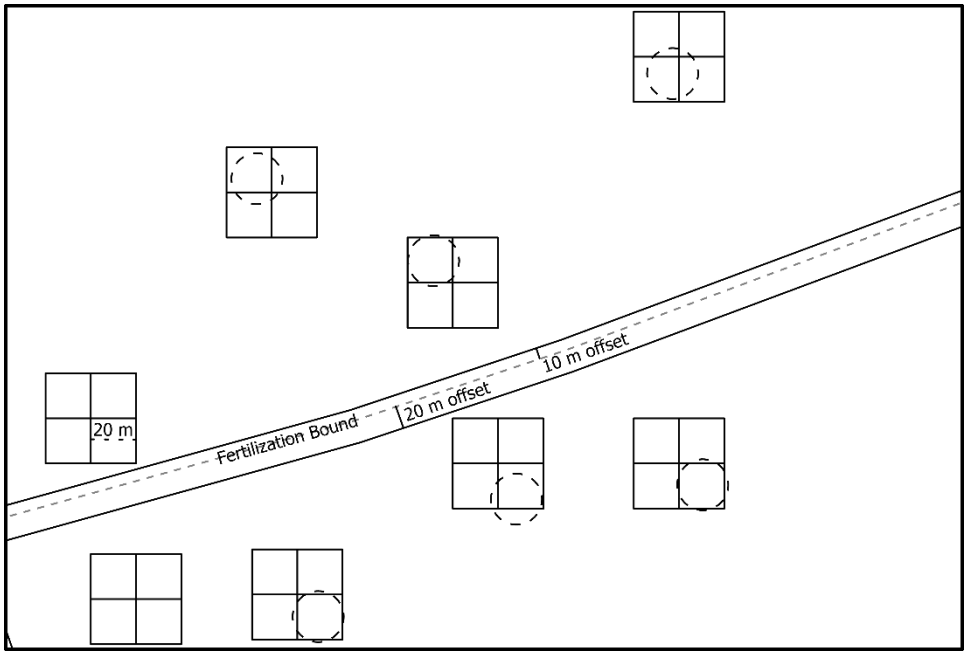

Figure 2.2. LiDAR paired block design in the DF49a area showing the fertilization boundary, buffered offsets, and sample plots' location within cells (dashed circles).

2.8. Area-Based Modelling

Non-parametric random forest (RF) regression models were estimated using the plot-level volume and biomass with the LiDAR predictor metrics. A Boruta variable selection method was employed to reduce the number of metrics used in model fitting. The Boruta method for feature selection is popularly used with machine learning applications in genetics, health sciences, and other disciplines where the number of predictor metrics is often much larger than the number of observations (Acharjee et al., 2020; Velusamy et al., 2020; Chiteka et al., 2019). This method copies each metric and randomly permutes the data creating a set of noise metrics. The combined set of original and noise metrics are then used to fit many RF models where each metric's importance score is recorded. Metrics with an overall importance distribution significantly greater than the highest scoring noise variable make up the final selected metrics (Kursa et al.,

2010). Next, with the subset of metrics selected, RF models were trained to estimate total stem volume and total stem biomass using the field data in each year. The RF models' training was done using the caret and random forest packages in R (Kuhn et al., 2008; Liaw et al., 2002). A five-times repeated 10-fold cross-validation method was used while fitting 1000 regression trees (White et al., 2015). This training method resulted in the removal of ten observations for each of the five repetitions resulting in 50 independent observations to assess model performance. Model performance was assessed using the independent observations and calculating the absolute and relative root mean square error (RMSE) and bias as described by White et al. (2015).

The RF model for both the volume and biomass attributes was then applied across the study area using the suite of raster-based metrics in order to produce estimation surfaces for each year. Each year's estimated volume and biomass values were extracted from the surfaces of each cell of the LiDAR blocks, and block-level estimates for each year were calculated as the average value of the four cells in each treatment. As an additional check on model performance, the 95th percentile of LiDAR height in each cell was also extracted for increment analysis. Cumulative and periodic annual increments for volume, biomass, and height were calculated for the block-level estimates, similar to the sample plots. The block-level increments were used in mixed-effects models to test the significance of the fixed treatment effect with a LiDAR block's random effect. Tests were done each year for increments for AUs individually and combined across all AUs. Results from these tests indicated if the treatments in the LiDAR blocks produced a similar fertilization effect over controls as in the sample plots. The similarity of increment magnitudes between the sample plots and LiDAR blocks was assessed through visual comparison.

3. Results

3.1. Sample Plots

In 2004, prior to the fertilization, average volumes in control plots (all trees) were slightly lower than in fertilized plots (Table 2.2). Cumulative volume increments for both the all trees and subset trees groups were not significantly different between treatments in all years (p-values > 0.3, Table A2). Weighted by their 2004 volumes, control plots (subset trees) had an average cumulative increment from the 2004 volume ratio of 0.076, 0.175, and 0.320 by 2008, 2011, and 2016, respectively. In the fertilized plots, the weighted average ratio was 0.076, 0.181, and 0.303 by 2008, 2011, and 2016, respectively (Table 2.2). By 2011 the un-weighted average cumulative volume increment in fertilized plots was 13% greater than in control plots. However, by 2016 the un-weighted average volume increment was only 3% greater in fertilized plots than in control plots (Table 2). Periodic annual volume increments were not significantly different between treatments in any period (p-values > 0.3, Table A3). For the 2009–2011 period, the fertilized plots saw an average increase of 17.2 $m^3\ ha^{-1}\ yr^{-1}$ compared to an increase in control plots of 14.8 $m^3\ ha^{-1}\ yr^{-1}$ (Table A4). In the 2012–2016 period, both treatments' overall rate decreased, with control plots having an average rate of 13.0 $m^3\ ha^{-1}\ yr^{-1}$ compared to a rate of 11.9 $m^3\ ha^{-1}\ yr^{-1}$ for the same period in the fertilized plots (Table A4). The impacts of 2011 tree felling in the plots can be seen in the cumulative increments for all trees, where the 2011 values are on average 96.6 $m^3\ ha^{-1}$ greater than the 2004 values, and the 2016 values on average are only 34.55 $m^3\ ha^{-1}$ greater than the 2004 values (Table 2.2).

Table 2.2. Plot level stem volumes ($m^3\,ha^{-1}$), cumulative volume increments, and control (C) or fertilized (F) treatment averages for the subset trees in the plots, as well as all trees.

		Subset Trees				All Trees			
Plot	Treat	2004 Volume	2005–2008 Inc	2005–2011 Inc	2005–2016 Inc	2004 Volume	2005–2008 Inc	2005–2011 Inc	2005–2016 Inc
1.1	C	516.8	34.8	82.2	173.1	651.1	40.0	91.2	38.8
8.3	C	338.8	26.4	58.6	139.7	446.5	34.5	73.4	31.9
10.2	C	491.1	41.1	94.3	117.8	580.6	48.3	107.4	28.4
Average (SE)	C	448.9 (55.6)	34.1 (4.2)	78.4 (10.5)	143.5 (16.1)	559.4 (60.2)	40.9 (4.0)	90.7 (9.8)	33.0 (3.0)
4.1	F	520.0	34.2	81.9	146.3	588.9	41.8	95.4	77.4
5.1	F	461.9	39.1	91.5	176.4	576.1	46.0	104.0	62.2
6.1	F	487.6	38.4	93.4	122.4	641.3	46.4	108.2	−31.3
Average (SE)	F	489.9 (16.8)	37.2 (1.5)	88.9 (3.6)	148.4 (15.6)	602.1 (19.9)	44.7 (1.5)	102.5 (3.8)	36.1 (34.0)

The biomass differences between treatment plots in 2004 were smaller than the volume differences. However, the control plots (all trees) had higher biomass values than the fertilized plots (Table 2.3). Similar to the plot-level volume increments, differences in cumulative biomass increments for both the all trees and subset trees groups between treatments were non-significant in all years (p-values > 0.3, Table A2). Fertilized plots continuously saw higher biomass gains with weighted ratios of 0.094, 0.229, and 0.372 in 2008, 2011, and 2016, respectively. In the same periods, control plots saw weighted ratios of 0.092, 0.216, and 0.293 (Table 2.3), respectively. By 2011 the un-weighted average cumulative biomass increment in fertilized plots was only 0.3% greater than in control plots. However, by 2016 the un-weighted average biomass increment was 20% greater in fertilized plots than in control plots (Table 2.3). For the period

between 2005 and 2008, the periodic annual biomass increment in control plots was 3.0 Mg ha^{-1} yr^{-1} compared to an average rate of 2.8 Mg ha^{-1} yr^{-1} over the same period in fertilized plots (Table A5). For the subsequent period from 2009 to 2011, rates in fertilized plots, 5.5 Mg ha^{-1} yr^{-1}, were greater than the 5.3 Mg ha^{-1} yr^{-1} in control plots. For the final period between 2012 and 2016, the average rate in the control plots (2.0 Mg ha^{-1} yr^{-1}) was higher than the average rate in fertilized plots (3.4 Mg ha^{-1} yr^{-1}) (Table A5). However, similar to the volume periodic annual increments, there were no significant differences in rates between treatments over any period (p-values > 0.3, Table A3).

Table 2.3. Plot level stem biomass (Mg ha^{-1}), cumulative biomass increments, and control (C) or fertilized (F) treatment averages for the subset trees in the plots, as well as all trees.

		Subset Trees				**All Trees**			
Plot	**Treat**	**2004 Biomass**	**2005–2008 Inc**	**2005–2011 Inc**	**2005–2016 Inc**	**2004 Biomass**	**2005–2008 Inc**	**2005–2011 Inc**	**2005–2016 Inc**
1.1	C	149.7	13.2	31.5	46.8	189.2	15.4	35.4	7.2
8.3	C	94.0	8.7	19.4	33.6	125.3	11.7	25.1	2.3
10.2	C	139.7	13.7	31.9	31.8	164.6	16.3	36.9	6.9
Average (SE)	C	127.8 (17.2)	11.8 (1.6)	27.6 (4.1)	37.4 (4.7)	159.7 (18.6)	14.5 (1.4)	32.4 (3.7)	5.5 (1.6)
4.1	F	128.9	11.1	26.8	46.5	146.2	13.3	31.0	29.1
5.1	F	108.9	11.0	26.3	51.2	136.1	12.9	29.9	24.0
6.1	F	124.4	11.9	29.9	37.0	161.6	14.4	34.4	−0.2
Average (SE)	F	120.7 (6.1)	11.3 (0.3)	27.7 (1.1)	44.9 (4.2)	148.0 (7.4)	13.5 (0.4)	31.7 (1.4)	17.6 (9.0)

3.2. CBM-CFS3 Plot Biomass Increments Using Tree-Ring and Default Growth Curves

Annual biomass carbon increments (g C m^{-2} yr^{-1}) using tree-ring curves varied more among control than treated plots across the 11-year period (Figure 2.3). Prior to fertilization, annual biomass carbon increment in control and treated plots increased over time, and while the 5-year treated (243 SE 8)[3] and control (270 SE 10)[2] plot means were significantly different (p = 0.023)[2], the 3-year means before fertilization were not (p = 0.173)[2]. Post-fertilization biomass increments in treated plots in-creased above control plots, with the 5-year means being significantly (p = 0.0002)[2] greater in treated (326 SE 6)[2] than control plots (271 SE 11)[2], a 20%[2] increase. Cumulative biomass carbon increments (Mg C ha^{-1}) from 2004 to 2008 and 2004 to 2011 were slightly greater in treated (11.8 SD 0.1, 21.8 SD 0.1) than control (11.0 SD 0.6, 19.2 SD 1.4) plots. Annual biomass carbon increments using default yield curves pre-fertilization ranged from 320 to 400 and were higher in plots to be fertilized (456 F) than control plots (123 C) (Figure 2.3). Post-fertilization, the model fertilizer effect predicted a 22% increase in 2007 and for the entire five-year period (Figure 2.3).

3.3. Area-Based Models

The Boruta variable selection method results are shown in Table 2.4. The table provides the metrics that had higher importance scores than the noise variables for each model. The method took 3512 iterations for the volume model and resulted in the selection of six LiDAR metrics, which consisted of both height and cover metrics (Table 2.4). The Boruta method for the biomass model ran for the set maximum of 6000 iterations and selected eleven total metrics. These metrics included similar height and cover metrics as the volume model and included several statistical metrics (Table 2.4).

[3] Values have been corrected since publication.

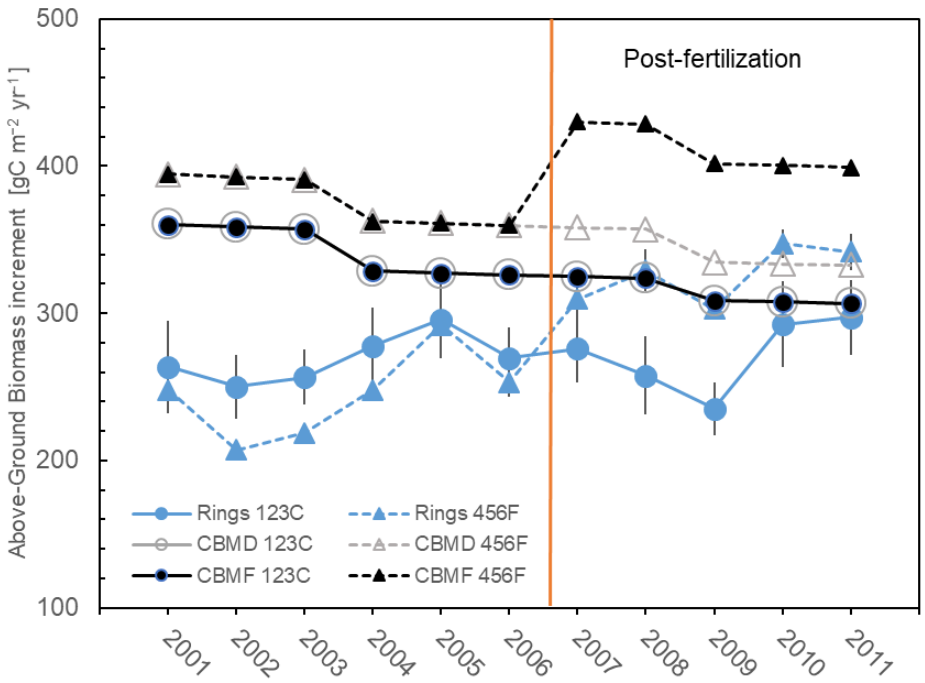

Figure 2.3. Annual above-ground biomass carbon increments from the CBM-CFS3 model for control (123C solid line, circles) and fertilized (456F, dashed line triangle) plots using yield curves derived from plot tree-ring data (Rings), default stand type yield curves without a fertilizer effect (CBMD gray lines, open symbols), or default yield curves with a fertilizer effect (CBMF black line, closed symbols). Rings data show plot mean with one standard error.

The fitted random forest (RF) volume model produced an R^2 value of 0.86, with a cross-validated RMSE of 67.33 m^3 ha^{-1} (12.55%) and a bias of 4.73 m^3 ha^{-1} (0.88%). Comparing the observed stem volumes to the modelled stem volumes showed a slight variable bias with no apparent patterns, except for the continual overestimating of volume in plot 8.3 (Figure 2.4A). The fitted biomass RF model also reported a high R^2 value of 0.92 with a cross-validated RMSE of 17.15 Mg ha^{-1} (11.91%) and a bias of 0.42 Mg ha^{-1} (0.29%). Similar to the volume model, the biomass model showed some variable bias. However, the consistent over-predictions in plot 8.3 were not as large as in the volume model (Figure 2.4B).

Table 2.4. LiDAR metrics selected and relative importance ranking for the volume (V, Vol) or biomass (B, Bio) models using Boruta variable selection method.

Predictor Class	Description	Vol Rank	Bio Rank
Canopy Cover	$\frac{All\ Returns\ Above\ Mean\ ht}{total\ 1st\ returns} * 100$	3	5
Canopy Cover	$\frac{1st\ Returns\ Above\ 2\ \mathrm{m}}{total\ 1st\ returns} * 100$	1	1
Canopy Cover	$\frac{1st\ Returns\ Above\ Mean\ ht}{total\ 1st\ returns} * 100$	6	-
Canopy Cover	$\frac{All\ Returns\ Above\ 2\ \mathrm{m}}{total\ all\ returns} * 100$	4	3
Canopy Cover	$\frac{All\ Returns\ Above\ 2\ \mathrm{m}}{total\ 1st\ returns} * 100$	2	2
Statistical	Average absolute deviation (AD) of ht	-	7
Statistical	Interquartile distance	-	9
Statistical	Second L moment	-	12
Statistical	Median of the AD from the overall mode	-	6
Statistical	Mode ht	-	10
Density	Cumulative percentage of returns in the Xth decile Volume—none; B = 6,7	-	7th: 4 6th: 11
Height	Xth percentile of height distribution V = 10^{h}; B = 95	5	8

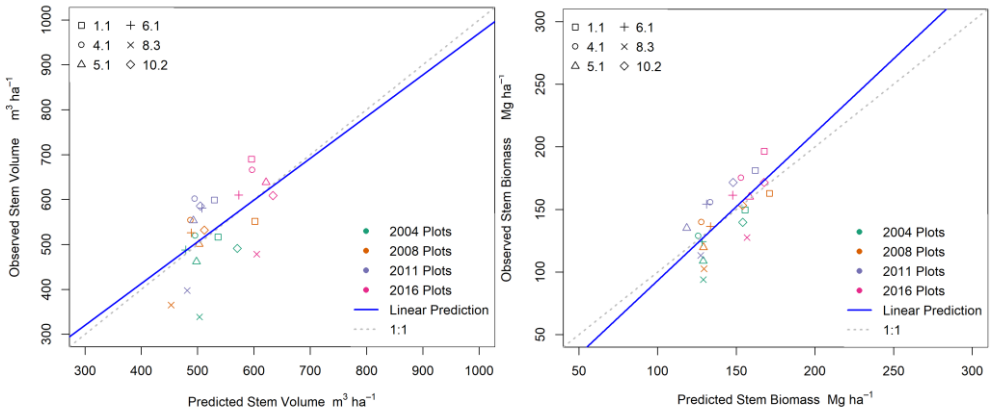

Figure 2.4. Observed plot level vs. RF predicted volume (A) and biomass (B) values in 2004 (green), 2008 (orange), 2011 (purple), and 2016 (pink).

Across all analysis units (AUs), the modelled 2004 volumes in control blocks were higher on average (582.2 m^3 ha^{-1}, SE 2.1) than in fertilized blocks (581.6 m^3 ha^{-1}, SE 3.3). Cumulative increments from 2004 averaged across all AUs are shown in Figure 2.5A, and individual AU results are shown in Figure A1. Similar to the sample plots, across all AUs, there were no significant differences in volume increments in any year (p-values > 0.1, Table A6). Relative to their 2004 volumes, control blocks saw an average increase of 0.5, 0.9, and 6.7 percent by 2008, 2011, and 2016, respectively. During the same time periods, fertilized blocks saw average increases of 0.7, 1.7, and 8.3 percent over their 2004 values. For AU 445, the 2005–2016 increment in fertilized blocks (44.1 m^3 ha^{-1}, SE 1.1) was significantly higher (p = 0.03) than in controls (38.9 m^3 ha^{-1}, SE 0.5). However, the number of pairs in that AU was low (3) (Figure A1E,F, Table A7). Periodic annual increments averaged across all AUs were also not significantly different between treatment blocks during any period (p-values > 0.2, Table A8). However, for the AU that contained the sample plots (AU 146) for the period between 2009 and

2011, the fertilized blocks (2.6 m^3 ha^{-1} yr^{-1}) increased at a significantly greater ($p = 0.03$) rate than in the control blocks (−0.7 m^3 ha^{-1} yr^{-1}) (Table A9).

Biomass model results in 2004 showed fertilized blocks having higher values (156.5 Mg ha^{-1}, SE 1.4) on average compared to control blocks (154.4 Mg ha^{-1}, SE 0.7) across all AUs. Relative to their 2004 biomass values, control blocks saw an average increase of 2.2, 1.8, and 5.2 percent by 2008, 2011, and 2016, respectively (Figure 2.5B). During the same time periods, fertilized blocks saw average increases of 2.0, 1.9, and 5.2 percent over their 2004 values (Figure 2.5B). Similar to the volume results, there were no significant differences between treatments when increments were averaged across all AUs (Tables A6 and A8), although the same individual AUs showed significant treatment differences in cumulative biomass increment (AU 445, Table A7) and periodic annual biomass increment (AU146, Table A8).

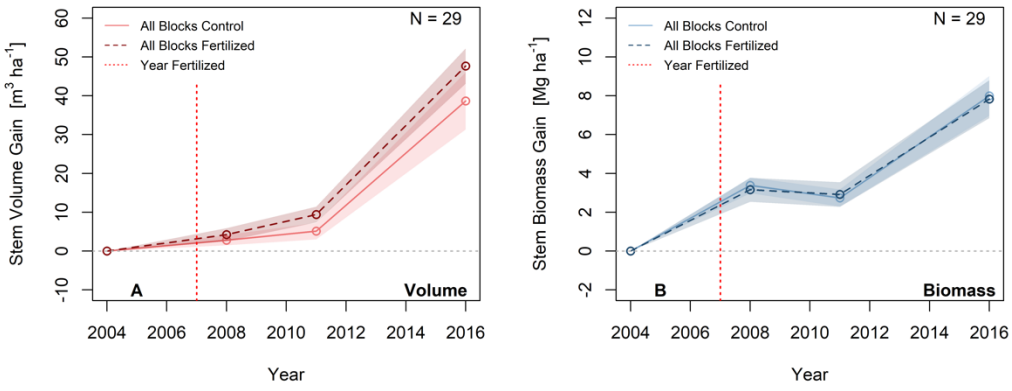

Figure 2.5. LiDAR block-level average (line) and standard error (shadow) of stem volume (A) and biomass (B) cumulative increments (gain) for control blocks (solid) and fertilized blocks (dashed).

In 2004 the average 95th percentile of LiDAR height was 31.3 m (SE 0.7) in the control blocks and 31.6 m (SE 0.6) in the fertilized blocks. Over the time series, the average cumulative height increments in fertilized blocks increased by 6.1% (SE 0.1), 8.3% (SE 0.2), and 12.6% (SE 0.3) over their 2004 heights by 2008, 2011, and 2016, respectively (Figure 2.6). During the same time periods, the average cumulative height increment in control plots increased by 5.9% (SE 0.1), 7.7% (SE 0.2), and 11.4% (SE 0.3) over their 2004 heights (Figure 2.6). Neither the average cumulative increment nor the average periodic annual increment across all AUs was significantly different ($p = 0.08$) between treatments by 2008 (Table A10). However, by 2011 the average cumulative height increment (2.61 m, SE 0.07) in fertilized blocks was significantly higher ($p = 0.02$) than in controls (2.39 m, SE 0.06), a 9% gain. Continuing this trend, by 2016, the average cumulative height increment (3.97 m SE 0.08) in fertilized blocks was significantly higher ($p = 0.02$) than in controls (3.56 m SE 0.06), for a 12% gain. Similar to the rates between 2005 and 2008, the average periodic annual increment between 2009 and 2011 was not significantly different ($p = 0.05$) between treatment blocks; however, for the period between 2012 and 2016, the rate in fertilized blocks (0.27 m yr^{-1}, SE 0.01) was significantly higher ($p = 0.02$) than in the control blocks (0.23 m yr^{-1}, SE 0.01). Height increment results for individual AUs can be seen in Figure A2 and Table A11.

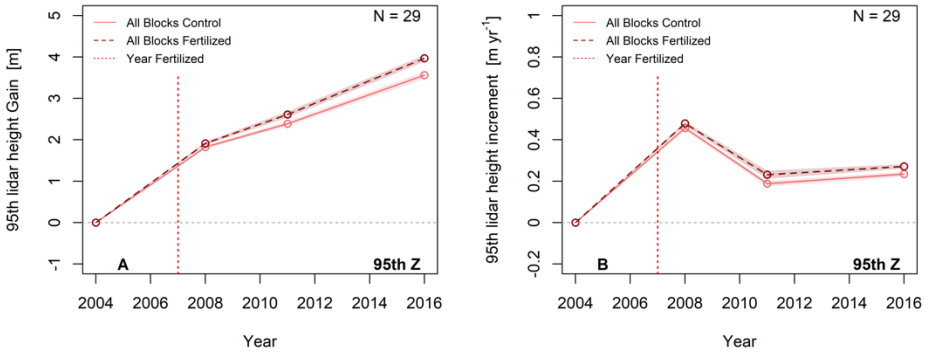

Figure 2.6. LiDAR block-level average (line) and standard error (shadow) of 95th percentile of LiDAR heights (A) and height periodic annual increments (B) for control blocks (solid) and fertilized blocks (dashed).

4. Discussion

This study investigated if area-based (AB) methods could be used with multi-temporal LiDAR data to detect fertilization effects across treated stands. Overall, the results show promise for LiDAR AB methods to be used to detect treatment impacts on stand volume, biomass, and height.

4.1. Method Comparisons

In the sample plots, the exclusion of felled trees appeared to have minimal impact on the analysis of treatment effects, as the all trees group showed from 2005 to 2011 that fertilized plots had an average un-weighted cumulative volume increment that was 13% greater than in control plots, which was similar to those seen in the subset trees group (Table 2.5). Weighted comparisons can be seen in Table A12. The differences between treatments had more variation in the biomass values whereby 2011, the subset trees group showed the fertilized cumulative biomass increments being less than the controls (Table 2.5). However, the differences between treatments were non-significant. Interestingly, CBM-CFS3 estimates using the tree-ring stand reconstruction approach showed that between 2005 and 2011, fertilized plots saw an increase in

above-ground biomass (AGB) carbon stocks, compared to controls, that was more like the plot volume results than biomass values (Table 2.5). This difference in relative biomass increase suggests there may be differences between the biomass equations used in CBM-CFS3 and those used in the NFI online biomass calculator, or this could be due to the differences between AGB and stem wood biomass.

Plot-level periodic annual volume increments (subset trees) between 2005 and 2008 were 9% greater in fertilized over control plots, which increased to 16% greater in fertilized over control plots between 2009 and 2011; however, these differences were not significant (Tables A4 and 8). When examining the felled crop trees, Filipescu et al. (2017) found that in fertilized plots, the volume 5-year average annual increment post-fertilization (2007–2011) was significantly greater than the average annual increment in control plots (Table 2.5). Average annual increments in AGB carbon from the stand reconstruction approach were similar, but slightly lower for the same post-treatment period as Filipescu et al. (2017) (Table 2.5). For the plot-level biomass, periodic annual increments (subset trees) between 2005 and 2008 were −7% less in fertilized over control plots, which increased to 4% greater in fertilized over control plots between 2009 and 2011; however, these differences were not significant (Tables A5 and 8).

Results from a flux tower in the main DF49 stand indicated that net ecosystem production (NEP) ranged from 268 to 410 (g C m^{-2} yr^{-1}) from 1998 to 2006 due to interannual variability in weather (Jassal et al., 2010). For the 4-year post-fertilization period, the mean NEP from 2007 to 2010 (561 SD 38) increased by 64% compared to NEP for the 4-year pre-fertilization period, 2003–2006 (341 SD 51). However, Jassal et al. (2010) found weather conditions differed between the periods and derived an empirical model for annual NEP and weather (annual air temperature, solar radiation, and 0–30 cm water content), which gave a lower mean estimate of

NEP without fertilization from 2007 to 2010 (427 SD32), with fertilized being 31% greater than unfertilized. This was comparable to the fertilization effect noted by Filipescu et al. (2017) (34%) but greater than that estimated using CBM-CFS3 with the tree-ring-based yield curves (14%) for the DF49a area. However, the effects noted by Filipescu et al. (2017) were based on the extrapolation of crop tree increments to the rest of the plot, while the tree-ring yield curves were based on the individual tree increments.

In the LiDAR blocks, cumulative volume (47.7 m^3 ha^{-1} F, 38.7 m^3 ha^{-1} C) and biomass (7.8 Mg ha^{-1} F, 8.0 Mg ha^{-1} C) increments by 2016 were a fraction of those observed in the sample plots (subset trees) (148.4 m^3 ha^{-1}/44.9 Mg ha^{-1} F, 143.5 m^3 ha^{-1}/37.4 Mg ha^{-1} C). Despite the differences in the magnitude of increments, the differences between treatments were largely non-significant in both the plot and LiDAR block-level results. However, the height increments in the LiDAR blocks showed significant differences between treatments in all years, other than 2008. Hilker et al. (2011) found there were no noticeable differences in canopy height between treatments around the DF49 area in 2008. However, since the forests were fertilized in 2007, the height response might not be observed after one growing season. Littke et al. (2014) found in paired single-tree fertilizations that fertilized tree height increments were greatest from 0 to 2 years and less from 2 to 4 years. They also reported that fertilized trees might show a basal area increment with little or no height increment. Hudak et al. (2012) found using a bi-temporal LiDAR approach with random forest modelling that AGB increased at an average rate of 4.1 Mg ha^{-1} yr^{-1} over the six years between acquisitions in a complex conifer forest, which is much higher than increment rates seen at the LiDAR blocks in this study and more similar to the rates observed in the sample plots.

Table 2.5. Treatment effect method comparison showing unweighted values (((Fertilized/Control)-1) x 100)[4] in pre- and post-treatment periods for stem volume (m^3 ha^{-1}), stem biomass (Mg ha^{-1}), and height (m) cumulative increment (gain) for plot subset trees and LiDAR blocks, and above-ground biomass carbon gain (Mg C ha^{-1}) from a model reconstruction approach using plot tree-ring growth curves. Comparisons are also shown for periodic annual increment (PAI) of above-ground biomass carbon (Mg C ha^{-1} yr^{-1}) from tree-ring curves for the same periods as volume growth (m^3 ha^{-1} yr^{-1}) in Filipescu et al. (2017)^.

Source	Attribute	Period	Pre-Treat	Post-Treat
Plot subset trees	Stem volume gain	Pre: 2005–2008 Post: 2005–2011	9%	13%
	Stem biomass gain	Pre: 2005–2008 Post: 2005–2011	−4%[3]	0.4%[3]
Lidar all blocks	Stem volume gain	Pre: 2005–2008 Post: 2005–2011	50%	83%
	Stem biomass gain	Pre: 2005–2008 Post: 2005–2011	−7%	7%
	Height gain	Pre: 2005–2008 Post: 2005–2011	5%	9%
Plot tree-ring growth curves	Biomass carbon gain	Pre: 2005–2008 Post: 2005–2011	7%	14%
	Biomass carbon PAI	Pre: 2002–2006 Post: 2007–2011	−10%	20%[3]
Plot crop trees^	Volume growth PAI	Pre: 2002–2006 Post: 2007–2011	−8%	22%

4.2. Sources of Uncertainty

While the results of this study clearly show the variation of treatment effects across methods and the treatment area, it is important to note that these results (as with all studies examining fertilization effects) are subject to the limitations of the applied methods. First, uncertainties exist related to the use of tree-ring analysis to produce plot or stand-level biomass estimates, including

[4] Values have been corrected since publication

uncertainties introduced from the subsampling of trees within a plot and those from the use of allometric equations (Alexander et al., 2017). In this study, the influence of subsampling uncertainty was eliminated by utilizing the tree-ring analysis from all trees within the plots (Metsaranta et al., 2018). Uncertainty from allometric equations was also minimized in this study by using volume allometric equations that were species- and biogeoclimatic zone-specific (Kozak, 1994) with parameters fit using plots from a harvested stand within the treatment area (Metsaranta et al., 2018). For the biomass calculations, regional equations were also used that specified the province (BC) and the ecozone (Pacific) of the data.

Another source of uncertainty comes from the removal of sampled trees from the LiDAR data. Stem mapping data often contain inaccuracies in absolute positioning due to GPS error (Silva et al., 2016), and similarly, LiDAR-identified treetops could have discrepancies in location between years due to differences in instrumentation, GPS error, and environmental conditions (White et al., 2017). To limit this uncertainty, trees that were removed were manually matched with segmented tree crowns using both the location and height of field trees to identify matches from the segmented LiDAR point cloud. Finally, uncertainty was introduced into the analysis through the use of random forest (RF) models, which are limited by the inability to extrapolate beyond the set of training data (White et al., 2017). The average 2004 values in LiDAR blocks were larger than the maximum of the 2004 values observed in sample plots, and suggest that the 2004 estimates approached the lower limit of the models. This would create lower yearly increments than reality if the actual 2004 values in these blocks were below the model's saturation point.

This study suggests that there is potential for the AB method to be used in a verification context. However, some challenges remain in optimizing the sampling design to describe

changes over the entire treatment area. The sampling intensity of the sample plots used in this study appears to be appropriate given the low RMSE (12.55%/11.91%) and bias (0.88%/0.29%) values of the volume model, which showed a similar goodness of fit as other RF volume models applied in complex coniferous forests (RMSE of 26% (White et al., 2014); RMSE of 33.24% (White et al., 2015)). However, in relation to the size of the plot level increments between years, the RMSE values were still high, and an increase in sample intensity might reduce the errors to an appropriate range for the increments. Additionally, the spatial distribution of the sample plots in future applications should be extended to include more of the variation within the treatment area. If available, plot locations could be determined by analyzing and stratifying the LiDAR point cloud structure utilizing a principal components analysis of LiDAR metrics (Van Ewijk et al., 2019).

As a method to augment sample plot estimates of treatment impacts, the AB approach offers the potential to increase the assessment's accuracy level and the spatial extent of the analysis. While more research is needed to determine the optimal sampling intensity and distribution for operational application, the fusion of the traditional sample design with a LiDAR area-based approach could offer the optimal design for a carbon verification context. As verification projects often balance the need for accuracy with project cost (Di Lallo et al., 2017), the fusion of these two methods provides the flexibility to leverage plot-level observations to gain insights into the wider treatment area. This method should also become more accessible, particularly with the increased availability of multiple LiDAR acquisitions and the use of UAV-based LiDAR systems (Hu et al., 2020).

5. Conclusions

This study demonstrated that the impacts of fertilization observed in a ground plot sampling design do not necessarily translate across spatial scales. This was due to the differences between fertilization effects experienced in sample plots and those found in the broader treatment area. However, in terms of utilization for carbon project verification, the fusion of traditional sample plot methods and the LiDAR AB approach shows promise for describing fertilization changes across an entire operational treatment area. Future research on the fusion of these methods should focus on optimizing the sampling intensity and spatial distribution of the sampling design to balance a high level of accuracy with sampling costs.

References

Acharjee, A., Larkman, J., Xu, Y., Cardoso, V.R., Gkoutos, G.V. (2020). A random forest based biomarker discovery and power analysis framework for diagnostics research. BMC Med. Genom., 13, doi:10.1186/s12920-020-00826-6.

Albaugh, T.J., Lee Allen, H., Fox, T.R. (2007). Historical patterns of Forest fertilization in the Southeastern United States from 1969 to 2004. South. J. Appl. For., 31, 129–137, doi:10.1093/sjaf/31.3.129.

Alexander, M.R., Rollinson, C.R., Babst, F., Trouet, V., Moore, D.J. (2017). Relative influences of multiple sources of uncertainty on cumulative and incremental tree-ring-derived aboveground biomass estimates. Trees, 32, 265–276, doi:10.1007/s00468-017-1629-0.

Bouvier, M., Durrieu, S., Fournier, R.A., Renaud, J. (2015). Generalizing predictive models of forest inventory attributes using an area-based approach with airborne LiDAR data. Remote Sens. Environ., 156, 322–334, doi:10.1016/j.rse.2014.10.004.

Brix, H. (1993). Fertilization and Thinning Effect on a Douglas-Fir Ecosystem at Shawnigan Lake: A Synthesis of Project Results; FRDA Report 196; Forestry Canada, Pacific Forestry Center: Victoria, BC, Canada.

Brockley, R.P. (2006). Effects of Fertilization on the Growth and Foliar Nutrition of Immature Douglas-Fir in the Interior Cedar-Hemlock Zone of British Columbia: Six-Year Results; Res. Rep. 27.; BC Ministry of Forests and Range Research Branch: Victoria, BC, Canada.

Brockley, R.P. (2007). Effects of 12 years of repeated fertilization on the foliar nutrition and growth of young lodgepole pine in the central interior of British Columbia. Can. J. For. Res., 37, 2115–2129, doi:10.1139/x07-081.

Chiteka, K., Arora, R., Sridhara, S.N. (2019). Method to predict solar photovoltaic soiling using artificial neural networks and multiple linear regression models. Energy Syst., 11, 981–1002, doi:10.1007/s12667-019-00348-w.

Coursolle, C., Margolis, H.A., Giasson, M., Bernier, P., Amiro, B.D., Arain, M.A., Barr, A.G., Black, T.A., Goulden, M.L., McCaughey, J.H…et al. (2012). Influence of stand age on the magnitude and seasonality of carbon fluxes in Canadian forests. Agric. For. Meteorol., 165, 136–148, doi:10.1016/j.agrformet.2012.06.011.

Dalponte, M,; Coomes, D.A. (2016). Tree-centric mapping of forest carbon density from airborne laser scanning and hyperspectral data. MEE, 7, 1236–1245, doi:10.1111/2041-210x.12575.

Di Lallo, G., Mundhenk, P., Marchetti, M., Köhl, M. (2017). Understanding measurement reporting and verification systems for redd+ as an investment for generating carbon benefits. Forests, 8, 271, doi:10.3390/f8080271.

Di Lucca, C.M., Goudie, J.W. (2011). Using TIPSY to predict the effect of stand management on quantity and value of carbon and biomass. In Carbon Management in BC Ecosystems, June 15–16, 2011; Columbia Mountains Institute of Applied Ecology: Nelson, BC, Canada, pp. 18–32.

Ferster, C.J., Coops, N.C., Trofymow, J.A. (2009). Aboveground large tree mass estimation in a coastal forest in British Columbia using plot-level metrics and individual tree detection from LiDAR. Can. J. Remote Sens., 35, 270–275, doi:10.5589/m09-014.

Ferster, C.J., Trofymow, J.A., Coops, N.C., Chen, B., Black, T.A. (2015). Comparison of carbon-stock changes, eddy-covariance carbon fluxes and model estimates in coastal Douglas-fir stands in British Columbia. For. Ecosyst., 2, 1–19, doi:10.1186/s40663-015-0038-3.

Filipescu, C.N., Trofymow, J.A., Koppenaal, R.S. (2017). Late-rotation nitrogen fertilization of Douglas-fir: Growth response and fibre properties. Can. J. For. Res., 47, 134–138, doi:10.1139/cjfr-2016-0306.

Fisher, J.I., Hurtt, G.C., Thomas, R.Q., Chambers, J.Q. (2008). Clustered disturbances lead to bias in large-scale estimates based on forest sample plots. Ecol. Lett., 11, 554–563, doi:10.1111/j.1461-0248.2008.01169.x.

Harrington, C.A., Devine, W.D. (2011). Stand development following precommercial thinning and fertilization treatments in a western redcedar (*Thuja plicata*) dominated forest. Can. J. For. Res., 41, 151–164, doi:10.1139/x10-193.

Hilker, T., Lepine, L., Coops, N.C., Jassal, R.S., Black, T.A., Wulder, M.A., Day, M. (2011). Assessing the impact of N-fertilization on biochemical composition and biomass of a Douglas-fir canopy—A remote sensing approach. Agric. For. Meteorol., 153, 124–133, doi:10.1016/j.agrformet.2011.03.0141.

Hu, T., Sun, X., Su, Y., Guan, H., Sun, Q., Kelly, M., Guo, Q. (2020). Development and performance evaluation of a very low-cost UAV-LiDAR system for forestry applications. Remote Sens., 13, 77, doi:10.3390/rs13010077.

Hudak, A.T., Strand, E.K., Vierling, L.A., Byrne, J.C., Eitel, J.U.H., Martinuzzi, S., Falkowski, M.J. (2012). Quantifying aboveground forest carbon pools and fluxes from repeat LiDAR surveys. Remote Sens. Environ. 123, 25–40, doi:10.1016/j.rse.2012.02.023.

Jang, W., Eskelson, B.N.I., de Montigny, L., Bealle Statland, C.A., Sattler, D.F., Ahmed, S. (2019). Stand growth responses after fertilization for thinned lodgepole pine, Douglas-fir, and spruce in forests of interior British Columbia, Canada. Can. J. For. Res., 49, 1471–1482, doi:10.1139/cjfr-2019-0188.

Jassal, R.S., Black, T.A., Cai, T., Ethier, G., Pepin, S., Brümmer, C., Nesic, Z., Spittlehouse, D.L., Trofymow, J.A. (2010). Impact of nitrogen fertilization on carbon and water balances in a chronosequence of three Douglas-fir stands in the Pacific northwest. Agric. For. Meteorol., 150, 208–218, doi:10.1016/j.agrformet.2009.10.005.

Klesse, S., DeRose, R.J., Guiterman, C.H., Lynch, A.M., O'Connor, C.D., Shaw, J.D., Evans, M.E. (2018). Sampling bias overestimates climate change impacts on forest growth in the southwestern United States. Nat. Commun., 9, doi:10.1038/s41467-018-07800-y.

Kozak, A. (1994). Development of Taper Equations by BEC Zones and Species; Report No. FS 189A HTA 90/08; BC Ministry of Forests: Victoria, BC, Canada, Available online: doi:https://www.for.gov.bc.ca/HFD/library/Documents/bib95354a.pdf (accessed on 08 November 2019).

Kuhn, M. (2008). Building predictive models in r using the caret package. J. Stat. Softw., 28, doi:10.18637/jss.v028.i05.

Kull, S.J., Rampley, G.J., Morken, S., Metsaranta, J., Neilson, E.T., Kurz, W.A. (2019). Operational-Scale Carbon Budget Model of the Canadian Forest Sector (CBM-CFS3) Version 1.2: User's Guide; Natural Resources Canada, Canadian Forest Service, Northern Forestry Centre: Edmonton, AB, Canada. (accessed on 29 February 2021).

Kursa, M.B., Rudnicki, W.R. (2010). Feature selection with the Boruta package. J. Stat. Softw., 36, doi:10.18637/jss.v036.i11.

Kurz, W.A., Dymond, C.C., White, T.M., Stinson, G., Shaw, C.H., Rampley, G.J., Smyth, C., Simpson, B.N., Neilson, E.T., Trofymow, J.A., Metsaranta, J., & Apps, M.J. (2009). CBM-CFS3: A model of carbon-dynamics in forestry and land-use change implementing IPCC standards. Ecol. Mod., 220, 480–504.

Liaw, A., Wiener, M. (2002). Classification and Regression by Random Forest. R. News, 2, 18–22.

Littke, K.M., Harrison, R.B., Zabowski, D., Briggs, D.G. (2014). Assessing nitrogen fertilizer response of coastal douglas-fir in the Pacific northwest using a paired-tree experimental design. For. Ecol. Manag., 330, 137–143, doi:10.1016/j.foreco.2014.07.008.

Metsaranta, J.M., Lieffers, V.J. (2009). Using dendrochronology to obtain annual data for modeling stand development: A supplement to permanent sample plots. Forestry 2009, 82, 163–173.

Metsaranta, J., Trofymow, J., Black, T., Jassal, R. (2018). Long-term time series of annual ecosystem production (1985–2010) derived from tree rings in Douglas-fir stands on Vancouver Island, Canada using a hybrid biometric-modelling approach. Forest Ecol. Manag., 429, 57–68, doi:10.1016/j.foreco.2018.06.040.

Næsset, E. (2002). Predicting forest stand characteristics with airborne scanning laser using a practical two-stage procedure and field data. Remote Sens. Environ., 80, 88–99, doi:10.1016/s0034-425700290-5.

Nabuurs, G.J., Masera, O., Andrasko, K., Benitez-Ponce, P., Boer, R., Dutschke, M., Elsiddig, E., Ford-Robertson, J., Frumhoff, P., Karjalainen, T… et al. (2007). Forestry. In Climate Change 2007: Mitigation. Contribution of Working Group III to the Fourth Assessment Report of the Intergov-ernmental Panel on Climate Change; Metz, B., Davidson, O.R., Bosch, P.R., Dave, R., Meyer, L.A., Eds.; Cambridge University Press, Cambridge, UK/New York, NY, USA.

National Forest Inventory. Canada's National Forest Inventory ground sampling guidelines: Specifications for ongoing measurements. Version 5.0. 2008. Available online: https://nfi.nfis.org/resources/groundplot/Gp_guidelines_v5.0.pdf (accessed on 15 August 2020).

Negrave, R.W., Prescott, C.E., Barker, J.E. (2007). Growth and foliar nutrition of juvenile western hemlock and western redcedar plantations on low- and medium-productivity sites on northern Vancouver Island: Response to fertilization and planting density. Can. J. For. Res., 37, 2587–2599, doi:10.1139/X07-089.

Omule, A.Y., Mitchell, A.K., Wagner, W.L. (2011). Fertilization and Thinning Effects on a Douglas-Fir Ecosystem at Shawnigan Lake: 32-Year Growth Response; Report No. FI-X-005; The Canadian Wood Fibre Centre: Victoria, BC, Canada. pp. 1–22.

Penner, M., Pitt, D.G., Woods, M.E. (2013). Parametric vs. non-parametric LiDAR models for operational forest inventory in boreal Ontario. Can. J. Remote Sens., 39, 426–443, doi:10.5589/m13-049.

Pojar, J., Klinka, K., Demarchi, D.A. (1991). Chapter 6: Coastal Western Hemlock Zone. In Ecosystems of British Columbia; BC Special Report Series No. 6; Meidinger, D., Pojar, J., Eds.; BC Ministry of Forests: Victoria, BC, Canada, pp. 95–111.

Prescott, C., DeMontigny, L., Harper, G. (2019). Eighteen-year growth responses to thinning and fertilization of a height-repressed lodgepole pine stand in interior British Columbia. For. Chron., 95, 207–221, doi:10.5558/tfc2019-029.

Prescott, C.E., Nery, V., Van Niejenhuis, A., Sajedi, T., Marshall, P. (2013). Nutrition management of Cedar and Hemlock plantations in coastal British Columbia. New Forests, 44, 769–784, doi:10.1007/s11056-013-9380-x.

Province of British Columbia. (2018). Tipsy, version 4.4. Forestry Analysis and Inventory Branch. BC Ministry of Forests, Lands, Natural Resource Operations and Rural Development. Available online https://www2.gov.bc.ca/gov/content/industry/forestry/managing-our-forest-resources/forest-inventory/field-forms-and-software/software-download (accessed on 29 February 2021).

Reid, A., de Montigny, L., Prescott, C., Sajedi, T. A. (2017). Systematic Review of Forest Fertilization Research in Interior British Columbia; Technical Report 111; Province BC: Victoria, BC, Canada. Available online: www.for.gov.bc.ca/ hfd/pubs/Docs/Tr/Tr111.htm (accessed on 20 August 2020).

Richards, K.R., Huebner, G.E. (2012a). Evaluating protocols and standards for forest carbon-offset programs, part A: Additionality, baselines and permanence. Carbon Manag., 3, 393–410, doi:10.4155/cmt.12.38.

Richards, K.R., Huebner, G.E. (2012b). Evaluating protocols and standards for forest carbon-offset programs, part B: Leakage assessment, wood products, validation and verification. Carbon Manag., 3, 411–425, doi:10.4155/cmt.12.39.

Roussel, J., Auty, D., Coops, N.C., Tompalski, P., Goodbody, T.R., Meador, A.S., Achim, A. (2020). LidR: An R package for analysis of airborne laser scanning (ALS) data. Remote Sens. Environ., 251, 112061, doi:10.1016/j.rse.2020.112061.

Routa, J., Kilpeläinen, A., Ikonen, V., Asikainen, A., Venäläinen, A., Peltola, H. (2019). Effects of intensified silviculture on timber production and its economic profitability in boreal Norway spruce and Scots pine stands under changing climatic conditions. Forestry, 92, 648–658, doi:10.1093/forestry/cpz043.

Saarsalmi, A., Mälkönen, E. (2001). Forest fertilization research in Finland: A literature review. Scand. J. For. Res., 16, 514–535, doi:10.1080/02827580152699358.

Shryock, B., Littke, K., Ciol, M., Briggs, D., Harrison, R. (2014). The effects of urea fertilization on carbon sequestration in Douglas-fir plantations of the coastal Pacific Northwest. Forest Ecol. Manag., 318, 341–348, doi:10.1016/j.foreco.2014.01.040.

Silva, C.A., Hudak, A.T., Vierling, L.A., Loudermilk, E.L., O'Brien, J.J., Hiers, J.K., Khosravipour, A. (2016). Imputation of individual longleaf pine (Pinus palustris Mill.) tree attributes from field and LiDAR data. Can. J. Remote Sens., 42, 554–573, doi:10.1080/07038992.2016.1196582.

Sullivan, T.P., Sullivan, D.S., Lindgren, P.M., Ransome, D.B., Zabek, L. (2020). Twenty-five years after stand thinning and repeated fertilization in lodgepole Pine Forest: Implications for tree growth, stand structure, and carbon sequestration. Forests, 11, 337, doi:10.3390/f11030337.

Temesgen, H., v. Gadow, K. (2004). Generalized height–diameter models—an application for major tree species in complex stands of interior British Columbia. Eur. J. For. Res., 123, 45–51, doi:10.1007/s10342-004-0020-z.

Timber Pricing Branch. Scaling Manual. (2011). Ministry of Forests Lands and Natural Resource Operations. Available online: https://www.for.gov.bc.ca/ftp/hva/external/!publish/web/manuals/Scaling/2011/Scaling2011NovMaster.pdf (accessed on 08 November 2019).

Trofymow, J.A, Stinson, G., Kurz, W.A. (2008). Derivation of a spatially explicit 86-year retrospective carbon budget for a landscape undergoing conversion from old-growth to managed forests on Vancouver Island, BC. Forest Ecol. Manag., 256, 1677–1691, doi:10.1016/j.foreco.2008.02.056.

Trofymow, J.A., Coops, N.C., Hayhurst, D. (2014). Comparison of remote sensing and ground-based methods for determining residue burn pile wood volumes and biomass. Can. J. For. Res., 44, 182–194, doi:10.1139/cjfr-2013-0281.

Van Ewijk, K., Treitz, P., Woods, M., Jones, T., Caspersen, J. (2019). Forest site and type variability in ALS-based forest resource inventory attribute predictions over three Ontario forest sites. Forests, 10, 226, doi:10.3390/f10030226.

Vejre, H., Ingerslev, M., Raulund-Rasmussen, K. (2001). Fertilization of Danish Forests: A review of experiments. Scand. J. For. Res., 16, 502–513, doi:10.1080/02827580152699349.

White, A.E.; Lutz, D.A.; Howarth, R.B.; Soto, J.R. (2018). Small-scale forestry and carbon offset markets: An empirical study of Vermont current use forest landowner willingness to accept carbon credit programs. PLoS ONE, 13, doi:10.1371/journal.pone.0201967.

White, J.C., Stepper, C., Tompalski, P., Coops, N.C., Wulder, M.A. (2015). Comparing ALS and image-iased point cloud metrics and modelled forest inventory attributes in a complex coastal forest environment. Forests, 6, 3704–3732, doi:10.3390/f6103704.

White, J.C., Tompalski, P., Vastaranta, M., Wulder, M.A., Saarinen, S., Coops, N.C. (2017). A best Practices Guide for Generating Forest Inventory Attributes from Airborne Laser Scanning Data Using the Area-Based Approach; Information Report FI-X-018; Natural Resources Canada, Canadian Forest Service, Canadian Wood Fibre Centre, Pacific Forestry Centre: Victoria, BC, Canada, 38p. Available online: http://cfs.nrcan.gc.ca/publications?id=38945 (accessed on).

White, J.C., Wulder, M.A., Buckmaster, G. (2014). Validating estimates of merchantable volume from airborne laser scanning (ALS) data using weight scale data. For. Chron., 90, 378–385, doi:10.5558/tfc2014072.

Woods, M., Lim, K., Treitz, P. (2008). Predicting forest stand variables from LiDAR data in the Great Lakes—St. Lawrence forest of Ontario. For. Chron., 84, 827–839, doi:10.5558/tfc84827-6.

Woods, M., Pitt, D., Penner, M., Lim, K., Nesbitt, D., Treitz, P. (2011). Operational implementation of LiDAR inventories in boreal Ontario advanced forest resource inventory technologies. For. Chron., 87, 512–528.

Velusamy, D., Ramasamy, K. (2020). Ensemble of heterogeneous classifiers for diagnosis and prediction of coronary artery disease with reduced feature subset. Comput. Methods Programs Biomed. 198, 105770, doi:10.1016/j.cmpb.2020.105770.

Appendix A

Table A1. LiDAR predictor metrics used and selected by the Boruta variable selection method.

Predictor Class	Description	(V)olume/ (B)iomass Model
Canopy Cover	(All Returns Above Mean ht/total 1st returns) * 100	V B
Canopy Cover	(All Returns Above Mode ht/total 1st returns) * 100	
Canopy Cover	((mean ht - min ht)/(max ht-min ht))	
Canopy Cover	Percentage 1st returns above 2m	V B
Canopy Cover	Percentage 1st returns above mean ht	V
Canopy Cover	Percentage 1st returns above mode ht	
Canopy Cover	Percentage All returns above 2m	V B
Canopy Cover	Percentage All returns above mean ht	
Canopy Cover	Percentage All returns above mode ht	
Canopy Cover	(All returns above 2m / Total 1st returns) * 100	V B
Statistical	Average absolute deviation (AD) of ht	B
Statistical	Coefficient of variation	
Statistical	Interquartile distance	B
Statistical	Kurtosis	
Statistical	First L moment	
Statistical	Second L moment	B
Statistical	L-moment coefficient of variation	
Statistical	L-moment kurtosis	
Statistical	L-moment skewness	
Statistical	Median of the AD from the overall median	
Statistical	Median of the AD from the overall mode	B
Statistical	Mode ht	B
Statistical	Quadratic mean of ht	
Statistical	Standard deviation of ht	
Statistical	Skewness of ht	
Statistical	Variance of ht	
Height	Xth percentile of height distribution (10,20,25,30,40,50,60,70,75,80,90,95)	V – 10 B – 95
Density	Cumulative percentage of returns in the Xth decile (1-9)	B – 6, 7

Table A2. Mixed effect model F and P-value results between treatments for volume and biomass cumulative increments with subset plot trees or all plot trees.

Attribute	Year	Trees	Degrees Freedom	Treatment Effect F-value (P-value)
Volume	2008	Subset	4	0.49 (0.52)
Volume	2011	Subset	4	0.91 (0.39)
Volume	2016	Subset	4	0.05 (0.84)
Biomass	2008	Subset	4	0.11 (0.76)
Biomass	2011	Subset	4	0.00 (0.99)
Biomass	2016	Subset	4	1.41 (0.30)
Volume	2008	All	4	0.78 (0.43)
Volume	2011	All	4	1.28 (0.32)
Biomass	2008	All	4	0.43 (0.55)
Biomass	2011	All	4	0.03 (0.87)

Table A3. Mixed effect model F and P-value results between treatments for volume and biomass periodic annual increments with all plot trees or subset plot trees.

Attribute	Year	Trees	Degrees Freedom	Treatment Effect F-value (P-value)
Volume	2008	Subset	4	0.49 (0.52)
Volume	2011	Subset	4	1.25 (0.33)
Volume	2016	Subset	4	0.05 (0.84)
Biomass	2008	Subset	4	0.10 (0.76)
Biomass	2011	Subset	4	0.05 (0.83)
Biomass	2016	Subset	4	1.05 (0.36)
Volume	2008	All	4	0.78 (0.43)
Volume	2011	All	4	1.64 (0.27)
Biomass	2008	All	4	0.43 (0.55)
Biomass	2011	All	4	0.01 (0.92)

Table A4. Plot level stem volumes (m^3ha^{-1}), periodic annual volume increments ($m^3ha^{-1}yr^{-1}$), and control (C) or fertilized (F) treatment averages for the subset trees in the plots, as well as all trees.

		Subset Trees				All Trees			
Plot	Treat	2004 Volume	2005-2008 PAI	2009-2011 PAI	2012-2016 PAI	2004 Volume	2005-2008 PAI	2009-2011 PAI	2012-2016 PAI
1.1	C	516.8	8.7	15.8	18.2	651.1	10.0	17.1	-10.5
8.3	C	338.8	6.6	10.7	16.2	446.5	8.6	13.0	-8.3
10.2	C	491.1	10.3	17.7	4.7	580.6	12.1	19.7	-15.8
Average (SE)	**C**	**448.9 (55.6)**	**8.5 (1.1)**	**14.8 (2.1)**	**13.0 (4.2)**	**559.4 (60.2)**	**10.2 (1.00)**	**16.6 (2.0)**	**-11.5 (2.2)**
4.1	F	520.0	8.6	15.9	12.9	588.9	10.4	17.9	-3.6
5.1	F	461.9	9.8	17.5	17.0	576.1	11.5	19.3	-8.3
6.1	F	487.6	9.6	18.4	5.8	641.3	11.6	20.6	-27.9
Average (SE)	**F**	**489.9 (16.8)**	**9.3 (0.4)**	**17.2 (0.7)**	**11.9 (3.3)**	**602.1 (19.9)**	**11.2 (0.4)**	**19.3 (0.8)**	**-13.3 (7.4)**

Table A5. Plot level stem biomass (Mg ha^{-1}), periodic annual biomass increments (Mg $ha^{-1}yr^{-1}$), and control (C) or fertilized (F) treatment averages for the subset trees in the plots, as well as all trees.

		Subset Trees				All Trees			
Plot	Treat	2004 Biomass	2005-2008 PAI	2009-2011 PAI	2012-2016 PAI	2004 Biomass	2005-2008 PAI	2009-2011 PAI	2012-2016 PAI
1.1	C	149.7	3.3	6.1	3.1	189.2	3.8	6.7	-5.6
8.3	C	94.0	2.2	3.6	2.8	125.3	2.9	4.5	-4.6
10.2	C	139.7	3.4	6.1	-0.02	164.6	4.1	6.9	-6.0
Average (SE)	**C**	**127.8 (17.2)**	**3.0 (0.4)**	**5.3 (0.8)**	**2.0 (1.0)**	**159.7 (18.6)**	**3.6 (0.4)**	**6.0 (0.8)**	**-5.4 (0.4)**
4.1	F	128.9	2.8	5.3	3.9	146.2	3.3	5.9	-0.4
5.1	F	108.9	2.7	5.1	5.0	136.1	3.2	5.7	-1.2
6.1	F	124.4	3.0	6.0	1.4	161.6	3.6	6.7	-6.9
Average (SE)	**F**	**120.7 (6.1)**	**2.8 (0.1)**	**5.5 (0.3)**	**3.4 (1.1)**	**148.0 (7.4)**	**3.4 (0.1)**	**6.1 (0.3)**	**-2.8 (2.1)**

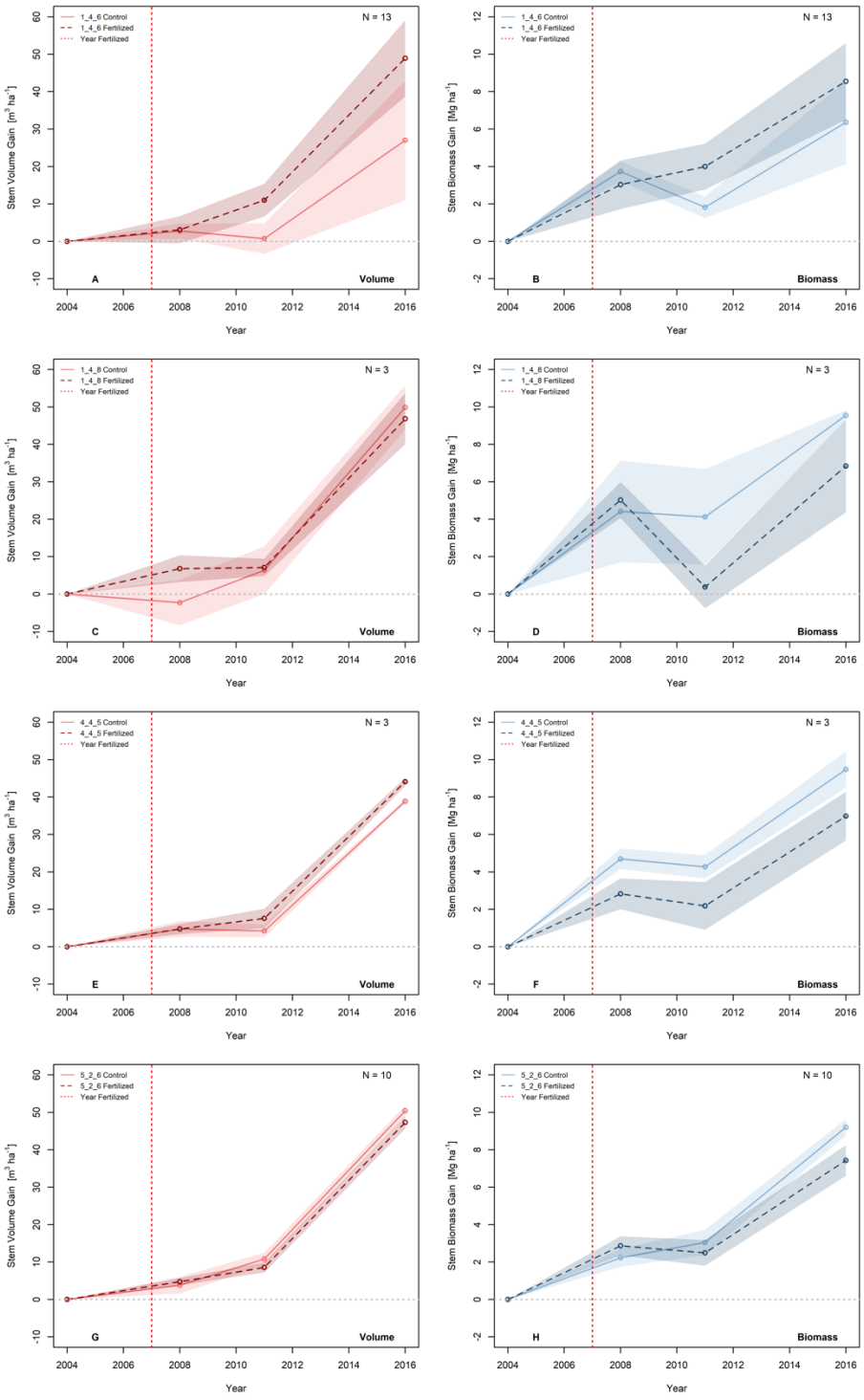

Figure A1: LiDAR block-level average (line) and standard error (shadow) stem volume (left) and biomass (right) increments for control blocks (solid) and fertilized blocks (dashed) in AU 146 (A,B), AU 148 (C,D), AU 445 (E,F), AU 526 (G,H).

Table A6: Mixed effect model F and P-value results between treatments for volume and biomass increments in the LiDAR blocks across all AUs.

Attribute	Year	AU	Degrees Freedom	Treatment Effect F-value (P-value)
Volume	2008	All	28	0.53 (0.47)
Volume	2011	All	28	2.33 (0.14)
Volume	2016	All	28	2.79 (0.11)
Biomass	2008	All	28	0.11 (0.74)
Biomass	2011	All	28	0.06 (0.80)
Biomass	2016	All	28	0.04 (0.85)

Table A7: Mixed effect model F and P-value results between treatments for volume and biomass increments in the LiDAR for individual AUs.

Attribute	Year	AU	Degrees Freedom	Treatment Effect F-value (P-value)
Volume	2008	146	12	0.01 (0.93)
Volume	2011	146	12	3.60 (0.08)
Volume	2016	146	12	3.98 (0.07)
Biomass	2008	146	12	0.34 (0.57)
Biomass	2011	146	12	4.35 (0.06)
Biomass	2016	146	12	2.03 (0.18)
Volume	2008	148	2	10.00 (0.09)
Volume	2011	148	2	0.02 (0.89)
Volume	2016	148	2	2.78 (0.24)
Biomass	2008	148	2	0.08 (0.81)
Biomass	2011	148	2	1.81 (0.31)
Biomass	2016	148	2	1.19 (0.39)
Volume	2008	445	2	0.00 (1.00)
Volume	2011	445	2	1.16 (0.39)
Volume	2016	445	2	**32.37 (0.03)**
Biomass	2008	445	2	3.57 (0.20)
Biomass	2011	445	2	4.48 (0.17)
Biomass	2016	445	2	**46.21 (0.02)**
Volume	2008	526	9	0.15 (0.71)
Volume	2011	526	9	1.24 (0.29)
Volume	2016	526	9	2.05 (0.19)
Biomass	2008	526	9	0.83 (0.39)
Biomass	2011	526	9	0.36 (0.56)
Biomass	2016	526	9	4.44 (0.06)

Table A8: Mixed effect model F and P-value results between treatments for volume and biomass periodic annual increments in the LiDAR blocks across all AUs.

Attribute	Year	AU	Degrees Freedom	Treatment Effect F-value (P-value)
Volume	2008	All	28	0.53 (0.48)
Volume	2011	All	28	1.74 (0.20)
Volume	2016	All	28	0.70 (0.41)
Biomass	2008	All	28	0.11 (0.74)
Biomass	2011	All	28	0.26 (0.61)
Biomass	2016	All	28	0.23 (0.64)

Table A9: Mixed effect model F and P-value results between treatments for volume and biomass periodic annual increments in the LiDAR blocks for individual AUs.

Attribute	Year	AU	Degrees Freedom	Treatment Effect F-value (P-value)
Volume	2008	146	12	0.01 (0.93)
Volume	2011	146	12	**6.09 (0.03)**
Volume	2016	146	12	0.87 (0.37)
Biomass	2008	146	12	0.34 (0.57)
Biomass	2011	146	12	**5.88 (0.03)**
Biomass	2016	146	12	0.00 (0.99)
Volume	2008	148	2	10.00 (0.09)
Volume	2011	148	2	8.82 (0.10)
Volume	2016	148	2	0.38 (0.60)
Biomass	2008	148	2	0.08 (0.81)
Biomass	2011	148	2	2.76 (0.24)
Biomass	2016	148	2	0.21 (0.69)
Volume	2008	445	2	0.00 (0.997)
Volume	2011	445	2	1.03 (0.42)
Volume	2016	445	2	0.32 (0.63)
Biomass	2008	445	2	3.57 (0.20)
Biomass	2011	445	2	0.01 (0.92)
Biomass	2016	445	2	0.28 (0.65)
Volume	2008	526	9	0.15 (0.71)
Volume	2011	526	9	3.12 (0.11)
Volume	2016	526	9	0.38 (0.55)
Biomass	2008	526	9	0.83 (0.39)
Biomass	2011	526	9	2.25 (0.17)
Biomass	2016	526	9	4.08 (0.07)

Table A10: Mixed effect model F and P-value results between treatments for 95th percentile of LiDAR height increments and periodic annual increments in the LiDAR blocks across all AUs.

Attribute	Year	AU	Degrees Freedom	Treatment Effect F-value (P-value)
95th - Inc	2008	All	28	3.30 (0.08)
95th – Inc	2011	All	28	**6.29 (0.02)**
95th – Inc	2016	All	28	**14.18 (0.001)**
95th – PAI	2008	All	28	3.30 (0.08)
95th – PAI	2011	All	28	4.15 (0.05)
95th – PAI	2016	All	28	**6.48 (0.02)**

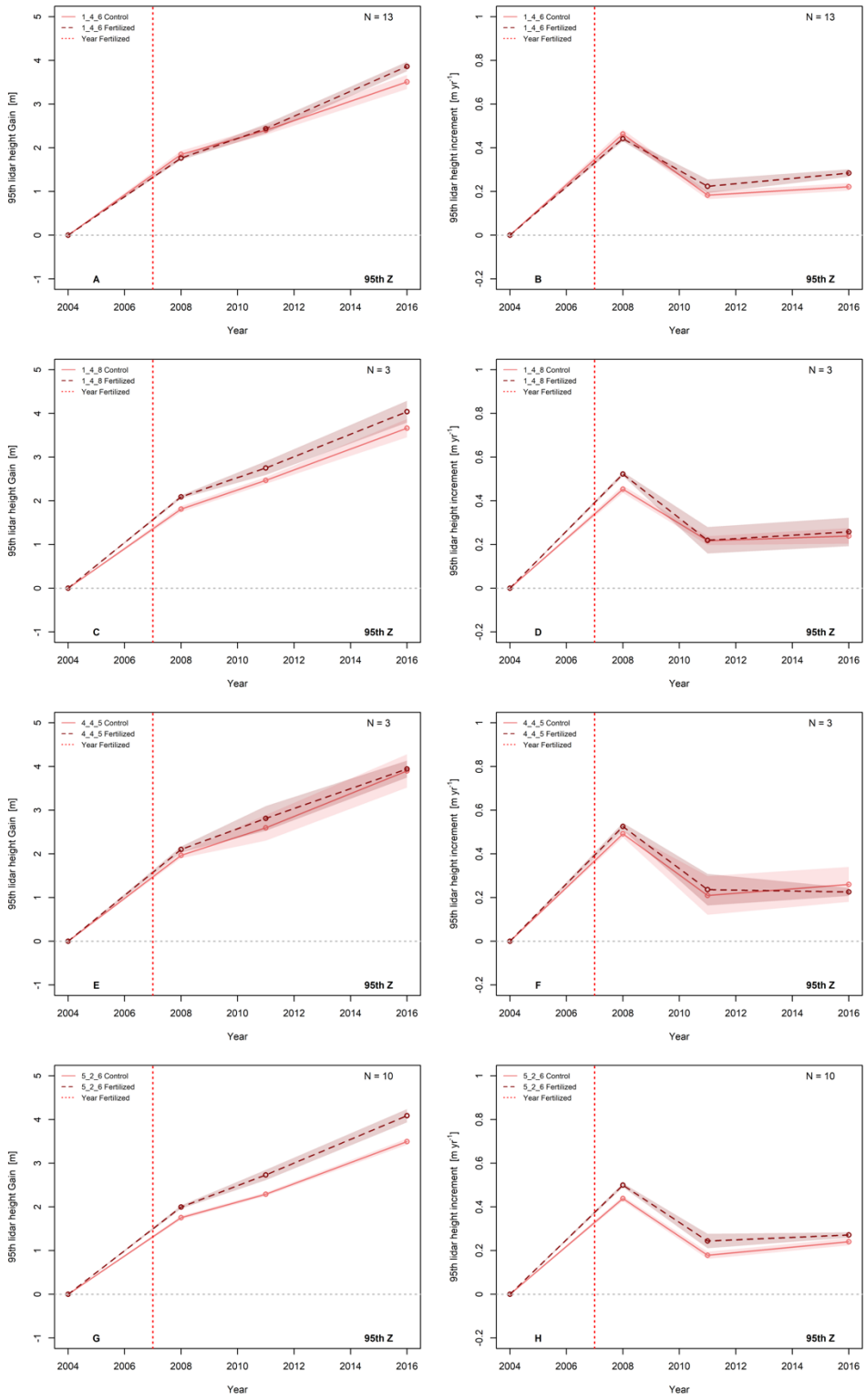

Figure A2: LiDAR block-level average (line) and standard error (shadow) 95th percentile of LiDAR height cumulative (left) and periodic annual (right) increments for control blocks (solid) and fertilized blocks (dashed) in AU 146 (A,B), AU 148 (C,D), AU 445 (E,F), AU 526 (G,H).

Table A11: Mixed effect model F and P-value results between treatments for 95th percentile of LiDAR height increments and periodic annual increments in the LiDAR blocks for individual AUs.

Attribute	Year	AU	Degrees Freedom	Treatment Effect F-value (P-value)
95th - Inc	2008	146	12	1.32 (0.27)
95th – Inc	2011	146	12	0.09 (0.76)
95th – Inc	2016	146	12	4.61 (0.05)
95th – PAI	2008	146	12	1.32 (0.27)
95th – PAI	2011	146	12	1.44 (0.25)
95th – PAI	2016	146	12	8.64 (0.01)
95th - Inc	2008	148	2	65.07 (0.02)
95th – Inc	2011	148	2	2.68 (0.24)
95th – Inc	2016	148	2	4.15 (0.18)
95th – PAI	2008	148	2	65.07 (0.02)
95th – PAI	2011	148	2	0.001 (0.98)
95th – PAI	2016	148	2	0.39 (0.60)
95th - Inc	2008	445	2	2.07 (0.29)
95th – Inc	2011	445	2	0.28 (0.65)
95th – Inc	2016	445	2	0.01 (0.93)
95th – PAI	2008	445	2	2.07 (0.29)
95th – PAI	2011	445	2	0.07 (0.82)
95th – PAI	2016	445	2	0.27 (0.65)
95th - Inc	2008	526	9	19.29 (0.002)
95th – Inc	2011	526	9	12.50 (0.01)
95th – Inc	2016	526	9	13.49 (0.01)
95th – PAI	2008	526	9	19.29 (0.002)
95th – PAI	2011	526	9	3.88 (0.08)
95th – PAI	2016	526	9	2.20 (0.17)

Table A12. Treatment effect method comparison showing weighted values ([Fertilized/2004 Fertilized x 100] – [Control/2004 Control x 100]) in pre and post treatment periods for stem volume (m^3 ha^{-1}), stem biomass (Mg ha^{-1}), and height (m) cumulative increment (gain) for plot subset trees and LiDAR blocks, and above ground biomass carbon gain (Mg C ha^{-1}) from a model reconstruction approach using plot tree ring growth curves. Comparisons are also shown for periodic annual increment (PAI) of above ground biomass carbon (Mg C ha^{-1} yr^{-1}) from tree-ring curves for the same periods as volume growth ($m^3ha^{-1}yr^{-1}$) in [22]. * Note: Plot tree ring growth curve PAI and Plot crop tree volume growth PAI values weighted as [Post-treat F/Pre-treat F x 100] - [Post-treat C/Pre-treat C x 100]

Source	Attribute	Period	Pre-Treat	Post-Treat
Plot Subset Trees	Stem volume gain	Pre: 2005-2008 Post: 2005-2011	0%	0.6%
	Stem biomass gain	Pre: 2005-2008 Post: 2005-2011	0%	1%
Lidar All Blocks	Stem volume gain	Pre: 2005-2008 Post: 2005-2011	0.2%	0.7%
	Stem biomass gain	Pre: 2005-2008 Post: 2005-2011	-0.2%	0.1%
	Height gain	Pre: 2005-2008 Post: 2005-2011	0%	0.7%
Plot Tree-ring growth curves	Biomass carbon gain	Pre: 2005-2008 Post: 2005-2011	0.2%	0.8%
	Biomass carbon PAI*	Pre: 2002-2006 Post: 2007-2011	-	28%
Plot crop trees [22]	Volume growth PAI*	Pre: 2002-2006 Post: 2007-2011	-	34%

Chapter 3: Combining Area-based and Individual Tree Metrics Can Improve Merchantable and Non-merchantable Wood Volume Estimates in Coastal Douglas-fir Forests.

Abstract

Forest management practices can increase climate change mitigation potential through applications focused on carbon budgets. One such application involves utilizing non-merchantable material (i.e. logging residues typically piled and burned) for bio-energy. However, limited data is available for estimating residue wood volumes until after timber has been harvested, at which point recovery of residual wood can become uneconomic. This research utilizes a hybrid method to develop models that provide pre-harvest estimates of the amount of merchantable and non-merchantable material that would result from harvesting and investigates the scalability and transferability of such measures to the harvest block level. Models were trained using 38 plots across two Douglas-fir dominated sites, expanded to ten harvest blocks, and transferred to eight blocks from two sites without training data before being compared against multiple independent block-level estimates. Model fit showed root mean square errors of 35% and 38% for merchantable and non-merchantable volume models, respectively. Merchantable volume estimates in blocks with training had a range (9%-34%) of average absolute differences from the harvest scale similar to transferred blocks without training (15%-20%). Non-merchantable model results were also similar in both trained and transferred harvest blocks, with the pre-harvest model results having lower differences from the geospatial survey than the field survey. The results from this study show promise for hybrid methods to improve estimates of merchantable wood volume compared to forest cover data and provide the ability to

predict non-merchantable volumes within the range of accuracy of post-harvest residue survey methods.

1. Introduction

Forests are a critical global resource, serving as the foundation for numerous national economies while at the same time driving the global carbon cycle. Canadian forests are a critical component of this natural resource as they make up over 9% of the world's total forest cover (Natural Resources Canada, 2020). As of 2018, a significant proportion (226 million hectares, or 65%) of these forests are considered actively managed, much of which has contributed over $25 billion to the national GDP through industrial operations (Natural Resources Canada, 2020). At the same time, forests play a critical role in the national and global carbon balance both negatively and positively.

The largest negative impact comes from the emissions of greenhouse gases (GHGs) from wildfires, such as in 2015 where Saskatchewan fires were estimated to have a total of 133.1 Tg of carbon dioxide equivalent (CO_2e) GHG emissions (Cambero et al., 2015). While the emissions from wildfires are largely out of human control, the emissions that result from forestry operations such as harvesting practices, silvicultural activities, and increased conservation are largely impacted by forest management policies. An examination of the mitigation potential of Canadian managed forests showed that changes to management policies could increase the mitigation potential of forest lands by 45.1 Tg CO_2e per year by 2050 (Smyth et al., 2014). Additionally, in British Columbia, similar changes in forest management practices which include utilizing more harvested material, producing longer-lived products, as well as utilizing harvest residues for bio-energy, were shown to have cumulative mitigation effects that could contribute up to 35% of the province's GHG reduction target by 2050 (Xu et al., 2018). These relatively

small changes in management practices have been recognized to increase the positive mitigation potential of managed forests, and the Intergovernmental Panel on Climate Change (IPCC) recognizes several management options to increase the climate change mitigation potential of forests. Some of these options include reducing deforestation, increasing afforestation, conducting selected silvicultural practices, and increasing the utilization of cut forest material for use as products in the bioeconomy (IPCC 2014, 2013).

In response to political pressures to reduce carbon emissions, many forest companies in Canada have begun utilizing waste from the milling process as a source for on-site bio-energy production (Barrette et al., 2018). This process involves using solid wood waste from manufacturing (i.e. chips, shavings, or sawdust) or black liquor produced from pulp mills to generate electricity which can be used onsite or sold back to the general electrical grid (Dymond & Kamp, 2014). It has been estimated that nationally bioenergy production could displace emissions from energy usage by 27 Mt CO_2e per year. However, this was most effective when bioenergy displaces energy produced from fossil fuels instead of other energy sources such as hydroelectricity (Smyth et al., 2017). While most of the bio-energy production in the context of forest processing has been utilizing feed sources (i.e. fuels) from milling waste, a relatively underutilized source of bio-material are residues from logging (Dymond & Kamp, 2014).

Generally, logging residues from harvest sites (i.e. non-merchantable trees and log processing remnants that are cut but left in a harvest block) are piled and burned or left dispersed across a harvest block (Trofymow et al., 2014). Logging residues are a viable feed source (Titus et al., 2021), although the amount of supply available generally remains unknown until after harvest is completed, creating challenges for increasing their utilization (Barrette et al., 2018). One solution to enhance the industry's ability to increase logging residue use would be to refine

the prediction and forecasting of non-merchantable timber volumes. Logging residue estimates could be improved from methods that can provide coarse-scale regional estimates (Dymond et al., 2010; Barrette et al., 2018) towards methods that focus on operational scales such as individual harvest blocks.

Remote sensing and geospatial models are one approach that has been successful in providing potential logging residue measurements. Satellite imagery, for example, has been used to conduct national-level assessments of potential biomass available from logging residues (Barrette et al., 2018) and salvage after wildfires (Mansuy et al., 2017). Additionally, geospatial models and spatially explicit carbon models have been used to estimate the availability of woody biomass for bioenergy (Sidders et al., 2008, Dymond et al., 2010). However, while studies have shown promise for predicting and forecasting available material, their focus on moderate resolution (>= 250 m) data, variable definitions of logging residues, and analysis at the spatial scale of forest management units offer limited capacity for use at a smaller scale, such as the individual harvest block. Yet, more recent remote sensing solutions have been developed to estimate forest attributes at smaller scales, such as enhanced forest inventory (EFI) methods. Such methods utilize high-resolution remote sensing data such as LiDAR or optical imagery and can be generally characterized into one of two styles that differ in scale: the area-based (AB) and the individual tree (IT) approaches.

The AB approach creates a generalized statistical model that accounts for the entire forest canopy profile within a rasterized grid cell. This approach uses LiDAR data and a network of training ground plots to develop a statistical model using either parametric (Ferster et al., 2009; Næsset, 2002; Woods et al., 2008) or non-parametric (White et al., 2014; Tompalski et al., 2019; Kelley et al., 2021) methods. Once a plot level model is developed, it can then be applied to the

larger area of interest, given it has similar characteristics as the training plots, by using a rasterized grid of LiDAR metrics similar to those used in the model development (White et al., 2013). The advantage of the AB approach, in general, is that both the dominant canopy trees and the sub-canopy trees are typically be accounted for, given that there exist appropriate LiDAR densities when developing the attribute models. While several studies have implemented the AB approach successfully with an improved level of accuracy over traditional inventories (White et al., 2014; Holopainen et al., 2010; Korhonen et al., 2008), some results indicate that the AB approach performs better in structurally homogenous stands such as those that are even-aged, which can present challenges when modelling attributes such as wood volume in more complex stands (Næsset, 2002; Woods et al., 2008).

Alternatively, the IT approach focuses on the larger dominant trees seen from the top of the canopy. IT approaches generally utilize image segmentation techniques to identify and delineate the crowns of individual trees. Some of these methods delineate tree crowns from a LiDAR canopy height model (CHM) up from the space between crowns (Gougeon & Leckie, 2003), down from an initial treetop point (Dalponte & Coomes, 2016), or directly from the point cloud itself (Li et al., 2012). The main advantage of using LiDAR data in the IT approach is that there is a more direct measurement of tree attributes like height and crown area, and when combined with appropriate imagery, IT segmentation can be used to classify tree species (Gougeon & Leckie, 2003). In addition, attributes such as species, height, and crown area can be used to further model additional attributes such as diameter at breast height (Jucker et al., 2017) and ultimately individual tree volume using allometric equations (Kozak, 1994). These estimates can then be summed up to the stand, harvest block, or landscape level for which there is data coverage and similar forest characteristics as the training data. The major limitation of the IT

approach is a sensitivity to errors of omission and commission, as it is limited to segmenting crowns from the larger upper canopy trees only (Blackburn et al., 2021). IT approaches that utilize terrestrial and mobile LiDAR have also been shown to have similar sensitivities to errors of omission due to occlusion, particularly with fixed position terrestrial systems (Donager et al., 2021). In such cases, mobile systems can provide an advantage as they offer multiple look angles and are the most suitable to be paired with airborne data to lessen the overall chance of omission and commission errors (Donager et al., 2021).

Several studies have proposed a hybrid EFI approach which combines methods from both the AB and IT approaches, and most have taken similar steps of summarizing metrics calculated for the ITs into a grid similar to the AB predictor metrics (Ferster et al., 2009; Hyyppä et al., 2012; Kankare et al., 2013, Blackburn et al., 2021). The main premise of this approach is that the inclusion of IT metrics allows for potential weighting towards the larger trees that make the largest contributions to total volumes. However, a limitation of using a hybrid method is the increased processing time, as the IT analysis needs to be completed and summarized into appropriate metrics before the model fitting can be continued, requiring considerable processing time for large areas. Yet, estimating the non-merchantable volume component presents a unique case where the increased times may be justified as IT variables such as stocking density and crown area could provide important information about the amount of non-merchantable material available.

While a hybrid approach has been shown to improve forest attribute estimates compared to other AB or IT approaches individually, applications of EFI methods have generally focused on merchantable volume components, with little effort to estimate the non-merchantable components (Næsset, 2002; Dalponte & Coomes, 2016; Gougeon & Leckie, 2003; White et al.,

2014). Additionally, limited research has been conducted to explore how EFI models scale to a harvest block and transfer to areas of similar conditions without prior training (White et al., 2014; Tompalski et al., 2019). This is desirable as creating a transferable model to other harvest blocks would reduce the cost of creating ground sample plots with every new harvest block. Traditionally, EFI models are fit using sample plot data and then expanded to a larger area or transferred to a new area and evaluated against additional sample plot data, where one limitation of the analysis is the sampling density and distribution of plots (Tompalski et al., 2019). Alternatively, after harvest, all merchantable wood transported off-site is scaled, allowing for a complete census of merchantable volume, which can then be compared to EFI model results on a harvest block-level (White et al., 2014).

Similarly, the traditional method to measure and estimate non-merchantable volumes in a harvest block is by using sample estimates from plots or transects and scaling up sample estimates to the stratum or block-level (Trofymow et al., 2019). These methods are limited because they also critically depend on the number and location of sample plots, which can greatly underestimate total non-merchantable volumes (Trofymow et al., 2014). However, recent methods have been developed to conduct a complete census of non-merchantable volume in the harvest block using a semi-automated log delineation method (SLD) (Trofymow et al., 2017).

This study aims to understand the application of an enhanced forest inventory method that combines the area-based and individual tree approaches to develop hybrid models (hereafter referred to as the HB models) that estimate the amount of pre-harvest merchantable and non-merchantable material that would result from harvesting operations. To accomplish this, we will address the following question: to what extent are estimates obtained using a HB model scalable to the harvest block level and transferable to blocks without plot level training data? In

answering this, we are also interested in examining the overall importance of individual tree-based summary metrics.

2. Methods

2.1 Study Area Descriptions

The study area for this research is composed of five sites in Pacific coastal forests located on Vancouver Island, British Columbia (B.C.), Canada. All sites are located within various subzones of the Coastal Western Hemlock biogeoclimatic zone (Pojar et al., 1991). In total, 18 sample blocks across the five sites were examined in this study.

2.1.1 Oyster River

The Oyster River (OR) site is located northwest of Courtenay B.C. (Figure 3.1) and from 1997 – 2010 was part of Fluxnet Canada's network of monitoring stations, which was a network of eddy-covariance flux towers across Canada in various forest types used to continuously monitor carbon exchanges between the forest and atmosphere (Coursolle et al., 2012). A central portion of this site was established in 1949 in a second-growth Douglas-fir (*Pseudotsuga menziesii*) dominated stand with some western hemlock (*Tsuga heterophylla*), western redcedar (*Thuja plicata*), and red alder (*Alnus rubra*) (Table 3.1) (Trofymow et al., 2008). The average estimated site index of these stands was 36 m, and the elevation at this site ranged from 259 meters to an average of 335 m and was moderately to strongly sloped (Table 3.1). Between 2010 and 2011, this central portion of the site was harvested in four blocks WH017, WH017a, WH017b, and WH017c (Trofymow et al., 2014).

2.1.2 Sooke Lake Watershed

The Sooke Lake watershed area is located near Victoria, B.C. and hosts two sites, Sooke Lake Watershed South (SWS) and Sooke Lake Watershed North (SWN) (Figure 3.1). Located at each site are young (est. 1960/1949), mature (est. 1892/1898), and old-growth (est. 1816/1695) stands

being monitored as part of the Coastal Forest Chronosequence project (Trofymow et al., 1997; Blackwell et al., 2002). Douglas-fir dominates the stands with additional western redcedar and western hemlock components and estimated site indices ranging from 24 to 39 m (Table 3.1). The average elevation at these sites ranged from 220 - 347 m at SWS and 250-491 m at SWN, and both sites had a range of slopes from moderate to very steep (Table 3.1). There was no harvesting in the three blocks at SWS or SWN. However, a nested sample design in which smaller inventory plots were nested inside larger stem-mapped demographic blocks (He & Duncan, 2000) allowed for a simulated harvest to be conducted, as described below, and post-harvest block-level data to be calculated.

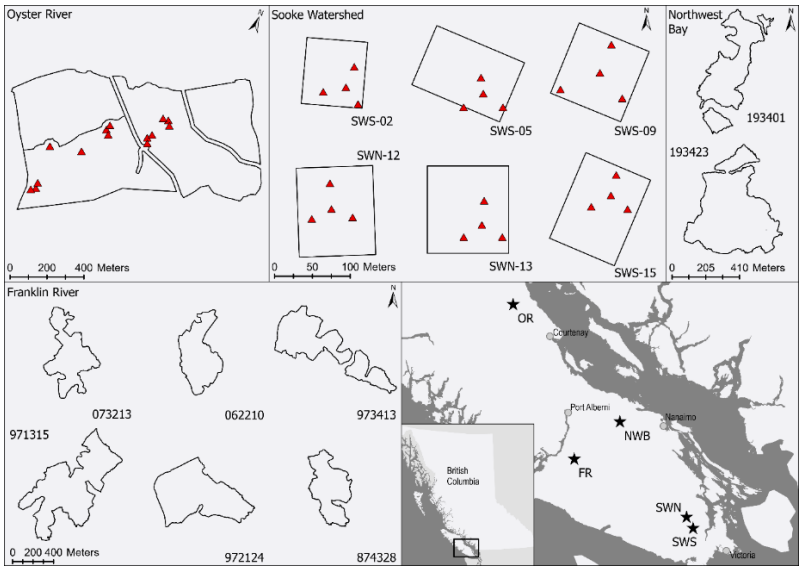

Figure 3.1. Study site map showing layouts of block boundaries (black lines) and sample plot locations (red triangles) at Oyster River (OR), Sooke Watershed South (SWS) and Sooke Watershed North (SWN), Northwest Bay (NWB), and Franklin River (FR). All sites are located in Douglas-fir dominated sites on Vancouver Island, with central site locations shown (stars) in the lower right panel.

2.1.3 Northwest Bay

The Northwest Bay (NWB) site is located west of Nanaimo B.C. (Figure 3.1) and had two blocks that were harvested in 2014 (Trofymow et al., 2019). Prior to harvest, both blocks were primarily

second-growth Douglas-fir with lesser amounts of western hemlock and western redcedar (Table 3.1). At NWB 193401, the stands were established between 1962 and 1965 and had site indices ranging from 18 m to 28 m with strong slopes (Table 3.1). NWB 193401 was higher in elevation (456 m) than most blocks at the OR, SWS, and SWN sites, although lower than SWN 15 (Table 3.1). At NWB 193423, the stands were established between 1959 and 1980 with site indices ranging from 21 m to 28 m and a slightly steeper slope than NWB 193401 (Table 3.1). The average elevation at NWB 193423 (612 m) was the highest of any of the blocks and was more than 150 m higher than NWB 193401 (Table 3.1). Both NWB 193401 and 193423 were harvested over the summer and fall of 2014 (Trofymow et al., 2017).

2.1.4 Franklin River

The Franklin River (FR) site is located south of Port Alberni, B.C. (Figure 3.1). The FR blocks were all composed of second-growth forests established between 1941 and 1948, and the main species present were mixtures of Douglas-fir, western hemlock, and western redcedar. However, some blocks had western hemlock as the dominant species and Douglas-fir as the secondary species, and one block included additional components of amabilis fir (*Abies amabilis*) (Table 3.1). The FR blocks had some of the lowest elevations of all sample blocks, but the overall range (132 – 348 m) was comparable with the other sites (Table 3.1). Alternatively, the slopes in the FR blocks were some of the highest (15 - 24°) but still within the range of other sites (Table 3.1). Harvesting of the six blocks at the FR site occurred between 2018 and 2019.

Table 3.1. Sample block site descriptions including earliest estimated establishment date (Est. Date), major species composition, main stand estimated site index (m), average block elevation (m ASL), average block slope (degrees) for blocks located at the Oyster River (OR), Sooke Watershed South (SWS), Sooke Watershed North (SWN), Northwest bay (NWB), and Franklin River (FR) sites. Major species include Douglas-fir (Fd), western hemlock (Hw), western red cedar (Cw), and amabilis fir (Ba).

Site	Block	Est. Date	Species	Site Index	Elevation	Slope	Harvest Year
OR	WH017	1949	FdHwCw	37.0	259	10	2011
OR	WH017a	1949	FdHwCw	36.0	328	11	2010
OR	WH017b	1949	FdHwCw	34.0	335	11	2011
OR	WH017c	1949	FdHwCw	37.0	275	7	2011
SWS	02	1960	FdHwCw	38.8	296	20	-
SWS	05	1892	FdCw	25.6	220	8	-
SWS	09	1816	FdCw	24.3	347	25	-
SWN	12	1949	FdCwHw	33.4	348	8	-
SWN	13	1898	FdCwHw	29.9	250	12	-
SWN	15	1695	Fd	29.9	491	21	-
NWB	193401	1962	FdCwHw	28.0	456	10	2014
NWB	193423	1959	FdHwCw	28.0	612	15	2014
FR	073213	1943	HwFd	34.2	281	15	2019
FR	062210	1945	FdHwCw	31.2	132	17	2018
FR	973413	1948	FdHw	29.5	316	23	2018
FR	971315	1941	HwFdBa	29.4	348	19	2019
FR	972124	1945	HwFd	27.5	192	17	2019
FR	874328	1943	FdHw	29.5	167	24	2019

2.2 Spatial Data

Spatial data for this study included pre-harvest LiDAR and imagery data, post-harvest imagery and photogrammetric point cloud, as well as pre- and post-harvest spatial boundaries. All spatial data were projected into a common coordinate system of NAD 1983 UTM zone 10n (EPSG: 29610), and block boundaries used to clip data to areas of interest were buffered by 100 m to limit the impacts of edge effects. Pre-harvest LiDAR acquisitions were performed in 2008 at the OR site (Hilker et al., 2010), 2012 at the SWS and SWN sites (Quinn, 2018), 2011 at the NWB site (Trofymow et al., 2014), and in 2016 at the FR site (S. Platt – Western Forest Products, personal communication, 10 January 2020) (Table 3.2). LiDAR points from each site were

classified into ground and non-ground points by vendors using various versions of the Terrascan software (Terrasolid, v021.023). All LiDAR point clouds were quality checked for errors such as duplicated points or air hits far above the canopy surface using the lidR package in R (Roussel et al., 2020). Point density was calculated using a 20 m resolution raster and was summarized in each block as the average of cells with centers within the block boundaries (Table 3.2). Point clouds were then normalized into heights above ground to remove the effects of local topography using the lidR package and a triangular irregular network (Roussel et al., 2020).

Pre-harvest orthoimagery was also acquired for the OR (2007), SWS (2013), SWN (2012/2013), NWB (2011), and FR (2016) sites. All imagery contained three channels (Red, Green, and Blue) and had various delivered spatial resolutions (Table 3.2). The imagery at the OR site, collected in 2007, had a timing offset from the LiDAR data, similar to imagery from the SWS site and SWN block 15 (Table 3.2). The imagery from SWN blocks 12 and 13 was collected coincidently with the LiDAR, similar to image acquisitions for the NWB and FR sites (Table 3.2). Imagery collected separately from the LiDAR acquisitions showed differences in absolute positioning of identifiable features compared to the LiDAR data. To geo-rectify imagery data to the LiDAR positioning, individual treetop positions were determined using image-based (Gougeon & Leckie, 2003) and point cloud-based (Roussel et al., 2020) methods. The treetop positions of large identifiable trees near the edge of gaps were used to rectify the imagery to match the absolute positioning of the LiDAR data.

Table 3.2: Point cloud and imagery characteristics and acquisition years. *Note imagery from SWN-15 from 2013 similar to SWS.

Site	Point Density	Image Resolution	LiDAR (Image) Year
OR	6.86	1.0	2008 (2007)
SWS	3.71	0.2	2012 (2013)
SWN	10.07	0.2	2012 (2012*)
NWB	23.13	0.1	2011 (2011)
FR	52.17	0.1	2016 (2016)

2.3 Spatial Data Processing

A point thinning method was used to address the large range in average point density between the different sites. This method randomly removed points from within a 25 m^2 window to a maximum density of 3 points m^{-2} and produced more consistent results across the entire block, particularly in areas of scan line overlap with the target density chosen based on the 25^{th} percentile of the calculated point densities in each block. Thinning was done to produce a similar point cloud structure through all study sites when generating point cloud metrics, as Tompalski et al. (2019) found that non-parametric implementations of the AB approach are sensitive to differences in point cloud structure among different sites. Canopy height models (CHMs) were produced using the thinned point clouds and a pit-free algorithm (Khosravipor et al., 2014), with intermediate TIN surfaces produced at 2, 5, 10, 15, 20, and 30 m, removing edges longer than 1.5 m.

An individual tree (IT) segmentation method was used to delineate individual tree crowns from the CHM and LiDAR point cloud to calculate metrics for each crown. A five-by-five Gaussian filter was used (sigma = 1.2) to smooth the CHMs for each block, and a local maximum filter with a circular 5 m radius window was used to identify treetop seed points. Using the treetop points and the smoothed CHM, the algorithm, based on the one described by Dalponte & Coomes (2016), segmented the point clouds into individual tree objects using a

minimum tree height of 2 m and two region growing thresholds (0.45, 0.55). The convex hull of identified LiDAR points was generated for each segmented tree and used as the IT crown delineations. This algorithm was chosen from a number of tested IT methods primarily for its ease of implementation and integration with the lidR package, as well as its observed consistency in the range of stand ages and conditions.

Next, a series of IT metrics were calculated from the segmented tree, including the crown area, the 95th percentile of the IT LiDAR height, and the average pixel values from the three imagery channels. Before the average imagery values were calculated, each image was resampled to 0.5 m to match the spatial resolution of the CHMs. Next, a bright pixel mask was created using the green channel and selecting pixels with a green value higher than the ITs average green value (Gougeon & Leckie, 2003). Next, the red, green, and blue channel averages were calculated for pixels within each ITs bright pixel mask. Finally, IT metrics were summarized using a rasterized grid with a 20 m resolution, matching the area of sample plots (0.04 ha), such that the average was calculated for the height, area, and imagery metrics for all trees that had their tops within a particular raster cell. Additionally, an IT density metric was calculated for each cell as the number of IT tops divided by the cell area (0.04ha).

A series of LiDAR metrics more common with traditional AB approaches were also generated using the same 20 m rasterized grid, similar in size to sample plots (0.04 ha). These predictor metrics included a combination of height, density, canopy cover, and statistical metrics similar to those produced and used by Kelley et al. (2021). In total, 34 AB metrics were created using the lidR package in R (Roussel et al., 2020) to be included with the six IT metrics (Table 3.3). Additionally, all point clouds and IT segmentations were clipped to the same extent as the

sample plots, and the same combination of 40 AB and IT metrics was generated at the plot level for the development of the HB model.

Table 3.3. Area based (AB) and individual tree (IT) style predictor metrics used for variable selection.

Class	Code	Description
AB	CanRelRatio	((mean ht - min ht)/(max ht-min ht))
AB	p1st_abv_2	Percentage 1st returns above 2m
AB	p1st_abv_Mean	Percentage 1st returns above mean ht
AB	p1st_abv_Mode	Percentage 1st returns above mode ht
AB	Zaad	Average absolute deviation (AD) of ht
AB	Zl1	First L moment
AB	Zl2	Second L moment
AB	Zlcv	L-moment coefficient of variation
AB	Zlkur	L-moment kurtosis
AB	Zlskew	L-moment skewness
AB	Zmadmed	Median of the AD from the overall median
AB	Zmadmod	Median of the AD from the overall mode
AB	ZquadMean	Quadratic mean of ht
AB	zq10-95	Xth percentile of height distribution (10,20,25,30,40,50,60,70,75,80,90,95)
AB	Zpcum1-9	Cumulative percentage of returns in the Xth decile (1-9)
IT	IT_TTDens	Individual tree density (# ha^{-1})
IT	IT_z95	95^{th} percentile of individual tree LiDAR points
IT	IT_crownarea	Individual tree crown area
IT	IT_redspec	Individual tree mean red channel
IT	IT_greenspec	Individual tree mean green channel
IT	IT_bluespec	Individual tree mean blue channel

2.4 Training Data From Plots at the OR, SWS and SWN Sites

Data from sample ground plots at OR, SWS, and SWN were used as the training data for the HB model. At the OR site, during the 2009 growing season, 14 circular sample plots with an area of

0.04 ha were measured following Canada's National Forest Inventory sampling guidelines (National Forest Inventory, 2008). Measurements recorded included species, diameter at breast height (DBH), and height for all trees >= 1.3m in height within the plot areas. At the SWS and SWN sites, similar measurements were recorded for trees within sample plots (4 per block) during the 2014 growing season. Sample plots in SWS 09 were 0.04 ha in size, whereas plots in all other blocks at SWS and SWN were 0.03 ha.

Total and merchantable volumes in the plots were determined from individual tree volumes calculated using the tree species, DBH, and height data, as input to regional taper equations developed by Kozak (1994). For each tree, jurisdictional timber criteria and available timber cruise data helped determine the merchantability parameters, set as a 30 cm stump height, 10 cm top height, 12.5 cm minimum DBH, and a 10 m log length (Timber Pricing Branch, 2011). At the old-growth plots in SWS-09 and SWN-15, the minimum DBH limit was increased to 17.5 cm to match merchantability limits of coastal old-growth stands (Timber Pricing Branch, 2011). The volume of each tree that met the merchantability limits was used to populate the initial merchantable volume pool (Figure 3.2). Next, sampled trees identified as dead standing had all merchantable volumes transferred to the non-merchantable pool (Figure 3.2). A final merchantable volume net-down of 6% for conifer species and 9% for deciduous species was subtracted from each live tree's merchantable volume and added to the non-merchantable volume pool. The net-down values were determined from averaging species-specific reductions applied in available timber cruise data from the FR blocks.

Tree volume that belonged to undersized stems (<12.5/17.5cm DBH) (not including stumps or tops) and/or the short (< 10m) logs were used to populate the initial non-merchantable volume pool (Figure 3.2), followed by the addition of dead trees and the net-down portion of the

live tree merchantable volume described above. Then, for each sample plot, the total merchantable and non-merchantable volumes for all trees were summed and plot merchantable and non-merchantable volume densities (m^3ha^{-1}) calculated and used for the HB model training.

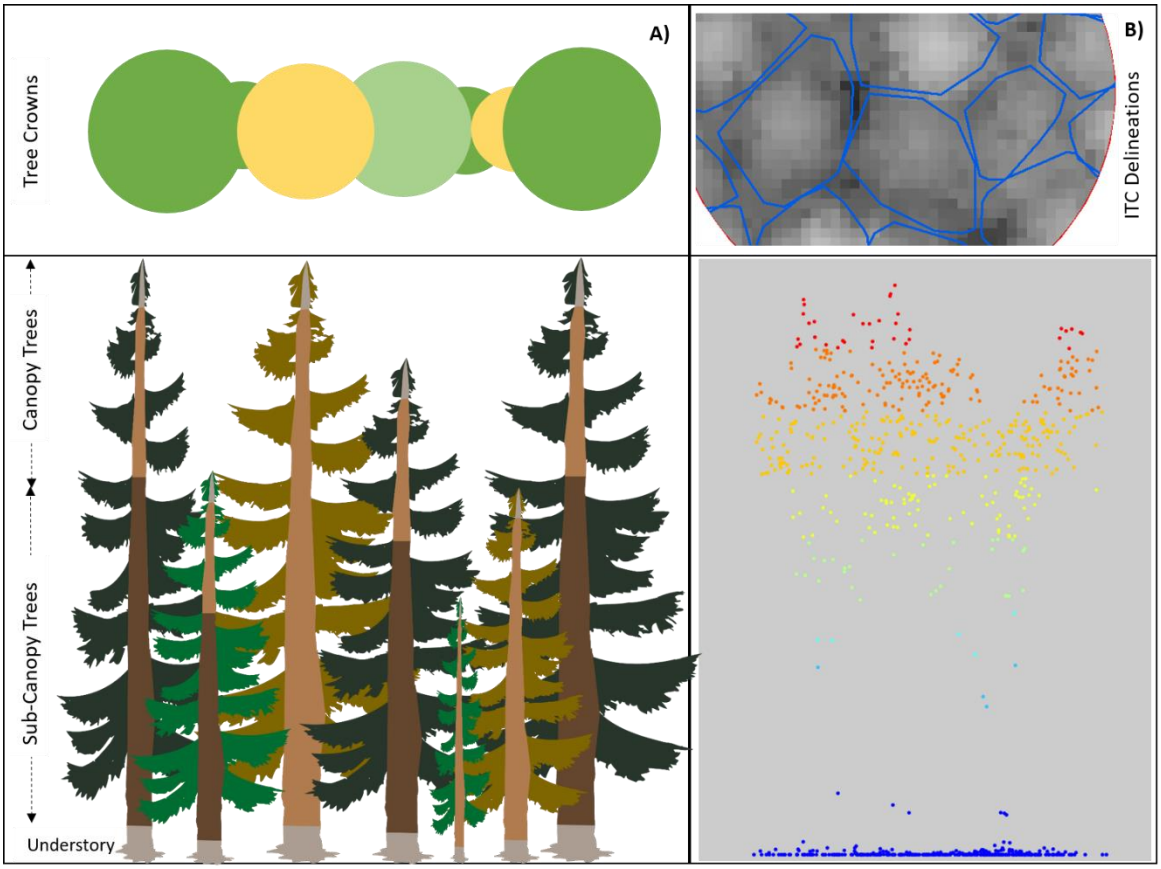

Figure 3.2. (A) Diagram depicting the areal appearance of the canopy and sub-canopy tree crowns (top) and the structure of a complex forest with live (dark and light green crown, respectively) and dead (yellow crown) trees that make up the canopy and sub-canopy. Also shown is the stem wood components of merchantable stem wood (>=12.5/17.5 cm DBH & 10 m length) (dark brown), non-merchantable stem wood (>= 10 cm diameter & < 10 m length) (light brown), and stumps and tops (grey). B) Data representations of an individual tree delineation for OR plot 11.3 (top) and the corresponding LiDAR point cloud (bottom).

2.5 Hybrid Model Development

The forty combined metrics for each of the 38 sample plots were used in a Boruta feature selection routine to select a subset of training metrics for both the merchantable and non-merchantable volume models. Boruta feature selection is a method popularly used for models with many predictor metrics and, more recently, in implementations of LiDAR EFI models (Kelley et al., 2021, Blackburn et al., 2021). First, for each volume component, the Boruta method adds copies of the predictor metrics that are randomly permuted noise metrics (Kursa & Rudnicki, 2010). Next, over 1000 random forest (RF) iterations, the algorithm tracks the RF variable importance scores and calculates the z-scores for each of the expanded set of predictor metrics, comparing z-scores between the original metrics and the noise metrics (Kursa & Rudnicki, 2010). The final selected metrics are those metrics that have a significantly higher z-score than the highest scoring noise variable.

RF models for both the merchantable and non-merchantable volume components were fit using the Boruta reduced predictor metrics. Models were trained using 1000 regression trees and the caret (Kuhn, 2008) and random forest (Liaw & Wiener, 2002) packages in R in a five-times repeated 10-fold cross-validation method (White et al., 2015). Using this training method results in 50 independent cross-validation observations used to assess model performance by calculating the absolute and relative root mean square error (RMSE) and bias (White et al. 2015). Each model was then expanded to the block areas using the suite of raster-based predictor metrics. For each cell with a centroid within the block boundaries, the cell's predicted volume density was multiplied by the cell area (0.04 ha), and the total block merchantable or non-merchantable volume was summed and divided by the total block area to calculate block-level densities (m^3ha^{-1}) of predicted merchantable and non-merchantable volume.

2.6 Sources of Block-level Data for Testing Hybrid Models

The HB models were trained and parameterized using plot data from the OR, SWN and SWS sites. The trained models were then expanded to the harvest blocks at the OR, SWN, and SWS sites and transferred to the harvest blocks at the NWB and FR sites, which had no prior training and were then tested against block-level data for all five sites. While the OR, NWB, and FR sites had post-harvest block-level measurements of merchantable and non-merchantable volumes, the demographic blocks at SWS and SWN were not harvested, and so a simulated harvest was conducted. In the SWS and SWN demographic blocks, species and diameter measurements were recorded for all trees and heights for a subset of trees. For those trees missing height measurements, a Chapman-Richards function was used to estimate height with parameters fit using data from trees that had both height and diameter measurements similar to Kelley et al. (2021) and Metsaranta et al. (2018). A simulated harvest was then done for all trees in a block, and total merchantable and non-merchantable volumes were calculated using the same merchantability limits as described above for the sample plots.

Estimates of block-level merchantable volumes (m^3ha^{-1}) derived from the HB models were compared to two independent sources of merchantable volume. The first came from traditional forest cover data used to calculate pre-harvest volumes in each block. The traditional forest cover data used was a mixture of polygonal inventories that were derived through air photo interpretation (for the SWS and SWN sites), such as the BC Vegetation Resource Inventory (Province of British Columbia, 2021) or from internal industry inventories derived from timber cruising (for the OR, NWB and FR sites). The second source of merchantable volume data at the OR, NWB, and FR sites, provided by the operating companies, was the scaled volume for logs transported to a log sort. Therefore, at the SWS and SWN sites, the calculated

merchantable volumes from the simulated harvest of the demographic blocks were used as a proxy for the harvest scale volumes.

Estimates of modelled block-level non-merchantable volumes (m^3ha^{-1}) at the OR, NWB, and FR sites were compared to two independent sources of post-harvest residue volumes. The first source was from the provincial standard waste and residue survey (WRS) sample plots measured on each block post-harvest (Province of British Columbia, 2018). The second used a geospatial semi-automated log delineation (SLD) method for dispersed residues while bulk pile volumes and packing ratios were used to determine accumulations and piled residues (P method) (Trofymow et al., 2017, 2019) to perform a complete census of residues in the entire post-harvest block. The harvest block and WRS sampling stratum boundaries were digitized for all blocks using very high resolution (2cm) post-harvest imagery obtained from remotely piloted aircraft. Non-merchantable WRS volume estimates were determined using the digitized stratum areas and the average stratum densities from WRS sampling plots. Total block density (m^3ha^{-1}) was calculated by summing all stratum totals and dividing by the total block area (Trofymow et al., 2014). Non-merchantable volume estimates were also determined using the SLD method for the dispersed and light-roadside stratums and the P method for the heavy-roadside and piled stratums (Trofymow 2017, 2019). The total block densities were determined by summing SLD and P stratum totals (SLDP method) and dividing by the total block area (Trofymow 2017). At the SWS and SWN sites, the calculated non-merchantable volume from the simulated harvest of the demographic blocks was used as a proxy for the WRS volume measurements.

2.7 Hybrid Model Testing and Comparisons

For each block, the total summed merchantable volume from the pre-harvest HB model, pre-harvest forest cover, and post-harvest scale was divided by the area of the digitized block

boundaries to determine total merchantable volume densities (m^3ha^{-1}). The block volume densities for the two pre-harvest sources were compared to the post-harvest scale in paired t-tests (Blackburn et al., 2021). The Shapiro-Wilk normality test was used to investigate if the differences between sources were normally distributed. Additionally, the difference between the post-harvest scale and each of the two pre-harvest methods (Post-harvest – Pre-harvest) was calculated for comparison.

Total non-merchantable volumes were also summed to a block total divided by the digitized area (m^3ha^{-1}) for the pre-harvest HB model results, the post-harvest WRS estimates, and the post-harvest SLDP estimates. Similar to the merchantable volumes, paired t-tests were used to compare the pre-harvest HB model with the two post-harvest methods, and the Shapiro-Wilk test was also used to test for normality of the method differences. Finally, the differences between each of the two post-harvest methods and the pre-harvest model results (Post-harvest – Pre-harvest) were calculated for comparison.

3. Results

3.1 Variable Selection

The Boruta feature selection method reduced the original 40 metrics to 16 metrics for the merchantable volume component (Figure 3.3). The average variable importance scores ranged from 2.5 to 7.7 for the selected variables, which were dominated mainly by height metrics. The average 95^{th} percentile of individual tree (IT) height was the only IT metric selected for the merchantable volume component. However, it scored higher on average than similar maximum height metrics (zq90 and zq95) from the traditional AB metrics and was within the top ten selected metrics (Figure 3.3). For the non-merchantable component, the Boruta method resulted in a more considerable reduction down to 10 metrics from the original 40 (Figure 3.3). The

average importance scores for the selected metrics ranged from 2.9 to 4.3 and contained a mixture of all types of predictor metric classes (height, density, statistical, and IT). The highest scoring IT variable was the average blue channel from the tree crowns and was the third-highest scoring variable overall for the non-merchantable volume component (Figure 3.3).

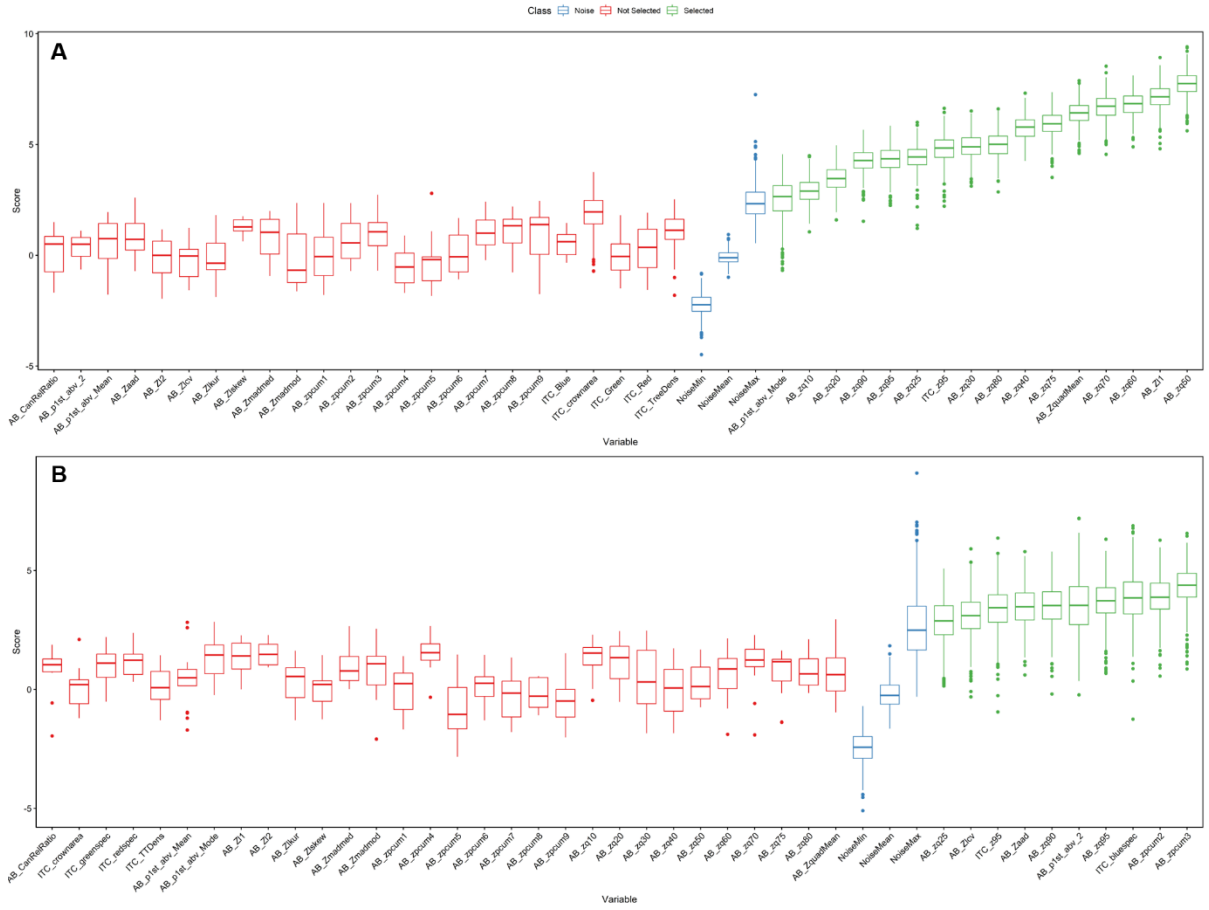

Figure 3.3: Boruta variable selection results showing the distribution of variable importance scores for the merchantable volume component (A) and non-merchantable volume component (B). Green indicates selected metrics, blue indicates noise or shadow metrics, and red is those metrics deemed not important to the model.

3.2 Model Fitting and Expansion

The Hybrid (HB) merchantable volume model showed an R^2 value of 0.75 with a cross-validated (CV) root mean square error (RMSE) of 240.11 m^3ha^{-1} (34.7%) and a bias of -45.07 m^3ha^{-1} (-

6.5%). Examining the plot level model predictions against the measured observations shows a variable bias, with predictions being the furthest from observations in the plots with the largest observed volumes, SWS 09 and SWN 15 (15-S) (Figure 3.4). The non-merchantable volume HB model showed a lower R^2 value of 0.49, but the CV RMSE of 52.28 m^3ha^{-1} (38.0%) was in a similar relative range as the merchantable volume model. The CV bias of -2.14 m^3ha^{-1} (-1.6%) for the non-merchantable volume was smaller than the merchantable model. The plot-level model predictions versus the observed measurements show a higher amount of variable bias than the merchantable volume model, although the largest discrepancies were also in the plots with the highest observed non-merchantable volumes (Figure 3.4).

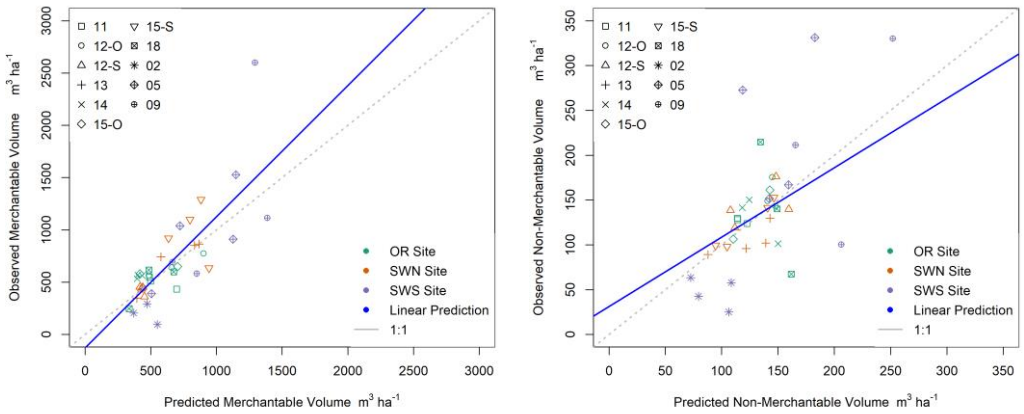

Figure 3.4: Observed plot level vs. RF predicted merchantable (Left) and non-merchantable volumes at the Oyster River (OR) (green), Sooke Watershed South (SWS) (Purple), and Sooke Watershed North (SWN) (orange) sites

Applying the merchantable volume HB model to the block level showed that the average merchantable volume in the OR blocks, 538 m^3ha^{-1}, was slightly lower than averages at the other sites with plot-level training data (SWS = 795 m^3ha^{-1}, SWN = 608 m^3ha^{-1}). However, this is due

mainly to the old-growth blocks SWS-09 and SWN-15 (Table 3.4). The NWB site had the lowest average merchantable volume model estimate of 339 $m^3ha^{-1,}$ and the average at the FR site of 655 m^3ha^{-1} was within the range of the other blocks that had training data. Similarly, the non-merchantable volume model showed a lower average value in the OR site (124 m^3ha^{-1}) than in the other training sites (SWS = 144 m^3ha^{-1}, and SWN = 129 m^3ha^{-1}).

Table 3.4. Block digitized areas and block-level HB random forest model estimates of merchantable (m^3ha^{-1}) and non-merchantable volumes (m^3ha^{-1}).

Site	Block	GIS Area	Merchantable Volume	Non-Merchantable Volume
OR	WH017	11.44	607.63	131.02
OR	WH017a	24.29	518.36	126.95
OR	WH017b	18.16	538.49	130.23
OR	WH017c	22.59	579.99	128.43
SWS	02	0.704	352.54	78.35
SWS	05	1.066	877.71	176.05
SWS	09	1.000	1156.14	178.38
SWN	12	1.188	406.05	130.02
SWN	13	1.240	670.08	140.23
SWN	15	1.139	749.32	116.19
NWB	193401	11.59	352.21	123.97
NWB	193423	20.30	363.03	128.66
FR	073213	17.58	774.20	155.55
FR	062210	16.64	606.05	138.79
FR	973413	27.95	615.02	136.68
FR	971315	36.58	550.36	142.80
FR	972124	29.92	635.92	147.93
FR	874328	16.35	750.96	150.26

However, while the NWB site still showed the lowest average non-merchantable volumes (120 m^3ha^{-1}), the difference from the range of the training sites was not as large. Additionally, the non-merchantable volumes estimated in the FR sites had shown on average 145 m^3ha^{-1}, which was slightly higher than the highest value in the training sites.

3.3 Comparison of HB Model Estimates with Block-level Data

3.3.1 Merchantable Volumes

Preharvest merchantable volume estimates from forest cover data were consistently lower on average in all blocks than the actual or simulated harvest scale data, with the largest average absolute difference being at the SWS, SWN, and NWB sites (Table 3.5). Paired t-test results showed a significant difference between the forest cover and harvest scale data ($t = -2.65$, p-value = 0.017). In addition, the pre-harvest HB model estimates showed more variability of over and under-estimations of the harvest scale compared to the forest cover data. On average, the HB model overestimated merchantable volumes at the SWS and SWN sites and showed underestimates at all other sites (Table 3.5). In contrast to the forest cover data, the results from paired t-test comparison of merchantable volume from the harvest scales to the HB model indicated no significant difference between the means of the two methods ($t = 1.30$, p-value = 0.211). On average, across all blocks, the absolute difference in merchantable volume between the harvest scale and the forest cover was 27% of the average harvest scale, whereas, for the HB model estimates, the average absolute difference was 17% of the average harvest scale.

3.3.2. Non-merchantable volumes

Preharvest estimates of non-merchantable volume from the HB model were continuously higher on average than the post-harvest estimates from the waste and residue survey (WRS) (Table 3.6). The paired t-test across all blocks showed that the means between these two methods were significantly different ($t = 6.08$, p-value = < 0.001). Alternatively, compared to the semi-automated log delineation plus piles (SLDP) estimates, the HB model results are more variable, with the majority of blocks showing model results to be lower than SLDP estimates (Table 3.6). The paired t-test across those blocks with an SLDP method applied showed no significant difference between method means ($t = -1.55$, p-value = 0.150). Across all blocks, the average

absolute difference between the WRS and HB model results was 47% of the WRS average, where the average absolute difference between the SLDP and HB model results was much lower and only 20% of the SLDP average (Table 3.6).

Table 3.5. Block merchantable volumes (m^3ha^{-1}) for the post-harvest scale (HS), pre-harvest forest cover (FC), pre-harvest hybrid model (HB), and differences in pre-harvest estimates from post-harvest validation. Average differences use the absolute value of block differences. SE – Standard Error.

Site	Block	HS Volume	FC Volume	HB Volume	FC-HS Volume	HB-HS Volume
OR	WH017	647	559	608	-88	-40
OR	WH017a	564	559	518	-5	-46
OR	WH017b	656	337	538	-319	-118
OR	WH017c	557	559	580	2	23
OR	Avg	606	504	561	104	57
	(SE)	(26)	(56)	(20)	(75)	(21)
SWS	02	270	533	353	263	83
SWS	05	946	672	878	-274	-69
SWS	09	994	741	1156	-253	162
SWS	Avg	737	649	796	263	104
	(SE)	(234)	(61)	(236)	(6)	(29)
SWN	12	293	396	406	103	113
SWN	13	436	598	670	162	234
SWN	15	976	497	749	-479	-226
SWN	Avg	568	497	608	248	191
	(SE)	(208)	(58)	(104)	(117)	(39)
NWB	193401	419	241	352	-178	-67
NWB	193423	519	202	363	-317	-156
NWB	Avg	469	222	358	248	112
	(SE)	(50)	(20)	(5)	(70)	(45)
FR	073213	825	550	774	-275	-51
FR	062210	672	582	606	-90	-66
FR	973413	738	569	615	-169	-123
FR	971315	755	700	550	-55	-205
FR	972124	838	841	636	3	-202
FR	874328	708	560	751	-148	43
FR	Avg	756	634	655	123	115
	(SE)	(27)	(47)	(36)	(39)	(30)
Total	Avg	656	539	617	177	113
	(SE)	(51)	(38)	(48)	(31)	(16)

Table 3.6. Block non-merchantable volumes (m^3ha^{-1}) for the post-harvest waste and residue survey (WRS) estimate, post-harvest semi-automated log delineation plus piles (SLDP) residue estimate, pre-harvest hybrid (HB) model predictions, and differences between pre-harvest estimates and post-harvest values. Average volume differences use the average absolute difference. SE – Standard Error.

Site	Block	WRS	SLDP	HB Model	HB - WRS	HB - SLDP
OR	WH017	120	157	131	-11	26
OR	WH017a	67	174	127	-60	48
OR	WH017b	58	178	130	-73	48
OR	WH017c	110	189	128	-19	60
OR	Avg	89	175	129	40	46
	(SE)	(15)	(7)	(1)	(15)	(7)
SWS	02	49	-	78	-30	-
SWS	05	163	-	176	-13	-
SWS	09	168	-	178	-10	-
SWS	Avg	127	-	144	17	-
	(SE)	(39)		(33)	(6)	
SWN	12	109	-	130	-21	-
SWN	13	74	-	140	-66	-
SWN	15	130	-	116	14	-
SWN	Avg	104	-	129	34	-
	(SE)	(16)		(7)	(16)	
NWB	193401	76	87	124	-48	-37
NWB	193423	72	85	129	-56	-44
NWB	Avg	74	86	127	53	41
	(SE)	(2)	(1)	(2)	(4)	(3)
FR	073213	75	166	156	-81	10
FR	062210	58	158	139	-80	19
FR	973413	117	168	137	-19	31
FR	971315	59	146	143	-84	3
FR	972124	80	133	148	-68	-15
FR	874328	108	178	150	-42	28
FR	Avg	83	158	146	63	18
	(SE)	(18)	(12)	(5)	(18)	(7)
Total	Avg	94	152	137	44	31
	(SE)	(8)	(8)	(5)	(6)	(5)

4. Discussion

Overall, this study demonstrates that a hybrid (HB) enhanced forest inventory modelling approach effectively estimates merchantable and non-merchantable volumes at the harvest block level. Individual tree (IT) metrics were ranked higher than Boruta noise variables in both HB

models, and for the non-merchantable model, IT metrics were among the top 3 ranked metrics (Figure 3.3b). For the merchantable volume HB model, selected metrics were primarily height percentiles, including the selected IT metric (Figure 3.3a). The selected metrics were similar to other applications of traditional area-based (AB) models (Latifi et al., 2010; White et al., 2014; Woods et al., 2008) and HB models (Kankare et al., 2013) that estimate forest volume, where height percentile metrics were consistently the highest-ranked or final selected metrics. One of the highest-ranked metrics for the non-merchantable HB model was the IT blue channel metric (Figure 3.3b). The high ranking of this metric is believed to be driven by ITs that are dead standing and made up entirely of non-merchantable wood, as was seen in sample plots at SWS 05. Interestingly, using the blue image channel from RGB imagery is similar to the procedures in the semi-automated log delineation (SLD) method to detect post-harvest logging residues (Trofymow et al., 2017).

Despite relying on much fewer training sample plots (38), HB model fits for both merchantable and non-merchantable volume components with RMSE values of 34.7% and 38.0%, respectively, were similar to total or merchantable volume estimates from other studies in complex coniferous forests using non-parametric modelling (RMSE: 23.3 – 31.4% (Latifi et al., 2010); RMSE: 17.9% (Vastaranta et al., 2013); RMSE: 33.2% (White et al., 2015)). For example, White et al. (2014) utilized 788 sample plots to fit an AB model with an RMSE of 26% when estimating merchantable volumes in Alberta, and Kankare et al. (2013) utilized 254 sample plots to fit a HB style model in coniferous forests of southern Finland with RMSEs ranging from 26.4% - 34.0%. In addition, recent implantations of a combination approach in pine forests of the southern United States utilized 1680 training plots to create HB style models of volume that had normalized RMSE values ranging from 34.6% to 42.6% (Blackburn et al., 2021).

The results from this study also highlight the potential for the transferability of EFI models. The HB merchantable volume model results had average absolute differences of 9% - 34% of the harvest scale in harvest blocks with available plot-level training data (Table 3.5). When the HB model was transferred to harvest blocks without pre-harvest plot-level training data, the average absolute difference from the harvest scale was within a similar range of 15% - 24%. A sample plot analysis of model transferability found that using the same LiDAR acquisition, models trained in one area could be successfully transferred to similar forest areas with no major increases to plot-level RMSE (Tompalski et al., 2019). However, Kotivuori et al. (2016) found that both forest structure and LiDAR sensor had considerable effects on volume model accuracy. For this study, LiDAR acquisitions took place over several years with various sensor platforms, possibly increasing the variability of results between sites.

Not surprisingly, the merchantable volume estimates from forest cover data for blocks with timber cruising data (OR, NWB, FR) were on average closer to harvest scales compared to forest cover estimates derived solely from air photo interpretation. At the Franklin River site, blocks that had hemlock as the leading dominant species instead of Douglas-fir also tended to show the largest differences between the harvest scale and the HB merchantable volume results, indicating a possible lack of stability in model transferability as stand species characteristics change. This is not surprising as western hemlock and Douglas-fir dominated stands will appear similar in point could structure despite having slightly different tapers and densities **(**Poudel et al., 2018; Miles & Smith, 2009). This is also similar to Tompalski et al.'s (2019) findings where random forest model predictions of wood volume decreased as the proportions of hemlock and Douglas-fir changed between sites with otherwise similar stand characteristics.

Comparing the merchantable volume results against the harvest scale showed that the HB model performed better than the forest cover data for this study. The HB model showed that the average absolute difference across all blocks was 17% of the average harvest scale, where for the forest cover data, the average absolute difference was 27% of the harvest scale. These results are higher than the AB model results reported by White et al. (2014) were on average, models predicted 6.7% less than the harvest scale. However, White et al. (2014) reported a difference of 23.7% between the merchantable volume estimates from forest cover data and the harvest scales. The stands examined by White et al. (2014) were higher elevation and covered a lower overall volume distribution compared to the coastal forest in this study and the old-growth plots that were at SWS and SWN, which could explain the increased differences between HB merchantable volume and harvest scales in this study.

Comparisons of non-merchantable volume estimates show that HB model results were higher and significantly different from waste and residue survey (WRS) estimates and lower and not significantly different from semi-automated log delineation plus piles estimates (SLDP). Previous research comparing WRS and SLDP methods found that particularly for the piled and heavy roadside stratums, WRS methods can lead to underestimates of residue volumes depending on sampling intensity (Trofymow et al., 2014). In the OR and NWB sites, the number of WRS sample plots per stratum was much greater than at the FR sites, and thus the differences between the WRS and SLDP methods were lower at these sites (Table 3.6). In another approach utilizing LiDAR data, Heinaro et al. (2021) attempted to segment the LiDAR point cloud to detect coarse woody debris under the canopy. Results indicated that point density and stand characteristics such as canopy cover significantly impacted making accurate ground classifications and resolving the under-canopy structure (Heinaro et al., 2021).

5. Conclusion

The results of this study demonstrate an ability for a hybrid enhanced forest inventory model to be used for pre-harvest estimations of non-merchantable volume that can be left post-harvest as logging residues. Additionally, this study highlighted that individual tree metrics could rank as important predictor metrics when using a Boruta variable selection method. This study also demonstrated the transferability of area-based models to areas with stable and similar point cloud structure, after point thinning, and similar forest structure characteristics. Future work should examine if completing segmentations before point cloud thinning offers any improvements or if the inclusion of other environmental or voxelized predictor metrics offers improved forest inventory estimates of merchantable and non-merchantable wood volumes. With further advancements, a hybrid enhanced forest inventory model could assist with forecasting non-merchantable wood volume available from future harvest blocks for use as bioenergy fuel or bioproducts such as wood pellets. Better forecasting of non-merchantable wood volumes allows for the economic evaluation of extracting these materials before they are cut and start to decompose. Additionally, the methods demonstrated here provide forest managers with the opportunity to analyze block-level harvest efficiencies rapidly.

References

Barrette, J., Paré, D., Manka, F., Guindon, L., Bernier, P., & Titus, B. (2018). Forecasting the spatial distribution of logging residues across the Canadian managed forest. Canadian Journal of Forest Research, 48(12), 1470-1481. doi:10.1139/cjfr-2018-0080

Blackburn, R. C., Buscaglia, R., & Sanchez Meador, A. (2021). Mixtures of airborne lidar-based approaches improve predictions of forest structure. Canadian Journal of Forest Research, https://doi.org/10.1139/cjfr-2020-0506

Blackwell, B. A., Trofymow, J. A., Hedberg, H. A., & Pacific Forestry Centre. (2002). Stand structure and species composition in chronosequences of forests on southern Vancouver Island. Natural Resources Canada, Canadian Forest Service, Pacific Forestry Centre.

Cambero, C., Sowlati, T., Marinescu, M., & Röser, D. (2015). Strategic optimization of forest residues to bioenergy and biofuel supply chain. International Journal of Energy Research, 39(4), 439-452. https://doi.org/10.1002/er.3233

Coursolle, C.; Margolis, H.A.; Giasson, M.; Bernier, P.; Amiro, B.D.; Arain, M.A.; Barr, A.G.; Black, T.A.; Goulden, M.L.; McCaughey, J.H. (2012). Influence of stand age on the magnitude and seasonality of carbon fluxes in Canadian forests. Agric. For. Meteorol. 165, 136–148, doi:10.1016/j.agrformet.2012.06.011.

Dalponte, M., & Coomes, D. A. (2016). Tree-centric mapping of forest carbon density from airborne laser scanning and hyperspectral data. Methods in Ecology and Evolution, 7(10), 1236–1245. https://doi.org/10.1111/2041-210X.12575

Donager, J. J., Sánchez Meador, A. J., & Blackburn, R. C. (2021). Adjudicating perspectives on forest structure: How do airborne, terrestrial, and mobile lidar-derived estimates compare? Remote Sensing, 13(12), 2297. doi:10.3390/rs13122297

Dymond, C. C., Titus, B. D., Stinson, G., & Kurz, W. A. (2010). Future quantities and spatial distribution of harvesting residue and dead wood from natural disturbances in Canada. Forest Ecology and Management, 260(2), 181-192. https://doi.org/10.1016/j.foreco.2010.04.015

Dymond, C. C., & Kamp, A. (2014). Fibre use, net calorific value, and consumption of forest-derived bioenergy in British Columbia, Canada. Biomass & Bioenergy, 70, 217-224. https://doi.org/10.1016/j.biombioe.2014.08.023

Ferster, C. J., Coops, N. C., & Trofymow, J. A. T. (2009). Aboveground large tree mass estimation in a coastal forest in British Columbia using plot-level metrics and individual tree detection from lidar. Canadian Journal of Remote Sensing, 35(3), 270–275. https://doi.org/10.5589/m09-014

Gougeon, F. A., Leckie, D. G., & Pacific Forestry Centre. (2003). Forest information extraction from high spatial resolution images using an individual tree crown approach. Victoria: Natural Resources Canada, Canadian Forest Service, Pacific Forestry Centre.

He, F., & Duncan, R. P. (2000). Density-dependent effects on tree survival in an old-growth Douglas fir forest. The Journal of Ecology, 88(4), 676-688. https://doi.org/10.1046/j.1365-2745.2000.00482.x

Heinaro, E., Tanhuanpää, T., Yrttimaa, T., Holopainen, M., & Vastaranta, M. (2021). Airborne laser scanning reveals large tree trunks on forest floor. Forest Ecology and Management, 491, 119225. https://doi.org/10.1016/j.foreco.2021.119225

Hilker, T., van Leeuwen, M., Coops, N. C., Wulder, M. A., Newnham, G. J., Jupp, D. L. B., & Culvenor, D. S. (2010). Comparing canopy metrics derived from terrestrial and airborne laser scanning in a douglas-fir dominated forest stand. Trees, 24(5), 819-832. doi:10.1007/s00468-010-0452-7

Holopainen, M., Vastaranta, M., Rasinmäki, J., Kalliovirta, J., Mäkinen, A., Haapanen, R., Melkas, T., Yu, X., & Hyyppä, J. (2010). Uncertainty in timber assortment estimates predicted from forest inventory data. European Journal of Forest Research, 129(6), 1131-1142. https://doi.org/10.1007/s10342-010-0401-4

Hyyppä, J., Yu, X., Hyyppä, H., Vastaranta, M., Holopainen, M., Kukko, A., … Alho, P. (2012). Advances in forest inventory using airborne laser scanning. Remote Sensing, 4(5), 1190–1207. https://doi.org/10.3390/rs4051190

IPCC 2014. (2013). Revised supplementary methods and good practice guidance arising from the Kyoto Protocol, Hiraishi, T., Krug, T., Tanabe, K., Srivastava, N., Baasansuren, J., Fukuda, M., and Troxler, T.G. (eds) Published: IPCC, Switzerland.

Jucker, T., Caspersen, J., Chave, J., Antin, C., Barbier, N., Bongers, F., Dalponte, M., van Ewijk, K.Y., Forrester, D.I., Haeni, M, Higgins, S.I., Holdaway, R.J., Iida, Y., Lorimer, C., Marshall, P.L., Momo, S., Moncrieff, G.R., Ploton, P., Lourens, P., … Coomes, D. A. (2017). Allometric equations for integrating remote sensing imagery into forest monitoring programmes. Global Change Biology, 23(1), 177–190. https://doi.org/10.1111/gcb.13388

Kankare, V., Vastaranta, M., Holopainen, M., Räty, M., Yu, X., Hyyppä, J., Hyyppä, H., Alho, P., & Viitala, R. (2013). Retrieval of forest aboveground biomass and stem volume with airborne scanning LiDAR. Remote Sensing, 5(5), 2257–2274. https://doi.org/10.3390/rs5052257

Kelley, J., Trofymow, J.A., Metsaranta, J. M., Filipescu, C. N., & Bone, C. (2021). Use of multi-temporal LiDAR to quantify fertilization effects on stand volume and biomass in late-rotation coastal Douglas-fir forests. Forests, 12(517), 517. https://doi.org/10.3390/f12050517

Khosravipour, A., Skidmore, A. K., Isenburg, M., Wang, T., & Hussin, Y. A. (2014). Generating pit-free canopy height models from airborne Lidar. Photogrammetric Engineering & Remote Sensing, 80(9), 863–872. https://doi.org/10.14358/PERS.80.9.863

Korhonen L., Peuhkurinen J., Malinen J., Suvanto A., Maltamo M., Packalen P., Kangas J. (2008). The use of airborne laser scanning to estimate sawlog volumes. Forestry: An International Journal of Forest Research, 81:4, Pages 499–510, https://doi-org.ezproxy.library.uvic.ca/10.1093/forestry/cpn018

Kotivuori, E., Korhonen, L., & Packalen, P. (2016). Nationwide airborne laser scanning based models for volume, biomass and dominant height in Finland. Silva Fennica (Helsinki, Finland : 1967), 50(4)https://doi.org/10.14214/sf.1567

Kozak, A. 1994. Development of Taper Equations by BEC Zones and Species. Retrieved from: https:// www.for.gov.bc.ca/hfd/library/documents/bib95354a.pdf. (accessed 20 October, 2018).

Kuhn, M. (2008). Building predictive models in R using the caret package. Journal of Statistical Software, 28(5), 1 - 26. doi:http://dx.doi.org/10.18637/jss.v028.i05

Kursa, M.B.; Rudnicki, W.R. (2010) Feature selection with the Boruta package. J. Stat. Softw. 36, doi:10.18637/jss.v036.i11.

Latifi, H., Nothdurft, A., & Koch, B. (2010). Non-parametric prediction and mapping of standing timber volume and biomass in a temperate forest: Application of multiple optical/LiDAR-derived predictors. Forestry (London), 83(4), 395-407.

Li, W., Guo, Q., Jakubowski, M. K., & Kelly, M. (2012). A new method for segmenting individual trees from the Lidar point cloud. Photogrammetric Engineering & Remote Sensing, 78(1), 75–84. https://doi.org/10.14358/PERS.78.1.75

Liaw, A. & Wiener, M., (2002). Classification and Regression by Random Forest. R News 2(3), 18--22.

Mansuy, N., Paré, D., Thiffault, E., Bernier, P. Y., Cyr, G., Manka, F., Lafleur, B., & Guindon, L. (2017). Estimating the spatial distribution and locating hotspots of forest biomass from harvest residues and fire-damaged stands in Canada's managed forests. Biomass & Bioenergy, 97, 90-99. https://doi.org/10.1016/j.biombioe.2016.12.014

Metsaranta, J. M., Trofymow, J. A., Black, T. A., & Jassal, R. S. (2018). Long-term time series of annual ecosystem production (1985–2010) derived from tree rings in Douglas-fir stands on Vancouver Island, Canada using a hybrid biometric-modelling approach. Forest Ecology and Management, 429, 57-68. doi:10.1016/j.foreco.2018.06.040

Miles, P.D., and Smith, W.B. (2009). Specific gravity and other properties of wood and bark for 156 tree species found in North America. USDA Forest Service, Northern Research Station, Newtown Square, Pennsylvania, Res. Note NRS-38.

Næsset, E. (2002). Predicting forest stand characteristics with airborne scanning laser using a practical two-stage procedure and field data. Remote Sensing of Environment, 80(1), 88-99. doi:10.1016/S0034-4257(01)00290-5

National Forest Inventory. (2008). Canada's National Forest Inventory ground sampling guidelines: Specifications for ongoing measurements. Version 5.0. Available online: https://nfi.nfis.org/resources/groundplot/Gp_guidelines_v5.0.pdf (accessed on 15 August 2020).

Natural Resources Canada. (2020). The State of Canada's Forests. Annual Report 2019. Natural Resources Canada, Canadian Forest Service, Ottawa. 88p. https://cfs.nrcan.gc.ca/publications?id=40219&lang=en_CA

Pojar, J.; Klinka, K.; Demarchi, D.A. (1991). Chapter 6: Coastal Western Hemlock Zone. In Ecosystems of British Columbia; BC Special Report Series No. 6; Meidinger, D., Pojar, J., Eds.; BC Ministry of Forests: Victoria, BC, Canada, pp. 95–111.

Poudel, K. P., Temesgen, H., & Gray, A. N. (2018). Estimating upper stem diameters and volume of Douglas-fir and western hemlock trees in the Pacific Northwest. Forest Ecosystems, 5(1), 1-12. https://doi.org/10.1186/s40663-018-0134-2

Province of British Columbia. (2018) Provincial Logging Residue and Waste Measurement Procedures Manual. https://www2.gov.bc.ca/assets/gov/farming-natural-resources-and-industry/forestry/timber-pricing/residue-and-waste/rwp_amend_28.pdf (accessed on 05/29/2021)

Province of British Columbia. (2021). Forest Inventory. https://www2.gov.bc.ca/gov/content/industry/forestry/managing-our-forest-resources/forest-inventory (accessed on 05/29/2021)

Quinn, G.S. (2018). Derivation of forest productivity and structure attributes from remote sensing imaging technology. Dissertation, University of Victoria. Retrieved from https://dspace.library.uvic.ca:8443/handle/1828/10471

Roussel, J.; Auty, D.; Coops, N.C.; Tompalski, P.; Goodbody, T.R.; Meador, A.S.; Achim, A. LidR: An R package for analysis of airborne laser scanning (ALS) data. Remote Sens. Environ. 2020, 251, 112061, doi:10.1016/j.rse.2020.112061.

Sidders, D., Joss, B., and Keddy, T. (2008). Project TID8 25B : GIS-based inventory and analysis of forestry and agriculture biomass. Natural Resources Canada, Ottawa, Ont.

Smyth, C. E., Stinson, G., Neilson, E., Lemprière, T. C., Hafer, M., Rampley, G. J., & Kurz, W. A. (2014). Quantifying the biophysical climate change mitigation potential of Canada's forest sector. Biogeosciences, 11(13), 3515–3529. https://doi.org/10.5194/bg-11-3515-2014

Smyth, C., Rampley, G., Lemprière, T. C., Schwab, O., & Kurz, W. A. (2017). Estimating product and energy substitution benefits in national-scale mitigation analyses for Canada. Global Change Biology. Bioenergy, 9(6), 1071-1084. https://doi.org/10.1111/gcbb.12389

Titus, B. D., Brown, K., Helmisaari, H. S., Vanguelova, E., Stupak, I., Evans, A., Clarke, N., Guidi, C., Bruckman, V. J., Varnagiryte-Kabasinskiene, I., Armolaitis, K., Vries, d., Wim, Hirai, K., Kaarakka, L., Hogg, K., & Reece, P. (2021). Sustainable forest biomass: A review of current residue harvesting guidelines. Energy, Sustainability and Society, 11(1), 1-32. https://doi.org/10.1186/s13705-021-00281-w

Timber Pricing Branch. (2011). Scaling Manual. Ministry of Forests Lands and Natural Resource Opperations. Retrieved from https://www.for.gov.bc.ca/ftp/hva/external/!publish/web/manuals/Scaling/2011/Scaling2011NovMaster.pdf

Tompalski, P., White, J. C., Coops, N. C., & Wulder, M. A. (2019). Demonstrating the transferability of forest inventory attribute models derived using airborne laser scanning data. Remote Sensing of Environment, 227, 110-124. https://doi.org/10.1016/j.rse.2019.04.006

Trofymow, J.A., Porter, G.L., Blackwell, B.A., Marshall, V., Arskey, R. and Pollard, D. (1997). Chronosequences selected for research into the effects of converting coastal British Columbia old growth forests to managed forests: An establishment report. Inf. Rep. BC-X-374. Nat. Res. Can. Can. For. Ser., Pacific Forestry Centre, Victoria, B.C. 137pp

Trofymow, J.A.; Stinson, G.; Kurz, W.A. (2008). Derivation of a spatially explicit 86-year retrospective carbon budget for a landscape undergoing conversion from old-growth to managed forests on Vancouver Island, BC. Forest Ecol. Manag., 256, 1677–1691, doi:10.1016/j.foreco.2008.02.056.

Trofymow, J. A., Coops, N. C., & Hayhurst, D. (2014). Comparison of remote sensing and ground-based methods for determining residue burn pile wood volumes and biomass. Canadian Journal of Forest Research, 44(3), 182–194. https://doi.org/10.1139/cjfr-2013-0281

Trofymow, J. A. , Gougeon, F., & Kelley, J. (2017). Determination of dispersed and piled post-harvest residues in coastal Douglas-fir cutblocks using unmanned aerial vehicle imagery and ground-based surveys. Information Report FI-X-015. Natural Resources Canada, Canadian Forest Service, Canadian Wood Fibre Centre, Pacific Forestry Centre, Victoria, BC. 39 p. Available online: http://cfs.nrcan.gc.ca/publications?id=38836

Trofymow, J. A., Kelley, J., & Gougeon, F. (2019). Comparison of geospatial and ground-based methods for determining post-harvest dispersed woody residues. Canadian Journal of Forest Research, 49(10), 1277-1288. doi:10.1139/cjfr-2018-0378

Vastaranta, M., Wulder, M. A., White, J. C., Pekkarinen, A., Tuominen, S., Ginzler, C., Kankare, V., Holopainen, M., Hyyppä, J., & Hyyppä, H. (2013). Airborne laser scanning and digital stereo imagery measures of forest structure: Comparative results and implications to forest mapping and inventory update. Canadian Journal of Remote Sensing, 39(5), 382-395. https://doi.org/10.5589/m13-046

White, J. C., Wulder, M. A., Varhola, A., Vastaranta, M., Coops, N. C., Cook, B. D., Pitt, D., Woods, M. (2013). A best practices guide for generating forest inventory attributes from airborne laser scanning data using an area-based approach Information Report FI-X-010; Natural Resources Canada, Canadian Forest Service, Canadian Wood Fibre Centre, Pacific Forestry Centre: Victoria, BC, Canada, 39p. Available online: https://cfs.nrcan.gc.ca/publications?id=34887

White, J. C., Wulder, M. A., & Buckmaster, G. (2014). Validating estimates of merchantable volume from airborne laser scanning (ALS) data using weight scale data. Forestry Chronicle, 90(3), 378–385. https://doi.org/10.5558/tfc2014072

White, J C., Stepper, C., Tompalski, P., Coops, N.C., Wulder, M.A., (2015). Comparing ALS and image-based point cloud metrics and modelled forest inventory attributes in a complex coastal forest environment. Forests, vol 6, 3704-3732 https://doi.org/10.3390/f6103704

Woods, M., Lim, K., & Treitz, P. (2008). Predicting forest stand variables from LiDAR data in the Great Lakes - St. Lawrence forest of Ontario. Forestry Chronicle, 84(6), 827–839. https://doi.org/10.5558/tfc84827-6

Xu, Z., Smyth, C. E., Lemprière, T. C., Rampley, G. J., & Kurz, W. A. (2018). Climate change mitigation strategies in the forest sector: Biophysical impacts and economic implications in British Columbia, Canada. Mitigation and Adaptation Strategies for Global Change, 23(2), 257-290. https://doi.org/10.1007/s11027-016-9735-7

Chapter 4: Conclusion

4.1 Summary

The overall focus of this thesis was to expand the applications of EFIs in monitoring and analysis. The first part of this thesis evaluated the utility of multi-temporal LiDAR-based EFI methods to quantify the effects of a silvicultural treatment, while the second evaluated the scalability and transferability of hybrid EFI methods for estimating both merchantable and non-merchantable wood volumes.

In the first study, the focus of Chapter 2, a process was evaluated that expanded the sampling of fertilization treatment effects to the wider treatment area by utilizing paired LiDAR blocks made up of raster cell estimates from a multi-temporal area-based (AB) model. Non-parametric random forest models and Boruta variable selection was used to train stem volume and stem biomass models, which were expanded to 29-paired LiDAR blocks across four different stand type analysis units. LiDAR block-level results of relative and periodic annual volume and biomass increments were compared against observed sample plot results and results from carbon budget model predictions using regional growth curves and growth curves derived from tree-ring reconstruction. Overall, applying a multi-temporal AB approach showed promise for detecting treatment impacts on stand volume, biomass, and height. Plot level estimates of stem volume gain post-treatment were similar to post-treatment tree-ring derived carbon budget model estimates of biomass carbon gain. However, the plot level estimates of stem biomass gain were largely different from the carbon budget model estimates suggesting differences in stand level and individual tree biomass equations used. Despite this study demonstrating that the impacts of fertilization on stem volume or biomass observed at a ground plot level do not necessarily translate across spatial scales, the methods show promise to be used in carbon verification projects as a means to rapidly expand the analysis from a network of sample plots to

the entire operational treatment area. Alternatively, the impacts of fertilization on stand height were similar across spatial scales highlighting the additional variability introduced by volume and biomass models. Although this study employed a relatively limited number of training plots compared to other studies utilizing similar methods, the relative root mean square errors (RMSE) of the stem volume and stem biomass models were similar to other applications of the AB method for estimating volume or biomass. However, despite the low relative RMSE values, the absolute RMSEs were high compared to the magnitude of volume and biomass increments. These relatively high RMSEs increased the variability of the results produced by the AB models, along with the need to remove sampled trees from the point cloud data. These findings suggest that for future applications of these methods, the number of sample plots might need to be increased according to the magnitude of the anticipated increments such that model variability is reduced. In these future applications, the optimization of sampling location and intensity should reduce overall variability and increase model accuracy allowing for the rapid and accurate expansion of the analysis on treatment impacts.

The second study was focused on evaluating the use of a hybrid (HB) EFI approach to model both merchantable and non-merchantable forest volumes while exploring the scalability of these models to harvest blocks and the transferability to additional blocks without prior training plots. Plot-level predictor metrics from 38 sample plots across three sites were produced, similar to traditional AB metrics, combined with individual tree summary metrics from LiDAR and imagery data, and then used to train HB models for merchantable and non-merchantable wood volume. The HB models were expanded to sample harvest blocks at the three sites, transferred to harvest blocks at two other sites, and compared to independent estimates of both merchantable and non-merchantable wood volume. Overall, results indicated success at transferring HB

models to additional blocks where the range of estimate accuracies was similar for harvest blocks with and without prior training sample plots. Additionally, model estimates at the block level were within a similar or higher accuracy range as other independent estimates of the same attribute. Results from non-merchantable volume variable selection indicated the average from image blue channels from individual trees as an important predictor variable and are believed to be tied to identifying dead standing trees. The HB model fits for both merchantable and non-merchantable wood volume models showed relative RMSE values within the range of other EFI applications, despite having fewer sample observations available for model training.

Additionally, the findings from this study show promise for transferring EFI models to areas without training data if point cloud attributes are stable between areas, although as stand characteristics change, accuracies decreased, similar to Tompalski et al. (2019). Interestingly, the model comparisons showed that average estimates for non-merchantable volumes were closer to the semi-automated log delineation plus pile residue method estimates than waste and residue survey estimates. However, the number of WRS sample plots was lower in some sites than others and thus a greater potential to under-sample the overall range of conditions in each stratum (Trofymow et al., 2017).

4.2 Applications

Overall, the applications of enhanced forest inventory (EFI) methods applied in this research highlight the potential for using these methods in applications that are not focused on timber production. The main contributions highlight 1) that EFI methods can expand monitoring of silvicultural treatments to the wider treatment area, and 2) EFI estimates of both merchantable and non-merchantable wood volume can be expanded to the harvest block level and transferred to additional blocks without prior training. Additionally, for both applications, EFI estimates

were shown to be within similar accuracy ranges as other independent estimates of similar attributes.

In the context of estimating silvicultural treatment impacts, the methods demonstrated in Chapter 3 offer the potential to rapidly expand the area of analysis and increase the overall accuracy of estimates for stand height, volume, and biomass. This is highly desirable in the context of carbon credit project validation as these projects often balance accuracy needs with overall project costs (Di Lallo et al., 2017). This is a critical contribution as carbon projects become increasingly popular because the expected outcomes of projects must be verified and consistent across the entire treatment area (Shryock et al., 2014; Reid et al., 2017). The methods presented herein can assist with this verification and consistency by establishing an initial assessment and providing the basis for future assessments without the need to expand or re-measure forest sample plots. Additionally, these methods should become increasingly more available with increased LiDAR data availability and UAV systems that lower the cost of data acquisition (Hu et al., 2020).

The hybrid EFI model approach used in this research further demonstrated the applicability of Boruta variable selection for selecting LiDAR-based predictor metrics. This is desirable as many LiDAR-based metrics used in EFI applications are highly correlated (Blackburn et al., 2021). Additionally, this research demonstrated that individual tree summary metrics were selected as important variables when estimating both merchantable and non-merchantable wood volumes, highlighting the importance of a hybrid approach. Similar to chapter 2, the findings from applications of EFI models in chapter 3 showed that relative RMSE values were similar to other applications, despite having much fewer sample plots available for training (White et al., 2014; Kankare et al., 2013). While this study highlighted the benefit of

utilizing a hybrid modelling approach for estimating merchantable and non-merchantable forest stand volumes, the hybrid method would also be applicable for increasing the accuracy of estimates of other forest attributes such as fire fuel, biomass, or carbon stocks. Additionally, the hybrid modelling methods from this study could also be paired with the multi-temporal approach demonstrated in Chapter 2 to estimate these forest attributes after other stand disturbances such as wildfires or insect outbreaks.

4.3 Future Research

Future research of enhanced forest inventory methods to assess the impacts of silvicultural treatments like fertilization should focus on several aspects. A primary focus should be on optimizing the sampling strategy, which could be done through a stratification of the LiDAR point cloud structure using a principal components analysis (van Ewijk et al., 2019). The second focus should investigate the influence of spatial and temporal autocorrelation in these applications of EFI methods. Lastly, the influence of GPS inaccuracies in multi-temporal remote sensing and plot location data should be further investigated.

Future research investigating the use and transferability of hybrid (HB) EFI models should focus on the influence of different sensors, acquisition dates, and point cloud structure on model transferability. As demonstrated in this study, HB models were successfully transferred to additional blocks of similar forest types. However, the point cloud structure was standardized between sensors and acquisitions through point cloud thinning. Tompalaski et al. (2019) found minimal increases of RMSE with differences in point density, but the data were from the same sensor, and errors increased when using non-parametric modelling approaches for estimating wood volumes. Alternatively, Keränen et al. (2016) found differences in model accuracy related to acquisition and sensor parameters and concluded that models should only be transferred when

point clouds have similar characteristics. Related to this, future applications of HB models should also investigate the influence of point density and the ability to segment understory trees for inclusion in individual tree summary metrics. Lastly, with the importance of the individual tree blue imagery channel related to non-merchantable volumes from dead standing trees, further research should investigate dead tree detection methods for including additional predictor metrics for non-merchantable wood volumes.

Overall, the research presented in this thesis demonstrated new applications of enhanced forest inventory methods for the assessment of silvicultural treatments and the estimation of merchantable and non-merchantable wood volumes. This work further demonstrates how these methods can be used for forest monitoring of non-timber primary attributes. We highlight that while there is room for further developments, there is great potential for EFI methods to expand assessment areas and increase overall estimate accuracies. This work will become even more critical in the future as cost barriers to data and processing are lowered, and the overall accessibility to methods is increased. Ultimately the methods presented in this research provide a base to increase the spatial resolution and accuracy of forest monitoring which serves as a key component for making informed decisions about forest management. Further, with the creation of freely publicly available remote sensing datasets, forest monitoring programs for non-timber primary attributes such as forest carbon can be developed to reach the same accuracy and spatial resolution levels as those already implemented for monitoring attributes important for timber production.

4.4 References

Blackburn, R. C., Buscaglia, R., & Sanchez Meador, A. (2021). Mixtures of airborne lidar-based approaches improve predictions of forest structure. Canadian Journal of Forest Research, https://doi.org/10.1139/cjfr-2020-0506

Di Lallo, G., Mundhenk, P., Marchetti, M., Köhl, M. (2017). Understanding measurement reporting and verification systems for redd+ as an investment for generating carbon benefits. Forests, 8, 271, doi:10.3390/f8080271.

Hu, T., Sun, X., Su, Y., Guan, H., Sun, Q., Kelly, M., Guo, Q. (2020). Development and performance evaluation of a very low-cost UAV-LiDAR system for forestry applications. Remote Sens., 13, 77, doi:10.3390/rs13010077.

Kankare, V., Vastaranta, M., Holopainen, M., Räty, M., Yu, X., Hyyppä, J., Hyyppä, H., Alho, P., & Viitala, R. (2013). Retrieval of forest aboveground biomass and stem volume with airborne scanning LiDAR. Remote Sensing, 5(5), 2257–2274. https://doi.org/10.3390/rs5052257

Keränen, J., Maltamo, M., & Packalen, P. (2016). Effect of flying altitude, scanning angle and scanning mode on the accuracy of ALS based forest inventory. International Journal Of Applied Earth Observation And Geoinformation, 52, 349-360. doi: 10.1016/j.jag.2016.07.005

Reid, A., de Montigny, L., Prescott, C., Sajedi, T. A. (2017). Systematic Review of Forest Fertilization Research in Interior British Columbia; Technical Report 111; Province BC: Victoria, BC, Canada. Available online: www.for.gov.bc.ca/ hfd/pubs/Docs/Tr/Tr111.htm (accessed on 20 August 2020).

Shryock, B., Littke, K., Ciol, M., Briggs, D., Harrison, R. (2014). The effects of urea fertilization on carbon sequestration in Douglas-fir plantations of the coastal Pacific Northwest. Forest Ecol. Manag., 318, 341–348, doi:10.1016/j.foreco.2014.01.040.

Tompalski, P., White, J. C., Coops, N. C., & Wulder, M. A. (2019). Demonstrating the transferability of forest inventory attribute models derived using airborne laser scanning data. Remote Sensing of Environment, 227, 110-124. https://doi.org/10.1016/j.rse.2019.04.006

Trofymow, J. A., Gougeon, F., & Kelley, J. (2017). Determination of dispersed and piled post-harvest residues in coastal Douglas-fir cutblocks using unmanned aerial vehicle imagery and ground-based surveys. Information Report FI-X-015. Natural Resources Canada, Canadian Forest Service, Canadian Wood Fibre Centre, Pacific Forestry Centre, Victoria, BC. 39 p. Available online: http://cfs.nrcan.gc.ca/publications?id=38836

Van Ewijk, K., Treitz, P., Woods, M., Jones, T., Caspersen, J. (2019). Forest site and type variability in ALS-based forest resource inventory attribute predictions over three Ontario forest sites. Forests, 10, 226, doi:10.3390/f10030226.

White, J. C., Wulder, M. A., & Buckmaster, G. (2014). Validating estimates of merchantable volume from airborne laser scanning (ALS) data using weight scale data. Forestry Chronicle, 90(3), 378–385. https://doi.org/10.5558/tfc2014072